isvr Institute of Sound and Vibration Research

Investigation of the Coupling of a Structure Consisting of a Beam and a Plate in Terms of Statistical Energy Analysis

J.W. Yoo, D.J. Thompson and N.S. Ferguson

ISVR Technical Memorandum No 931

April 2004

University of Southampton

SCIENTIFIC PUBLICATIONS BY THE ISVR

Technical Reports are published to promote timely dissemination of research results by ISVR personnel. This medium permits more detailed presentation than is usually acceptable for scientific journals. Responsibility for both the content and any opinions expressed rests entirely with the author(s).

Technical Memoranda are produced to enable the early or preliminary release of information by ISVR personnel where such release is deemed to the appropriate. Information contained in these memoranda may be incomplete, or form part of a continuing programme; this should be borne in mind when using or quoting from these documents.

Contract Reports are produced to record the results of scientific work carried out for sponsors, under contract. The ISVR treats these reports as confidential to sponsors and does not make them available for general circulation. Individual sponsors may, however, authorize subsequent release of the material.

UNIVERSITY OF SOUTHAMPTON

INSTITUTE OF SOUND AND VIBRATION RESEARCH

DYNAMICS GROUP

Investigation of the Coupling of a Structure Consisting of a Beam and a Plate in Terms of Statistical Energy Analysis

by

J.W. Yoo, D.J. Thompson and N.S. Ferguson

ISVR Technical Memorandum No: 931

April 2004

Authorised for issue by
Professor M.J. Brennan
Group Chairman

CONTENTS

1. INTRODUCTION

In earlier reports, a wave method [1] and a Fourier transform method [2] have been introduced in order to describe the dynamic behaviour of simple beam-plate coupled structures. Using these methods, the dissipated power and power flow between substructures were calculated and the power balance was investigated. In this report the beam-plate coupling is expressed in terms of the Statistical Energy Analysis (SEA) framework, a commonly used high frequency analysis method. First the use of SEA is briefly reviewed.

Approaching the high frequency region, corresponding to short structural wavelengths relative to the geometry, the dynamic behaviour of structures generally becomes much more sensitive to small structural changes and the prediction is often inaccurate due to the increasing uncertainty of the structure. Therefore, nominally identical structures can show significant differences in the high frequency region [3]. In such cases, therefore, the structural analysis often needs to be treated as providing a mean value estimate rather than the detailed response of the structure. For this reason various methods have been developed, amongst which the most widely accepted is SEA [4].

The application of SEA to acoustic and vibration analysis is based on a system which is considered to be an ensemble of nominally identical systems and correspondingly, a general solution is presented when the subsystems are assumed to be drawn from the ensemble of similar subsystems [4, 5]. Nominally identical subsystems may have the same gross physical and geometrical properties, but modal characteristics vary due to differences in detailed properties. If they are randomly different in a statistical sense, then the characteristics of the subsystem can be defined in terms of the ensemble average of many such similar but not identical systems. The response of a particular system is then one of the ensemble of possible system responses.

However, the application based on the ensemble is often impractical, and as it is known that the variance of the response decreases as the frequency averaging bandwidth increases [4], low ensemble variance can be assumed if the system has high modal overlap or wide analysis bands are used. Thus, the frequency average technique can be used to approximate the ensemble average. The frequency average arises from analysis based on a frequency band, for example an octave or one-third octave band, so that the energy is actually the frequency band average energy.

The system to be analysed may be divided into a number of subsystems. The frequency - and spatially - averaged response in terms of energy are required. Then the coupling between subsystems is defined in terms of a coupling loss factor (CLF), which describes the relationship between the power flow between connected subsystems and the stored energy in the subsystems. It is defined in an analogous way to the dissipation loss factor (DLF) in that it relates the fraction of power transferred between subsystems to the stored energy in the source subsystem. The values of the CLFs for particular connections are highly dependent on the physical and geometrical properties and generally require numerical calculations [4, 6]. Values can also be estimated using a wave method [5, 7].

If a system is considered as one of an ensemble of nominally identical systems, the mathematically 'typical' model of the system can be modelled from the ensemble point of view [4]. Then an exact coupling loss factor can also be defined, which is not affected by details of the structure but depends only on gross properties.

Although research related to the mid-frequency region is more important for the further study on which this report will be based, the present report discusses the CLFs and related parameters in an SEA sense, which are predicted from the model previously formulated [2]. This is because, although a statistical method is normally accepted for high frequency analysis, it is still important to understand the physical behaviour of the structure in the mid-frequency region. From this point of view, it seems useful to mention previous studies. Although many studies related to SEA have been carried out, in the present report some of them concerning coupled structures consisting of beams and/or plates are introduced.

Wester and Mace used an explicit ensemble average formulation [8] to analyse two line-coupled finite rectangular plates. The response of the system was described using a wave approach. The subsystem is assumed to be drawn from ensembles in which the reflection coefficient phase lag is uniformly distributed as a random variable [5]. Accordingly, the ensemble power was presented and compared with the estimates of the CLFs obtained using traditional SEA methods. It was shown that the traditional SEA hypothesis of proportionality between the coupling power and the difference in subsystem mean modal energies is exact for the ensemble average response of the plate systems in which the two plate wavenumbers are equal, regardless of the strength of coupling. Also a CLF traditionally calculated for use in SEA by a wave method, in which semi-infinite subsystems and diffuse fields are assumed, was found generally to over-estimate the exact value based on the ensemble average predictions at low frequencies (low modal overlap). At these low frequencies the subsystems are described as being strongly coupled.

Fahy and Mohammed [9] investigated the relationship between the CLF, modal overlap factor and the variance of the power flow for the coupled plate system by a computational experiment. For the coupled plate system presented, it was shown that it is necessary to have at least five resonance frequencies in a band for reliable estimates of the CLF to be obtained. In addition, the estimates of the CLF based on a diffuse field transmission coefficient generally exceed the actual value when the geometric average modal overlap factor is much less than unity. Accordingly, the computational examples showed that the CLF derived from tests on one physical sample could be unrepresentative of the ensemble average value when modal overlap factors are small.

The wave transmission coefficients of various joints of beam-plate structures were studied by Langley and Heron [10]. The equations of motion of the junction, which consists of semi-infinite plates connected through a beam, are formulated based on the dynamic stiffness matrix and some example junctions such as L, T and cross type coupled structures were investigated. The DLF of the structure was taken as zero, and the corresponding transmission coefficients were presented as a function of the angle of an incident wave. The diffuse incidence transmission coefficient was also determined. Then, a CLF was calculated from the transmission coefficient in an SEA sense. Although the influence of the energy dissipation in the beam could not be considered, as it was also assumed that the beam of the junction has no damping, it was shown that the procedure presented could be used in practical situations.

Heron subsequently introduced Advanced Statistical Energy Analysis (ASEA) [11]. ASEA allows for coupling between sub-systems that are physically separate by a so-called 'tunnelling mechanism' in which, even though the subsystems are physically separated from each other coupling may exist in an SEA sense. The energy of each subsystem is divided into free energy that is freely available for transfer to other subsystems and fixed energy that is dissipated within the subsystem. The system is interpreted as a series of mathematical models, and in fact, the results depend on the number of transfers of power across a subsystem and if only one junction is considered then an ASEA model is identical to a standard SEA model. A numerical example for a system consisting of six rods is considered and the normalized mean square velocity compared with that from the exact result. ASEA converges to the exact results whereas SEA is shown to overpredict by up to 60dB.

Ji developed a mode-based method as an approximate solution in which a set of basis functions is introduced for interface decomposition between a stiff beam and a flexible plate [12]. Using beam modal shape functions as the basis functions, the dynamic response of the

coupled beam and the power transmitted to the plate are expressed in terms of unloaded modal properties of the beam and the plate as well as the modal correlation matrix between them. The results are detailed for the structure consisting of a straight beam or an L-shaped beam attached to a plate. It was shown that neither the dimensions nor the boundary conditions of the plate are important for determining the vibration response. Therefore it is reasonable to describe a large flexible receiver by a simple standing wave model.

Grice and Pinnington [13] used a wave analysis to study a built-up structure consisting of a beam and plate in which the beam is seen as a source and the plate as a receiver. If the wavenumber in the plate is at least twice the wavenumber in the beam, the plate can be idealized as a set of independent plate strips that have a locally reacting impedance. Then the dynamic behaviour of the beam can be described in terms of the locally reacting impedance of the plate and the dispersion relationship of the coupled structure. As the coupled structure can be divided into a structure carrying long wavelengths (beam) and a structure carrying short wavelengths (plate), one can expect that each substructure can be analysed by different methods. Grice and Pinnington introduced such a hybrid method [14] where a finite element method is used for modelling of the beam and the plate is modelled as a number of plate strip impedances. The hybrid method was used to calculate the response of two different plate-beams, with a rectangular plate and a trapezoidal plate, and good agreement with measurements was shown.

Another hybrid method was developed by Langley and Bremner [15]. In this method, the degrees of freedom of a system are partitioned into a global set and a local set. The important assumption is that the local modes have a high degree of modal overlap and the main effect of the local modes is to add damping and an effective mass to the global modes, which can be referred to as a fuzzy structure. Then, the long wavelength component is modelled deterministically, while the short wavelength component is modelled by using SEA so that each subsystem can be assigned a single degree of freedom corresponding to the vibrational energy of the local modes. An example for a simple rod system was presented and it was shown that the method can be used to predict the dynamic behaviour in low and high frequency regions. However, application to other system in not straight forward.

The difficulties of SEA mainly occur because of the uncertainty due to variability in the CLFs. The variability in the CLF of two coupled rectangular plates was investigated by Park [16]. In order to quantify the variability of the effective CLF, a wide range of parameter variations such as the thickness ratio, the length ratio, the length-to-width ratio and damping loss factor were studied using finite plate simulations. Variations in both modal density and

modal overlap were considered, either together or separately. Although the variability of the effective CLFs reduced as frequency increased, significant variability still remains when modal overlap is greater than about 0.4. Upper and lower bounds for the CLF developed by Craik *et al* [17] were considered. It was shown that better agreement is found when the modal overlap of both systems in taken into account, rather than that of the receiver alone, as originally proposed by Craik *et al* [17]. Also the variance was investigated to find the variability of the effective CLF in terms of the combined modal overlap factor and combined number of modes for each subsystem. An empirical formula for the variance of the effective CLF was derived, which showed improved confidence intervals of the CLFs compared with previously published estimates [17, 18].

SEA is generally used for the high frequency analysis in various areas such as aircraft and spacecraft problems and more recently automotive vehicles. One successful example of the latter was given by Fraser [19]. Wave Intensity Analysis (WIA) proposed by Langley was also used to model a curved panel [20, 21] and the complex joint modelling technique was studied, so that the transmission of the energy of bending motion between panels connected by a curved section of panel can be investigated. Based on different kinds of joints such as between the roof and the windscreen or between the windscreen and the firewall, SEA was used to predict the energy level difference of the panels. It was shown that the interior saloon sound pressure level (SPL) was predicted accurately by the complex joint SEA model and the most important noise paths were identified.

In most applications, SEA parameters are derived from the wave method or modal formulations. Although, for example, the wave approach can conveniently be used for simpler structures, it has been shown that there are some limitations in the previously described application of the wave approach for the analysis of a beam-plate coupled structure [1]. By contrast, the Fourier method produced good results for the analysis of a beam-plate-beam coupled structure [2]. Thus, in the present report, in order to study SEA and its application to the beam-plate system, the Fourier method is used. The equations of motion for the coupled structure are the same as have been used previously and are not mentioned in the present report except where it is necessary.

The frequency average technique is used here instead of using the ensemble average. Also predictions of the spatial sum of the energy of a subsystem are made instead of the response at any particular point in the subsystem.

In SEA, a complex system is notionally divided into a number of subsystems that are connected through junctions. SEA parameters such as CLFs will depend on how the

subsystems are chosen. For a beam-plate coupled structure, the subsystems can conveniently be chosen as the beam and the plate. As the cases in which the external force is applied to the beam and then to the plate were analysed previously using the Fourier approach [2], SEA parameters are evaluated for these cases based on the power balance equations. An equivalent loss factor (ELF) for an infinite beam is obtained based on the wave method and is considered as an asymptotic representation. Similarly, the case in which incident waves exist in an infinite plate is considered, in order to obtain a lower bound for the CLF based on a diffuse field assumption, which can also be used as an asymptotic estimate. Then, some relationships such as variability and consistency are investigated and comparisons made between the various CLFs.

In applying SEA to the beam-plate system it is recognised that the long wavelengths in the beam cause it to have low modal density and low modal overlap, causing the CLF estimates to contain potentially large variability.

Finally, the effective CLFs obtained for the single beam coupled structure are used in a SEA model to predict the subsystem energies of a beam-plate-beam coupled structure. The SEA model used assumes only direct coupling, i.e. no indirect coupling between the beams. Then, the predicted energies are compared with those calculated exactly with the Fourier technique and discrepancies are noted and explained.

2. BACKGROUND TO SEA

2.1 Power balance and coupling loss factor

The principal objective of SEA is to establish a model which can be used to predict the average responses of a coupled structure in terms of the gross parameters of the subsystems of the original structure. The main parameters required in this process are the subsystem dissipation loss factors and the coupling loss factors. As the system is described in terms of subsystem energies, the analysis procedure normally starts with a power balance equation for each of the subsystems. It is generally necessary to consider structures consisting of several coupled subsystems. However, it seems natural and simpler to start with a structure consisting of just two subsystems, in this case a beam-plate coupled structure. The power balance relationships for two coupled subsystems, 1 and 2, where external forces are separately applied to only one subsystem at a time are illustrated in Figure 1.

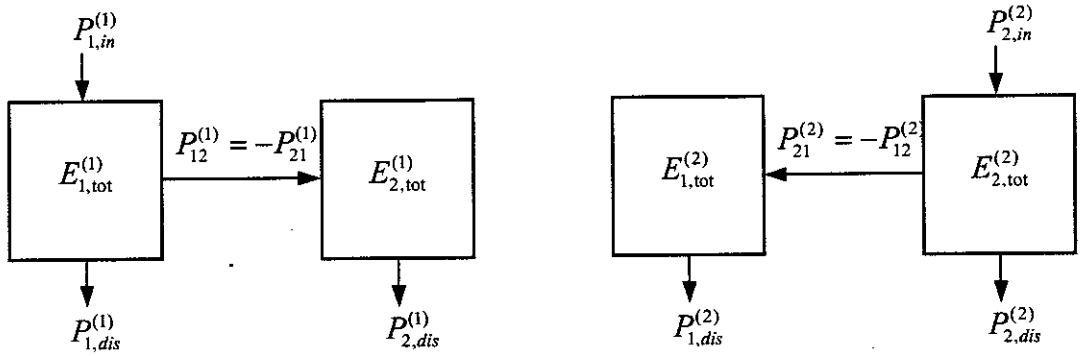

(a) Power input to subsystem 1 (b) Power input to subsystem 2

Figure 1. Power flows in coupled structure consisting of two subsystems

As explained before, introducing the ensemble average notation, the power balance equations can be expressed as

$$\overline{P}_{1,in}^{(1)} = \overline{P}_{1,dis}^{(1)} + \overline{P}_{2,dis}^{(1)} = \overline{P}_{1,dis}^{(1)} + \overline{P}_{12}^{(1)}, \tag{2.1}$$

$$\overline{P}_{2,in}^{(2)} = \overline{P}_{2,dis}^{(2)} + \overline{P}_{1,dis}^{(2)} = \overline{P}_{2,dis}^{(2)} + \overline{P}_{21}^{(2)}. \tag{2.2}$$

where P_{in} and P_{dis} are the input power and dissipated power, and $P_{12}(=-P_{21})$ is the net power transferred from subsystem 1 to 2. The superscripts are introduced to distinguish the case in

which the excitation is applied to subsystem 1 or 2. The powers are the time-averaged values and '−' denotes an ensemble average. Note that $\overline{P}_{12}^{(1)} \neq \overline{P}_{12}^{(2)}$.

In SEA, it is assumed that the power flow between subsystems is proportional to the difference in average modal energy. Then, equations (2.1) and (2.2) can be rewritten in terms of energies, coupling loss factors and damping loss factors as follows.

$$\overline{P}_{1,in}^{(1)} = \overline{P}_{1,dis}^{(1)} + \overline{P}_{12}^{(1)} = \omega\left(\eta_1 \overline{E}_1^{(1)} + \eta_{12}^{(1)} \overline{E}_1^{(1)} - \eta_{21}^{(1)} \overline{E}_2^{(1)}\right), \tag{2.3}$$

$$0 = \overline{P}_{2,dis}^{(1)} + \overline{P}_{21}^{(1)} = \omega\left(\eta_2 \overline{E}_2^{(1)} + \eta_{21}^{(1)} \overline{E}_2^{(1)} - \eta_{12}^{(1)} \overline{E}_1^{(1)}\right), \tag{2.4}$$

$$\overline{P}_{2,in}^{(2)} = \overline{P}_{2,dis}^{(2)} + \overline{P}_{21}^{(2)} = \omega\left(\eta_2 \overline{E}_2^{(2)} + \eta_{21}^{(2)} \overline{E}_2^{(2)} - \eta_{12}^{(2)} \overline{E}_1^{(2)}\right), \tag{2.5}$$

$$0 = \overline{P}_{1,dis}^{(2)} + \overline{P}_{12}^{(2)} = \omega\left(\eta_1 \overline{E}_1^{(2)} + \eta_{12}^{(2)} \overline{E}_1^{(2)} - \eta_{21}^{(2)} \overline{E}_2^{(2)}\right). \tag{2.6}$$

where η_1 and η_2 are the dissipation loss factors (DLFs) of corresponding subsystems, E_1 and E_2 are total energies, and η_{12} and η_{21} are the coupling loss factors (CLFs). Energy is also time-averaged. If the input power, the total energy stored in each system and DLFs are known from other approaches, for example a wave method, a Fourier transform method, etc, equations (2.3) - (2.6) can be used to obtain the equivalent SEA parameters CLFs $\eta_{12}^{(1)}$, $\eta_{21}^{(1)}$, $\eta_{21}^{(2)}$ and $\eta_{12}^{(2)}$. Hence, imposing the SEA model on the system and using the predicted responses, one may invert the equations to obtain the SEA parameters which would provide the same subsystem response. This is known as the Power Injection Method (PIM) [22]. Strictly $\eta_{ij}^{(1)} \neq \eta_{ij}^{(2)}$, although in SEA it is usually assumed that $\eta_{ij}^{(1)} = \eta_{ij}^{(2)}$ i.e. the coupling loss factors are independent of which system is being excited. If this assumption is made, and the DLFs are known, only two of the above equations are required. In fact these equations are not independent and cannot be used to separate $\eta_{ij}^{(1)}$ and $\eta_{ij}^{(2)}$.

2.2 The effective CLF

As explained, the actual CLF is defined in terms of the ensemble average over substructures that are different in detail but are members of same specified statistical distribution. However, in real applications, it is often difficult to realise an ensemble.

Alternatively the power balance equations hold for an individual realisation and a CLF-like term may be obtained for a particular realisation. This is referred to as the effective CLF $\hat{\eta}_{ij}$ [16]. Assuming $\hat{\eta}_{ij}^{(1)} = \hat{\eta}_{ij}^{(2)}$, the power balance equation including the effective CLF can be written as

$$P_{12}^{(1)} = \omega\left(\hat{\eta}_{12}E_1^{(1)} - \hat{\eta}_{21}E_2^{(1)}\right) \tag{2.7}$$

$$P_{21}^{(2)} = \omega\left(\hat{\eta}_{21}E_2^{(2)} - \hat{\eta}_{12}E_1^{(2)}\right) \tag{2.8}$$

or in matrix form,

$$\begin{Bmatrix}\hat{\eta}_{12}\\ \hat{\eta}_{21}\end{Bmatrix} = \omega^{-1}\begin{bmatrix}E_1^{(1)} & -E_2^{(1)}\\ -E_1^{(2)} & E_2^{(2)}\end{bmatrix}^{-1}\begin{Bmatrix}P_{12}^{(1)}\\ P_{21}^{(2)}\end{Bmatrix}. \tag{2.9}$$

Therefore, if the subsystem i is excited first by the external force and then the subsystem j is excited, then the effective CLFs for the coupled structure can be obtained by equation (2.9). Note that, here, the power flows and the stored energies are presented by space-averaged and frequency-averaged representation such as the octave band frequency average and therefore the frequency ω is the centre frequency of the corresponding octave band.

2.3 Consistency of the two coupled subsystems

As SEA requires the power flow between subsystems to be proportional to the difference in average modal energy, for the whole system consisting of two subsystems as in Figure 1, the consistency or reciprocity relationship can also be investigated, which is an important hypothesis often used in SEA [4].

If the external excitation is applied first to the subsystem i and then to subsystem j, then the equation for the consistency relationship may be given as

$$n_i\eta_{ij}^{(i)} = n_j\eta_{ji}^{(j)}. \tag{2.10}$$

where n_i, n_j are respectively the modal densities of subsystems i and j and η is the CLF.

It is known if the coupling power proportionality (CPP) is exact then equation (2.10) holds [23]. The CPP means that the coupling power from one subsystem to another is proportional to the difference in their modal energy. The expressions for the CPP are simply

equations (2.7) and (2.8), so that the effective CLFs can be obtained based on the assumption of the exact CPP. Therefore, it is expected that the consistency relationship should hold for the present beam-plate coupled structure based on the power balance equations provided that there are sufficient modes in a frequency band. However, note that the consistency equation is not a necessary condition for the power balance equations, and has not been assumed in the results in previous sections. If consistency were imposed there in principle, assuming knowledge of the modal densities, one would only require one CLF to be evaluated.

The numerical results testing the consistency equation will be shown later in section 5.3 where the effective CLFs are considered.

2.4 Modal density

As presented in equation (2.10), the consistency relationship relates the modal density of subsystems as well as CLFs. Thus, it is necessary to determine the modal density of the subsystems used here, normally a beam and a plate.

2.4.1 Finite beam system

Any finite structure has natural modes of vibration and the mode count $N(\omega)$ is normally used to define the number of modes occurring below a particular frequency ω. The mode count can be obtained based on the boundary conditions of the finite system and the dispersion relationship. For a one-dimensional system such as a beam, the expression for the mode count is known [4]

$$N(k_b) = \frac{k_b L}{\pi} + \delta_{BC} \tag{2.11}$$

where k_b is the travelling wave number, L is the length of the system in which the wave propagates and δ_{BC} is a constant which is dependent upon the boundary conditions. The constant δ_{BC} for particular boundary conditions is given by [24]

$$\delta_{BC} = 1 - \delta_L - \delta_R . \tag{2.12}$$

where δ_L and δ_R are dependent on boundary conditions. For example, for a free boundary condition $\delta = 0$ and for a sliding boundary $\delta = 1/4$.

The modal density of a structure is defined as the number of modes per unit frequency interval, $\Delta N/\Delta\omega$. For the mode count $N(\omega)$, the modal density function can be written as

$$n(\omega)=\frac{dN}{d\omega}=\frac{dN}{dk}\cdot\frac{dk}{d\omega}. \tag{2.13}$$

Therefore, the modal density of flexural vibration in a beam becomes, from equation (2.12) and (2.13)

$$n(\omega)=\frac{dN}{dk}\frac{dk}{d\omega}=\frac{dN}{dk}\frac{1}{c_g}=\frac{L}{\pi}\frac{k}{2\omega}. \tag{2.14}$$

where c_g is the group velocity of flexural waves in the structure and is given by $c_g=2\omega/k$. This is independent of the boundary condition in most cases.

2.4.2 Finite rectangular plate system

The general form for the mode count of a rectangular plate is given by Lyon and DeJong [4] as

$$N(k_p)\simeq\frac{k_p^2S_p}{4\pi}+\Gamma_{BC}L_{tot}k_p \tag{2.15}$$

where k_p is the plate free wavenumber, S_p is the area of the plate, L_{tot} is the perimeter length of the plate and Γ_{BC} depends on the boundary conditions.

Xie [24] introduced a more developed equation for the mode count, so that the boundary effects can be considered as follows.

$$N(k_p)=\frac{k_p^2S_p}{4\pi}+\left(1-\delta_{x,L}-\delta_{x,R}\right)\frac{k_p}{\Delta k_y}+\left(1-\delta_{y,T}-\delta_{y,B}\right)\frac{k_p}{\Delta k_x}+\Delta \tag{2.16}$$

where $\delta_{x,L}$, $\delta_{x,R}$, $\delta_{y,T}$ and $\delta_{y,B}$ are the one-dimensional boundary effects corresponding the boundary conditions of the four edges, Δ is a small number, and Δk_x and Δk_y are the changes in trace wavenumbers from one mode to the next, which are π/L_x and π/L_y for the present case.

For the present report, a coupled structure consisting of a beam and a plate is considered in which the plate is assumed to be sliding along three edges including the coupling junction and the opposite edge to the junction is assumed to be pinned. Correspondingly, the mode count number for the present plate is given by

$$N(k_p) = \left(\frac{\pi}{L_x} \frac{\pi}{L_y} \right)^{-1} \left(\frac{\pi k_p^2}{4} + \frac{k_p}{2} \frac{\pi}{L_x} \right) = \frac{S_p}{4\pi} k_p^2 + \frac{L_y k_p}{2\pi}. \tag{2.17}$$

Then, the modal density can be evaluated from equation (2.13).

3. CLF BASED ON WAVE TRANSMISSION AND EQUIVALENT LOSS FACTOR (ELF)

The finite system effective CLFs $\hat{\eta}_{21}$ can be obtained from equation (2.9) by considering both the beam-excited response and the plate-excited response. However, before mentioning the effective CLFs $\hat{\eta}_{21}$ based on the power balance relationship, the wave coefficient is presented in this section. Often in SEA, the CLF is based on the transmission coefficient and a diffuse field assumption [4] for the transmission between two semi-infinite systems e.g. plates.

As well as the transmission efficiency and a possible lower bound for the CLF, the equivalent loss factor (ELF) of the beam is also mentioned in this chapter, which can also be used as an asymptotic representation of η_{12}.

3.1 Power transmission between a semi-infinite plate and an infinite beam

For the coupled structure consisting of an infinite beam and infinitely long semi-infinite width plate as in Figure 2, consider an incident harmonic wave in the plate with wavenumber k_p and heading θ with respect to the normal to the coupling junction (at $y=0$). The plate free wavenumber k_p is given by $k_p^4 = \left(m_p''/D_p\right)\omega^2$ where m_p'' is mass per unit area, ω is angular frequency and D_p is the bending stiffness of the plate. It is assumed that the plate has no damping and the beam has light damping*.

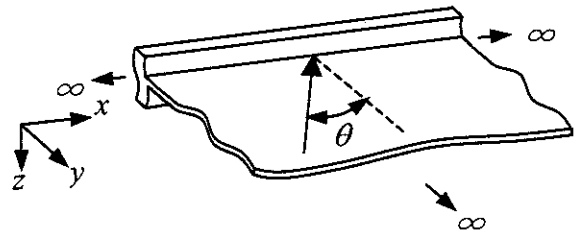

Figure 2. Coupled structure consisting of an infinite beam and a semi-infinite plate and the incident wave on the plate.

* Note that for two coupled semi-infinite plates, normally both subsystems are considered to be undamped. However, in the present case, as will be seen, in the absence of damping no power is transmitted to the beam.

The displacement amplitude of the coupled beam can be expressed as

$$\tilde{w}_b = \tilde{A}e^{-ik_x x}. \tag{3.1}$$

where k_x is the component of the incident wavenumber along the beam direction. Matching the trace wavenumber in the plate with the wavenumber in the beam, one has

$$k_x = k_p \sin\theta \tag{3.2}$$

Accordingly, the motion of the plate can be represented by the trace wave matching as follows:

$$\tilde{w}_p = \left(\tilde{B}_1 e^{k_{y1}y} + \tilde{B}_2 e^{k_{y2}y} + \tilde{B}_3 e^{k_{y3}y}\right) e^{-ik_x x} \tag{3.3}$$

where $\tilde{B}_1$ is the amplitude of a wave travelling away from the junction, $\tilde{B}_2$ is the amplitude of a nearfield wave decaying away from the junction, and $\tilde{B}_3$ is the amplitude of the incident wave. The plate trace wavenumbers can be expressed in terms of the beam and free plate wavenumbers, namely

$$k_{y1} = -\sqrt{k_x^2 - k_p^2} = -ik_p \cos\theta \tag{3.4}$$

$$k_{y2} = -\sqrt{k_x^2 + k_p^2} = -k_p\sqrt{1+\sin^2\theta} \tag{3.5}$$

$$k_{y3} = ik_p \cos\theta \tag{3.6}$$

The equation of motion of the Euler-Bernoulli beam is

$$\tilde{D}_b \frac{d^4\tilde{w}_b(x)}{dx^4} - m_b'\omega^2\tilde{w}_b(x) = -\tilde{f}_1(x) \tag{3.7}$$

where $\tilde{f}_1(x)$ is the force per unit length, acting on the beam due to the plate, $\tilde{D}_b$ is the bending stiffness which is complex due to damping and m_b' is the mass per unit length. Substituting equation (3.1) into equation (3.7) gives

$$\tilde{A}\left(\tilde{D}_b k_x^4 - m_b' \omega^2\right) e^{-ik_x x} = -\tilde{f}_1(x). \tag{3.8}$$

The boundary conditions that apply for the coupled structure consisting of an infinite beam and a semi-infinite width plate are:

i) Equal displacement at the coupling junction

$$\tilde{w}_b = \tilde{w}_p\Big|_{y=0} \tag{3.9}$$

Therefore, from equations (3.1) and (3.3),

$$\tilde{A} = \tilde{B}_1 + \tilde{B}_2 + \tilde{B}_3. \tag{3.10}$$

ii) Infinite torsional stiffness of the beam is assumed (as in [1, 2]) which implies

$$\left.\frac{\partial \tilde{w}_p}{\partial y}\right|_{y=0} = 0 \tag{3.11}$$

from which

$$\left[\left(\tilde{B}_1 k_{y1} e^{k_{y1} y} + \tilde{B}_2 k_{y2} e^{k_{y2} y} + \tilde{B}_3 k_{y3} e^{k_{y3} y}\right) e^{-ik_x x}\right]_{y=0} = 0$$

$$\tilde{B}_1 k_{y1} + \tilde{B}_2 k_{y2} + \tilde{B}_3 k_{y3} = 0. \tag{3.12}$$

iii) Force equilibrium; the force acting on the junction can be expressed in terms of the shear force in the coupled plate

$$D_p\left[\frac{\partial^3 \tilde{w}_p}{\partial y^3} + (2-\nu)\frac{\partial^3 \tilde{w}_p}{\partial x^2 \partial y}\right]_{y=0} = \tilde{f}_1(x) \tag{3.13}$$

Using equation (3.3),

$$\frac{\partial^3 \tilde{w}_p}{\partial y^3} = \left(\tilde{B}_1 k_{y1}^3 e^{k_{y1} y} + \tilde{B}_2 k_{y2}^3 e^{k_{y2} y} + \tilde{B}_3 k_{y3}^3 e^{k_{y3} y}\right) e^{-ik_x x}.$$

$$\frac{\partial^3 \tilde{w}_p}{\partial x^2 \partial y} = -k_x^2 \left(\tilde{B}_1 k_{y1} e^{k_{y1} y} + \tilde{B}_2 k_{y2} e^{k_{y2} y} + \tilde{B}_3 k_{y1} e^{k_{y3} y}\right) e^{-ik_x x}.$$

Therefore,

$$D_p\left[\tilde{B}_1k_{y1}^3+\tilde{B}_2k_{y2}^3+\tilde{B}_3k_{y3}^3-(2-\nu)k_x^2\left(\tilde{B}_1k_{y1}+\tilde{B}_2k_{y2}+\tilde{B}_3k_{y1}\right)\right]\ e^{-ik_xx}=\tilde{f}_1(x),$$

and as $\tilde{B}_1k_{y1}+\tilde{B}_2k_{y2}+\tilde{B}_3k_{y3}=0$, equation (3.13) becomes

$$D_p\left(\tilde{B}_1k_{y1}^3+\tilde{B}_2k_{y2}^3+\tilde{B}_3k_{y3}^3\right)\ e^{-ik_xx}=\tilde{f}_1(x). \tag{3.14}$$

From equations (3.10) and (3.12),

$$\tilde{B}_2=\frac{-\tilde{B}_1k_{y1}-\tilde{B}_3k_{y3}}{k_{y2}}. \tag{3.15}$$

$$\tilde{A}=\frac{\tilde{B}_1(k_{y2}-k_{y1})+\tilde{B}_3(k_{y2}-k_{y3})}{k_{y2}}. \tag{3.16}$$

Substituting equation (3.15) into equation (3.14) gives

$$D_p\left[\tilde{B}_1k_{y1}\left(k_{y1}^2-k_{y2}^2\right)+\tilde{B}_3k_{y3}\left(k_{y3}^2-k_{y2}^2\right)\right]\ e^{-ik_xx}=\tilde{f}_1(x). \tag{3.17}$$

Also, substituting equation (3.16) into equation (3.8) gives

$$\frac{\left[\tilde{B}_1(k_{y2}-k_{y1})+\tilde{B}_3(k_{y2}-k_{y3})\right]\left(\tilde{D}_bk_x^4-m_b'\omega^2\right)}{k_{y2}}\ e^{-ik_xx}=-\tilde{f}_1(x). \tag{3.18}$$

Therefore, eliminating $\tilde{f}_1(x)$ from equations (3.17) and (3.18) results in

$$\begin{aligned}&\tilde{B}_1\left[\left(\tilde{D}_bk_x^4-m_b'\omega^2\right)\left(k_{y1}-k_{y2}\right)-D_pk_{y1}k_{y2}\left(k_{y1}^2-k_{y2}^2\right)\right]\\&=\tilde{B}_3\left[\left(\tilde{D}_bk_x^4-m_b'\omega^2\right)\left(k_{y2}-k_{y3}\right)-D_pk_{y2}k_{y3}\left(k_{y3}^2-k_{y2}^2\right)\right].\end{aligned} \tag{3.19}$$

Hence, the ratio of the amplitude of the reflected wave to the amplitude of the incident wave can be written as

$$\tilde{r}=\frac{\tilde{B}_1}{\tilde{B}_3}=\frac{\left(k_{y2}-k_{y3}\right)\left[\left(\tilde{D}_bk_x^4-m_b'\omega^2\right)-D_pk_{y2}k_{y3}\left(k_{y2}+k_{y3}\right)\right]}{\left(k_{y1}-k_{y2}\right)\left[\left(\tilde{D}_bk_x^4-m_b'\omega^2\right)-D_pk_{y1}k_{y2}\left(k_{y1}+k_{y2}\right)\right]}. \tag{3.20}$$

As presented in equations (3.3) - (3.6) each wavenumber can be expressed in terms of the plate free wavenumber and the angle of the incident wave. Also, the uncoupled wavenumber of the damped beam is given by $\tilde{k}_b^4=\left(m_b'/\tilde{D}_b\right)\omega^2$. Thus, equation (3.20) can written as follows.

$$\tilde{r}=\frac{\tilde{B}_1}{\tilde{B}_3}=\frac{\left(-k_p\sqrt{1+s^2}-ik_pc\right)\left[\left(\tilde{D}_bk_x^4-m_b'\omega^2\right)+iD_pk_p^2\sqrt{1+s^2}\,c\left(-k_p\sqrt{1+s^2}+ik_pc\right)\right]}{\left(+k_p\sqrt{1+s^2}-ik_pc\right)\left[\left(\tilde{D}_bk_x^4-m_b'\omega^2\right)+iD_pk_p^2\sqrt{1+s^2}\,c\left(+k_p\sqrt{1+s^2}+ik_pc\right)\right]}$$

$$=\frac{\left(+\sqrt{1+s^2}+ic\right)\left(k_p^4s^4-\tilde{k}_b^4\right)-2D_pik_p^3\sqrt{1+s^2}\,c/\tilde{D}_b}{\left(-\sqrt{1+s^2}+ic\right)\left(k_p^4s^4-\tilde{k}_b^4\right)-2D_pik_p^3\sqrt{1+s^2}\,c/\tilde{D}_b} \tag{3.21}$$

where $s=\sin\theta$ and $c=\cos\theta$.

For convenience, if μ is given by

$$\mu=\frac{m_p''}{m_b'k_p}=\frac{D_pk_p^3}{\tilde{D}_b\tilde{k}_b^4} \tag{3.22}$$

then equation (3.21) becomes

$$\tilde{r}=\frac{\tilde{B}_1}{\tilde{B}_3}=\frac{\left(+\sqrt{1+s^2}+ic\right)\left(k_p^4s^4-\tilde{k}_b^4\right)-2i\mu\tilde{k}_b^4\sqrt{1+s^2}\,c}{\left(-\sqrt{1+s^2}+ic\right)\left(k_p^4s^4-\tilde{k}_b^4\right)-2i\mu\tilde{k}_b^4\sqrt{1+s^2}\,c}. \tag{3.23}$$

If ξ the free wavenumber ratio is defined by

$$\xi=\frac{k_b}{k_p}, \tag{3.24}$$

then

$$\frac{\tilde{k}_b^4}{k_p^4}=\xi^4\left(1+i\eta_b\right)^{-1}. \tag{3.25}$$

Accordingly, equation (3.23) becomes

$$\tilde{r}=\frac{\tilde{B}_1}{\tilde{B}_3}=\frac{\left(+\sqrt{1+s^2}+ic\right)\left[s^4\left(1+i\eta_b\right)-\xi^4\right]-2i\mu\xi^4\sqrt{1+s^2}\,c}{\left(-\sqrt{1+s^2}+ic\right)\left[s^4\left(1+i\eta_b\right)-\xi^4\right]-2i\mu\xi^4\sqrt{1+s^2}\,c}. \tag{3.26}$$

Therefore, the power reflection coefficient, which is the ratio of the power reflected from the junction to the power incident in the plate, can be written as

$$\rho_\theta=\rho(\theta)=\left|\tilde{r}\right|^2=\left|\frac{\tilde{B}_1}{\tilde{B}_3}\right|^2. \tag{3.27}$$

Also, the transmission coefficient, indicating the proportion of power that is transmitted to the beam, can be obtained from the reflection coefficient as follows.

$$\tau_\theta = 1 - \rho_\theta . \tag{3.28}$$

In SEA it is usually assumed that a diffuse field is present, so that travelling wave energy in the subsystem is distributed uniformly in all directions. The reflection coefficient for the diffuse field can be obtained from an angular average of ρ_θ.

$$\rho_d = \frac{\int_0^{\frac{\pi}{2}} \rho_\theta \cos\theta d\theta}{\int_0^{\frac{\pi}{2}} \cos\theta d\theta} = \int_0^{\frac{\pi}{2}} \rho_\theta \cos\theta d\theta . \tag{3.29}$$

Assuming that there is no significant power dissipation at the junction, then a power transmission coefficient for the semi-infinite system such as the structure shown in Figure 2 will be

$$\tau_{21,d} = 1 - \rho_d . \tag{3.30}$$

where subscript 21 means that power is transmitted from the plate (subsystem 2) to the beam (subsystem 1) for consistency with the previous section. As a diffuse field is assumed, the total normal incident power in the diffuse field due to the incident wave as shown in Figure 2 is given by

$$P_{inc,d} = \int_0^{\frac{\pi}{2}} P_{inc}(\theta)\cos\theta d\theta = P_{inc}\int_0^{\frac{\pi}{2}} \cos\theta d\theta = P_{inc} \tag{3.31}$$

where $P_{inc} = P_{inc}(\theta)$ is the constant incident power for any arbitrary angle θ, which is independent of θ. Similarly the transmitted power is also given by

$$P_{21,d} = \int_0^{\frac{\pi}{2}} \tau_{21}(\theta) P_{inc}(\theta)\cos\theta d\theta = P_{inc,d}\int_0^{\frac{\pi}{2}} \tau_{21}(\theta)\cos\theta d\theta = P_{inc,d}\tau_{21,d} . \tag{3.32}$$

A coupling loss factor (CLF) of a finite system cannot be obtained directly from the transmission coefficient and the relationship between the incident power and the energy which is assumed equally distributed in the subsystem. For a finite beam the net power transferred to the beam depends upon its damping and when it is undamped there will be no net power transferred to it.

For a diffuse field on the plate (subsystem 2), the relationship between the incident power arriving at the perimeter and total energy of the plate may be expressed as [25]

$$P_{inc,P} = E_2 c_g \frac{L_{tot}}{\pi S_2} \tag{3.33}$$

where E_2 is the total energy stored in the plate, c_g is the group velocity of the plate ($c_g = 2c_B = 2\omega/k_p$), L_{tot} is the perimeter of the plate and S_2 is the area of the plate. Therefore, the power flowing to the junction of length L becomes

$$P_{inc} = E_2 c_g \frac{L_{tot}}{\pi S_2} \frac{L}{L_{tot}} = E_2 c_g \frac{L}{\pi S_2}. \tag{3.34}$$

The net power transmitted to the beam from the plate P_{21} is dependent upon the beam damping and is given by

$$P_{21} = \eta_{21}\omega E_2 - \eta_{12}\omega E_1. \tag{3.35}$$

If one assumes negligible power is transmitted from the beam back to the plate (i.e. $\eta_{12}\omega E_1 \ll \eta_{21}\omega E_2$) then, from equations (3.32), (3.34) and (3.35) an approximation for the coupling loss factor of two-dimensional subsystems can be represented in terms of the power transmission coefficient [25] as

$$\eta_{21} \approx \frac{\tau_{21,d} c_g L}{\pi\omega S_2}. \tag{3.36}$$

In practice $\eta_{12}\omega E_1 \neq 0$ so the estimate for η_{21} given above represents a lower bound for the actual CLF (provided η_{12} is positive). Also, strictly the system analysed violates the assumptions on which the expression in equation (3.36) is based.

3.2 CLF estimates of a beam-plate coupled structure based on the semi-infinite structure wave transmission

Now, an approximation for a lower bound for the CLF of a coupled structure consisting of a finite beam and a finite plate such as the structure shown in Figure 3 may be obtained from the power transmission coefficient derived in section 3.1 and the procedure described in section 3.1 using a slightly more rigorous approach.

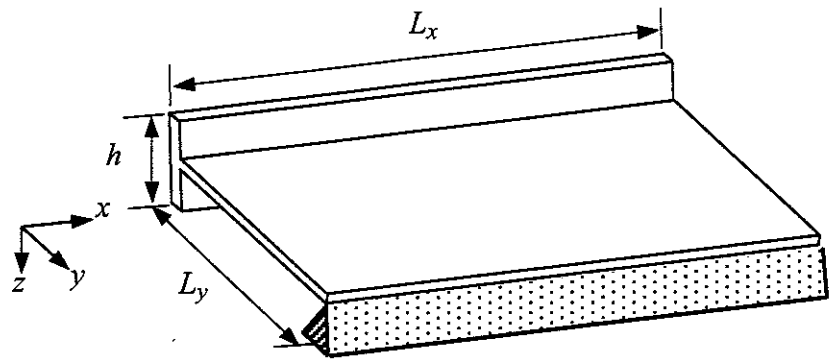

Figure 3. A built-up structure consisting of a finite beam attached to a finite plate with a pinned opposite edge.

As explained in section 3.1, the total energy in the plate (subsystem 2) is made up of the incident and the reflected wave at the junction. Thus the energy for any angle of incidence θ in the plate is given by

$$E_2(\theta) = \frac{1}{2} m_p'' S_2 \omega^2 \left(\left| \tilde{B}_1 \right|^2 + \left| \tilde{B}_3 \right|^2 \right) = \frac{1}{2} m_p'' S_2 \omega^2 \left| \tilde{B}_3 \right|^2 (1 + \rho_\theta). \tag{3.37}$$

If an equivalent reflection coefficient ρ_e for the diffuse field assumption is introduced as*

$$\rho_e = \frac{\int_0^{\frac{\pi}{2}} \rho_\theta d\theta}{\int_0^{\frac{\pi}{2}} d\theta} = \frac{\int_0^{\frac{\pi}{2}} \rho_\theta d\theta}{\frac{\pi}{2}}, \tag{3.38}$$

and a corresponding equivalent transmission coefficient is

$$\tau_{21,e} = 1 - \rho_e \tag{3.39}$$

then, the total energy stored in the plate is given by

$$E_2 = \int_0^{\frac{\pi}{2}} E_2(\theta) d\theta = \frac{1}{4} \pi m_p'' S_2 \omega^2 \left| \tilde{B}_3 \right|^2 (1 + \rho_e). \tag{3.40}$$

Apart from this, the total energy per unit area (energy density) due to the incident wave motion is

$$\varepsilon = \frac{m_p'' \omega^2 \left| \tilde{B}_3 \right|^2}{2}. \tag{3.41}$$

* Note that $\rho_e \neq \rho_d$ due to the omission of the $\cos\theta$ term here.

Therefore, the normal incident power per unit length due to the wave travelling at an angle θ to the normal to the coupling junction may be written as

$$P_{inc} = \varepsilon c_g \cos\theta = \frac{m_p'' \omega^3 \left|\tilde{B}_3\right|^2}{k_p} \cos\theta \tag{3.42}$$

where c_g is the group velocity of the plate. Accordingly the normal component of the power incident along the length L_x of the junction is given by

$$P_{inc} = \varepsilon c_g L_x \cos\theta = \frac{m_p'' \omega^3 \left|\tilde{B}_3\right|^2 L_x}{k_p} \cos\theta . \tag{3.43}$$

Then the incident power assuming a diffuse field can be simply given by the integral over θ (see equation (3.31))

$$P_{inc,d} = \frac{m_p'' \omega^3 \left|\tilde{B}_3\right|^2 L_x}{k_p}, \tag{3.44}$$

and the net transmitted power becomes

$$P_{21,d} = \tau_{21,d} P_{inc,d} = \tau_{21,d} \frac{m_p'' \omega^3 \left|\tilde{B}_3\right|^2}{k_p} L_x . \tag{3.45}$$

Applying equation (3.35) and assuming $\eta_{12}\omega E_1 \ll \eta_{21}\omega E_2$, then a lower bound for the CLF is given from equations (3.40) and (3.45).

$$\eta_{21} > \frac{4\tau_{21,d} L_x}{(1+\rho_e)\pi k_p S_2} = \frac{2\tau_{21,d}}{2-\tau_{21,e}} \frac{c_g L_x}{\pi \omega S_2} . \tag{3.46}$$

Equation (3.46) can be compared with equation (3.36). It has the same form. However it can be seen that there is a correction in the denominator of $\left(2-\tau_{21,e}\right)/2$, due to the difference between the incident power and the reflected power at the coupling junction for a semi-infinite plate. This equation is a little different to the one presented in [16] where a correction factor of $\left(2-\tau_{21,d}\right)/2$ is used; this was initially given in terms of the transmission coefficient τ_θ by Lyon and DeJong [4]. However, the difference between them seems negligible in the present case, as will be shown in the following section.

The consistency relationship for two coupled subsystems is described in section 2.3. Using this assumption, the power flow equation (3.35) can be rewritten in terms of one CLF and the modal densities as follows.

$$P_{21} = \omega \eta_{21} \left(E_2 - \frac{n_2}{n_1} E_1 \right) \tag{3.47}$$

where n_1 and n_2 are the asymptotic modal density of the beam and the plate respectively. Then combining equations (3.45) and (3.47) gives

$$\eta_{21} = \frac{\tau_{21,d} m_p'' \omega^2 \left| \tilde{B}_3 \right|^2 L_x}{E_2 \left(1 - \frac{n_2 E_1}{n_1 E_2} \right) k_p}. \tag{3.48}$$

Therefore, substituting equation (3.40) in equation (3.48) results in

$$\eta_{21} = \frac{2\tau_{21,d}}{\left(2 - 2\tau_{21,e}\right)} \frac{c_g L_x}{\omega \pi S_2} \left(1 - \frac{n_2 E_1}{n_1 E_2} \right)^{-1}. \tag{3.49}$$

It can be seen that equation (3.49) is slightly different from equation (3.46).

The total energy of the beam can be presented based on the transmission coefficient and the diffuse field assumption as follows.

$$E_1 = \int_0^{\frac{\pi}{2}} E_1(\theta) d\theta = \int_0^{\frac{\pi}{2}} \frac{1}{2} m_b' L_x \omega^2 \left| \tilde{B}_3 \right|^2 \tau_\theta d\theta = \frac{1}{4} \pi m_b' L_x \omega^2 \left| \tilde{B}_3 \right|^2 \tau_e. \tag{3.50}$$

Thus the energy ratio E_1/E_2 required in equation (3.49) can be found from equations (3.40) and (3.50) i.e.

$$\frac{E_1}{E_2} = \frac{m_b' \tau_e}{m_p'' L_y (2 - \tau_e)}. \tag{3.51}$$

As the CLF presented by equation (3.49) is based on the assumption of the consistency relationship, this expression is also an estimate for CLF η_{21} rather than the exact one.

3.3 Numerical analysis

3.3.1 Baseline model

In this section, numerical results are given for the CLF calculated using equation (3.46). Although equation (3.46) represents the coupling parameter of the finite structure shown in Figure 3, it is necessary to note that the CLF is calculated from the transmission coefficient of the semi-infinite model assumption as in Figure 2. Accordingly it seems meaningful first to examine the transmission coefficient.

The material properties and the dimensions used for the baseline model (see Figure 3) are presented in Table 1. The length of the beam is regarded as 3.0 m, which in fact has no

influence on the results as $S_2 = L_x \times L_y$ (see equation (3.46)). Note that the damping of the plate is assumed to be zero as the CLF is calculated based on the power transmission coefficient, so that the CLF from the plate to the beam is not a function of the plate dissipation.

Table 1. Material properties and dimensions of the baseline model shown in Figure 3.

Material	Perspex
Young's modulus, E (GNm^{-2})	4.4
Poisson's ratio, ν	0.38
Density, ρ (kgm^{-3})	1152.0
Beam length, L_x (m)	3.0
Plate width, L_y (m)	0.75
Thickness, t (mm)	5.9
Height of the beam, h (mm)	68.0
DLF of the beam, η_b	0.03
DLF of the plate, η_p	0.0

Firstly, the transmission coefficient τ_θ is investigated, which indicates how much power is transmitted to the receiver beam. Figure 4 shows the transmission coefficient τ_θ of the baseline model where it can be clearly seen that τ_θ is a function of the incident angle of the wave as well as the frequency. It is interesting to note that the maximum power transmission occurs at a lower incident angle (closer to normal) with increasing frequency, which can also be confirmed in Figure 5.

Note that the coupled beam wavenumber k_x is calculated from $k_x = k_p \sin\theta$. Hence k_x is smaller than k_p, and reduces as θ reduces. The results shown in Figure 4 correspond to the same phenomenon explained previously [1] in the relationship between the coupled beam wavenumber k_x and the free plate wavenumber k_p, because the equivalent mass (m_p''/k_p) of the plate impedance is reduced with increasing frequency (see Figure 14 in section 3.5).

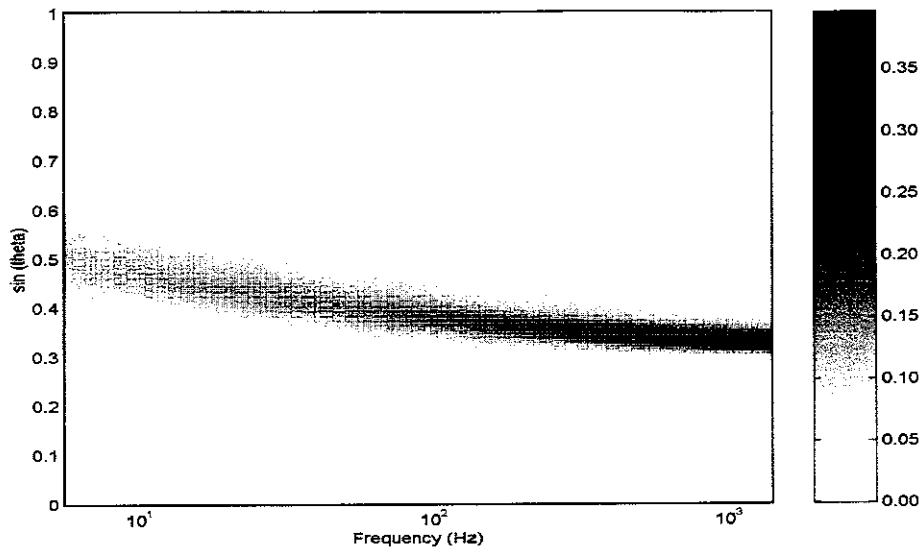

Figure 4. Transmission coefficient τ_θ of the baseline model ($\eta_p = 0.0$, $\eta_b = 0.03$) as a function of angle of incidence and frequency. A darker value corresponds to a larger transmission coefficient.

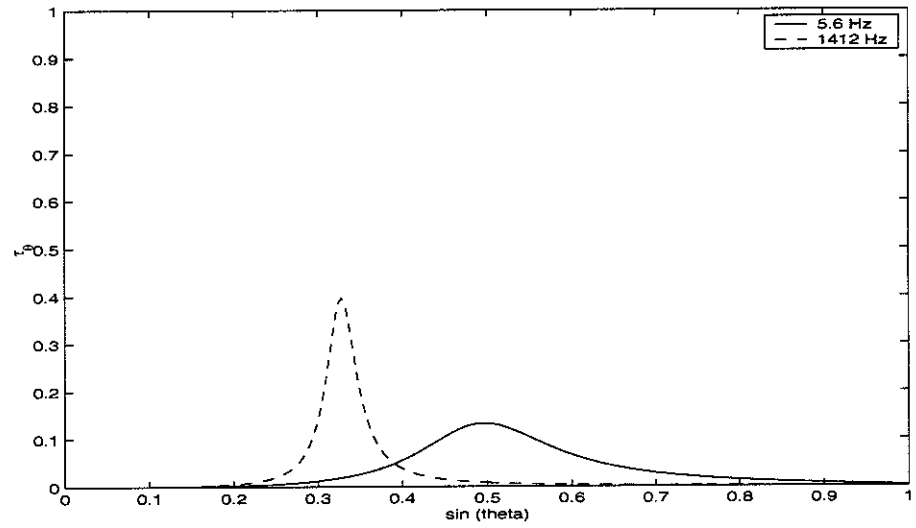

Figure 5. Transmission coefficient τ_θ of the baseline model at different frequencies ($\eta_p = 0.0, \eta_b = 0.03$) as a function of incident angle θ.

The corresponding diffuse field transmission coefficient $\tau_{21,d}$ is shown in Figure 6. Less total power is transmitted to the receiver beam with increasing frequency, which indicates the coupling becomes weaker as frequency increases.

Also the equivalent transmission coefficient $\tau_{21,e}$ introduced in the previous section is shown in Figure 6 and the corresponding correction factors $(2-\tau_{21,d})/2$ and $(2-\tau_{21,e})/2$ are given in Figure 7 to compare their difference. It can be seen that the difference between them is negligible as mentioned (maximum difference of 0.4%).

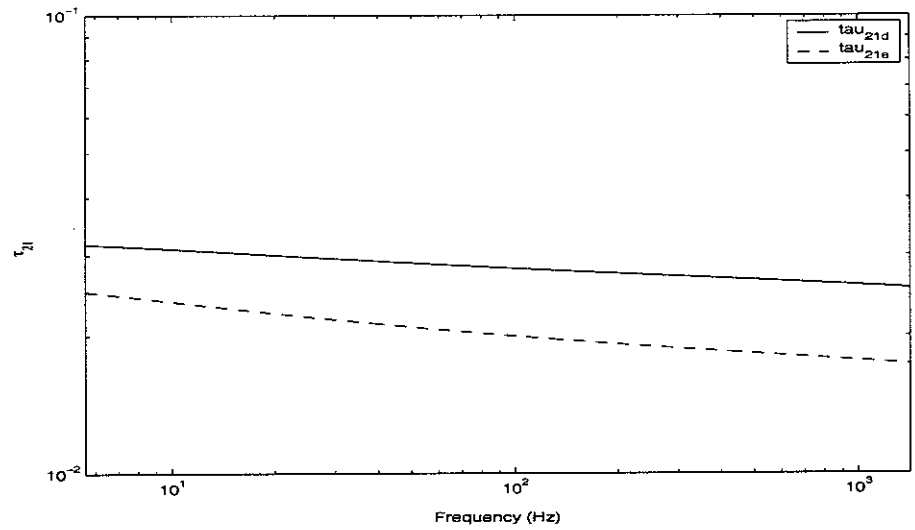

Figure 6. The diffuse field transmission coefficient $\tau_{21,d}$ and the equivalent transmission coefficient $\tau_{21,e}$ of the baseline model ($\eta_p = 0.0$, $\eta_b = 0.03$).

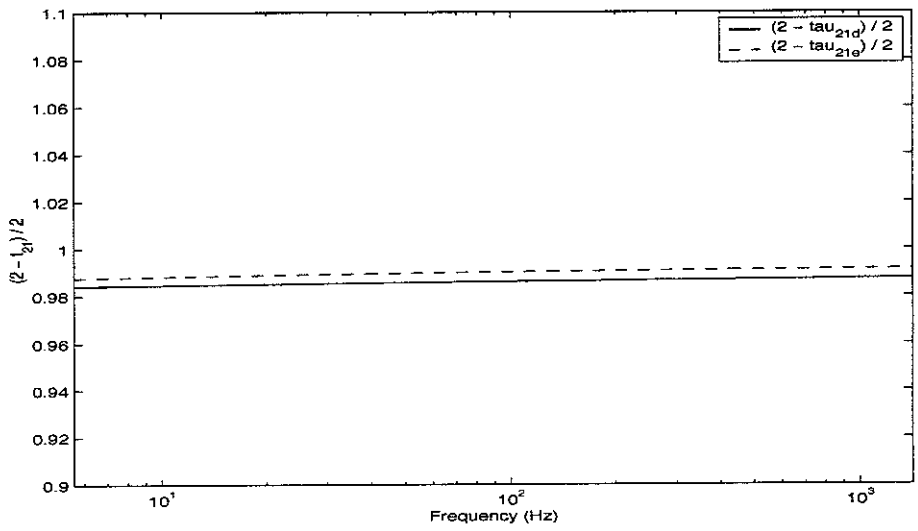

Figure 7. Comparison of correction factors $(2-\tau_{21,d})/2$ and $(2-\tau_{21,e})/2$ of the baseline model ($\eta_p = 0.0$, $\eta_b = 0.03$).

3.3.2 Effect of different beam heights and thicknesses

Next the effect of changing the height and thickness of the beam is considered. These investigations will effectively be used in comparing with the results in following sections, so that different kinds of coupling situations can be examined. The other dimensions are as used previously. One would expect that the CLFs decrease as the height of the beam increases, which corresponds to weaker coupling with increasing height.

In Figure 8, the power transmission coefficient τ_θ is shown as a function of the incident angle and frequency for a beam height of 360 mm. Comparing this with Figure 4, as beam height increases, it seems that the incident angle for the maximum power transmission has much less dependence on frequency. This phenomenon can be explained from examination of equations (3.24) and (3.26). Note that the only frequency-related term in equation (3.26) is the equivalent mass ratio μ. If the beam height increases the ratio of the free wavenumber of the beam to the plate ξ decreases and therefore, the term including μ, $2i\mu\xi^4\sqrt{1+s^2}\,c$ becomes small so that the influence of the frequency is reduced. As the term related to μ has a small value, if $s^4(1+i\eta_b)-\xi^4$ becomes greater one can expect that $\rho_\theta \to 1$. Meanwhile, the maximum power transmission occurs when $\sin\theta$ becomes close to ξ. In such cases, accordingly, the term related to μ becomes important as $s^4(1+i\eta_b)-\xi^4$ has a small value as well.

In fact, as the beam height increases so that the beam wavenumber is much smaller than that of the plate, the incident angle of the maximum power transmission, in other words the minimum power reflection, is closer to zero. This means that the power transmission is maximum when the incident wave propagating into the beam is at a normal angle to the beam axis ($s^4 \to 0$), when the beam wavenumber is much smaller than that of the plate ($\xi^4 \to 0$). A very similar phenomenon occurs for an incident wave on the beam with $k_b \ll k_p$, when the transmitted propagating wave radiates into the plate at an angle which is almost normal to the axis of the beam [26].

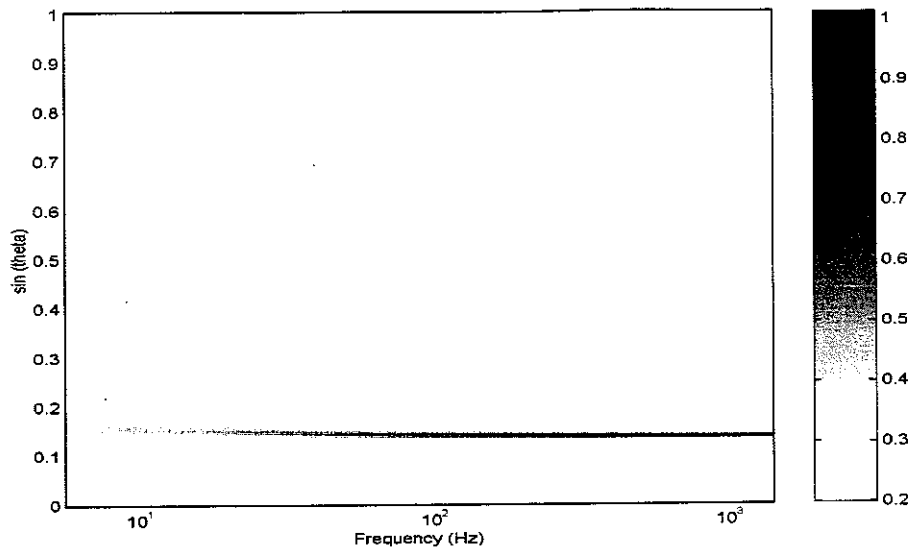

Figure 8. Transmission coefficient τ_θ for a beam height of 360 mm ($t_b = 5.9\,\text{mm}$, $\eta_p = 0.0$, $\eta_b = 0.03$)

It is interesting to compare the transmission coefficients τ_θ with different heights of the beam (Figures 4 and 8). The maximum transmission coefficient τ_θ is found to be greater when the beam height increases. This is because the transmission coefficient τ_θ of the baseline model is present over a wider range of the incident angle. Note that as the height of the beam increases, the power tends to be transmitted only over a particular narrow range of angle as shown in Figure 8. In fact therefore, the diffuse field transmission coefficient $\tau_{21,d}$ decreases with increasing beam height. The same phenomenon occurs similarly when the thickness of the beam increases.

The power transmission coefficient τ_θ is shown in Figure 9 for the 400 mm thickness case. It seems that the incident angle of the maximum power transmission becomes independent of frequency as the thickness increases. This can similarly be explained as in 360 mm height case. In this case, the phenomenon is mainly related to the mass ratio $\mu = m_p''/m_b' k_p$. As seen in equation (3.26), it is clear that the mass ratio μ decreases as the thickness of the beam increases and the term including μ becomes smaller, so that the influence of the frequency on τ_θ is less important. Note however, that this term is again important when $s^4(1+i\eta_b)-\xi^4$ has also a small value. Meanwhile, if the mass ratio increases,

then the effect of $2i\mu\xi^4\sqrt{1+s^2}\,c$ also increases, and accordingly equation (3.26) becomes dependent on the frequency as seen in Figure 4.

As explained before, the incident angle for maximum transmission depends on the height of the beam and reduces to zero as the height becomes very large. In this case, $\sin\theta$ decreases down to approximately 0.3 at the minimum. This can also be inferred from equation (3.26). The maximum power transmission occurs when $\sin\theta \approx \xi = k_b/k_p$, which can be confirmed from $\xi = 0.306$ ($h = 68\,mm$) as seen in Figure 9. Therefore, the maximum power transmission occurs for the particular material and geometry when the incident angle becomes about 18° and decreases with increasing height.

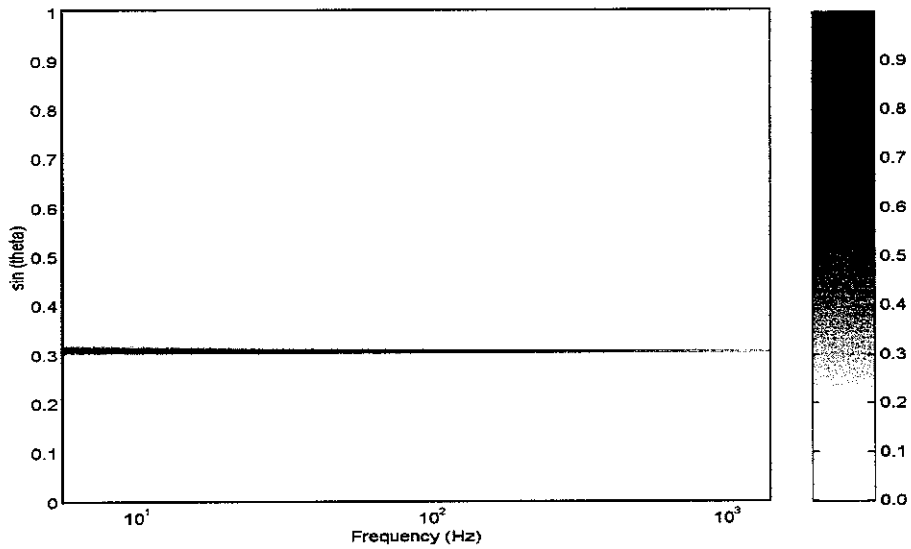

Figure 9. Transmission coefficient τ_θ for a beam thickness of 400 mm ($h = 68\,\text{mm}$, $\eta_p = 0.0$, $\eta_b = 0.03$)

3.3.3 CLF estimates and effect of the beam damping

Based on the diffuse field assumption the CLF lower bound (equation (3.46)) was obtained and the estimate for η_{21} (equation (3.49)) was derived using the consistency relationship in section 3.2. The corresponding numerical results are shown here.

As explained in section 3.1, the net power transfer to the beam is dependent on the beam damping. Therefore, firstly the CLF lower bounds are presented in Figure 10 in order to compare the effect of the beam damping (see equation (3.46)).

It can be seen that the CLF lower bounds increase with increasing DLFs of the beam, which means more energy is dissipated in the beam and correspondingly more power is transferred to the beam. This relationship can be confirmed as the CLF lower bound is

obtained from equation (3.35) with the assumption $\eta_{12}\omega E_1 \ll \eta_{21}\omega E_2$, so $P_{21} \approx \omega\eta_{21}E_2$ whilst $P_{21} = \omega\eta_1 E_1$.

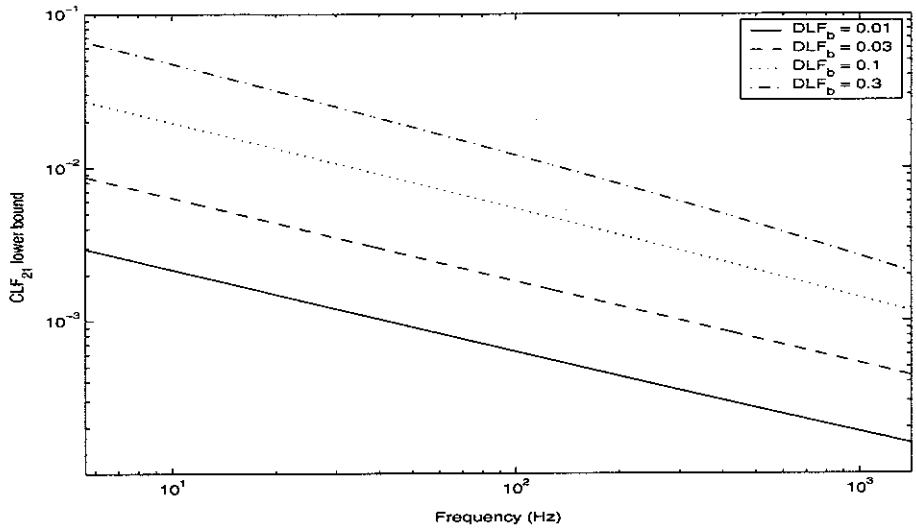

Figure 10. Comparison of CLF lower bounds with different DLFs of the beam for the baseline model.

In addition to the CLF lower bound, the CLF based on the consistency relationship is found (see equation (3.49)). The corresponding results are shown in Figure 11, also for different DLF values for the beam. The effect of the beam damping is similar to that on the CLF lower bound shown in Figure 10.

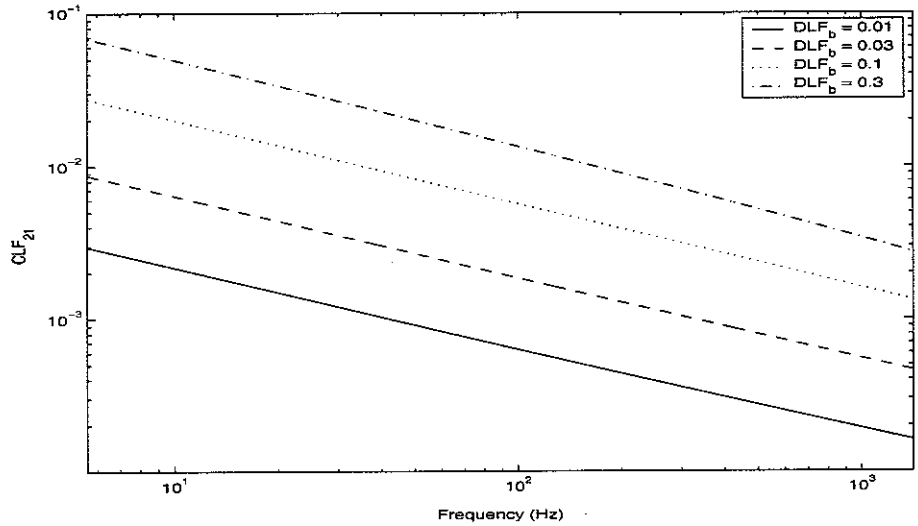

Figure 11. Comparison of η_{21} based on the consistency assumption and using the predicted η_{12} with different DLFs of the beam of the baseline model.

The difference between the CLF lower bound and the estimate for η_{21} based on the consistency relationship is shown in Figure 12 for two different values of beam damping. As seen in the figures, the difference is small (maximum difference of 4.8 and 23.3 %

respectively). Although the difference is small for both cases, it increases with increasing damping of the beam. This means that the effect of the term related to the power transmitted from the beam back to the plate ($\eta_{12}\omega E_1$) also increases with increasing beam damping (see equation (3.35)).

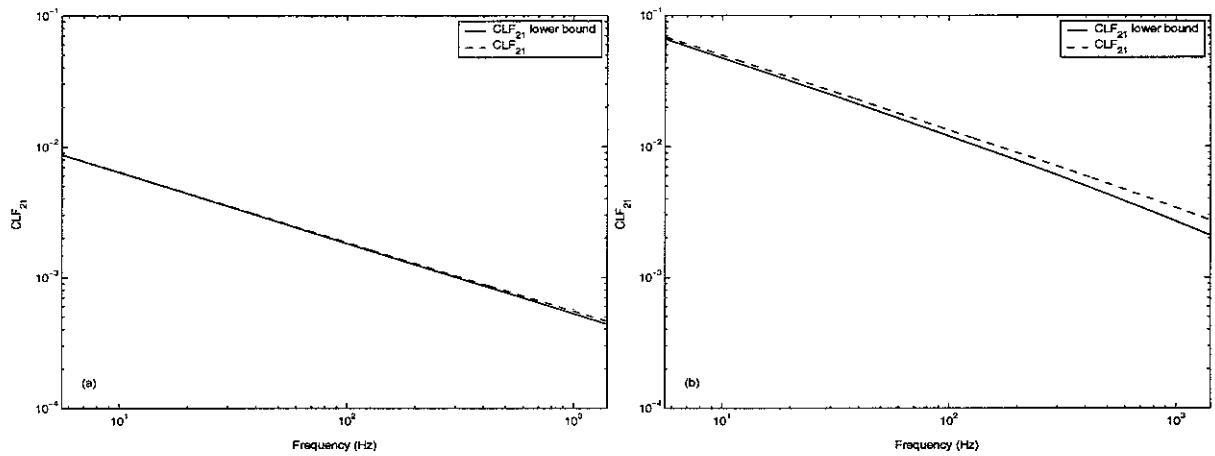

Figure 12. Comparison of CLF lower bounds and η_{21} based on the consistency assumption; (a) $\eta_b = 0.03$ (b) $\eta_b = 0.3$.

As the difference between the CLF lower bound and the CLF based on the consistency relationship is small and it is known that the consistency relationship only holds when the coupling power proportionality (CPP) is exact, as explained in section 2.3, in the following sections only the CLF lower bounds are compared with the effective CLFs $\hat{\eta}_{21}$.

3.4 Equivalent loss factor and CLF

In an earlier study [1], the structural behaviour of the beam-plate coupled system was investigated by the wave method. In this section some physically important characteristics of the wave method are reviewed and the relationship with the effective CLFs is presented.

Consider the coupled structure consisting of an infinite beam and a semi-infinite plate shown in Figure 13 where the edge of the plate along the joint is assumed to be sliding.

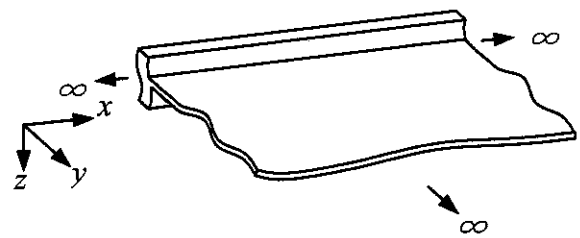

Figure 13. A built-up structure consisting of an infinite beam attached to a semi-infinite width plate.

The general dispersion relationship for a 'free' wave in the beam of this structure is given by [1]

$$D_b \tilde{k}_x^4 = m_b' \omega^2 - i\omega \tilde{Z}_p' \tag{3.52}$$

where D_b is the bending stiffness, $\tilde{k}_x$ is the coupled wavenumber, m_b' is the mass per unit length of the beam, ω is frequency and $\tilde{Z}_p'$ is the plate impedance per unit length along the beam. For the semi-infinite plate, if the plate free wavenumber k_p is much smaller than k_x, then the line impedance of the plate can be approximated as

$$\tilde{Z}_p' \approx \frac{D_p k_p^3}{\omega}(1+i) = \frac{m_p'' \omega}{k_p}(1+i) \tag{3.53}$$

where $\tilde{D}_p$ is the bending stiffness, and m_p'' is the mass per unit area of the plate. The real part of the impedance acts as a damping effect and the imaginary part is mass-like. For the finite plate of the width $y = L_y$, using the same assumption ($k_p >> k_x$), the approximate impedance is given by [1]

$$\tilde{Z}_p' \approx \frac{D_p 2k_p^3}{\omega}\left(\frac{1-\beta_y \tilde{r}}{(1+\beta_y \tilde{r}) - i(1-\beta_y \tilde{r})}\right) \tag{3.54}$$

where $\beta_y = e^{-ik_y 2L_y}$ represents a phase shift over length $2L_y$, $\tilde{r}$ is the complex reflection coefficient at the edge of the plate $y = L_y$. Combining equations (3.52) and (3.53) for the semi-infinite plate and equations (3.52) and (3.54) for the finite plate, the corresponding wavenumber relationship can be identified. The wavenumbers obtained for the semi-infinite plate case and the finite plate case are shown in Figure 14 and Figure 15 respectively. The material properties for this figure are the same as presented in Table 1 except that the DLFs η_b and η_p are changed, to 0.0 and 0.01 respectively. It can be seen that the slope of the coupled wavenumber k_x is lower than that of uncoupled wavenumber k_b as the mass effect in the impedance reduces with increasing frequency due to increasing k_p.

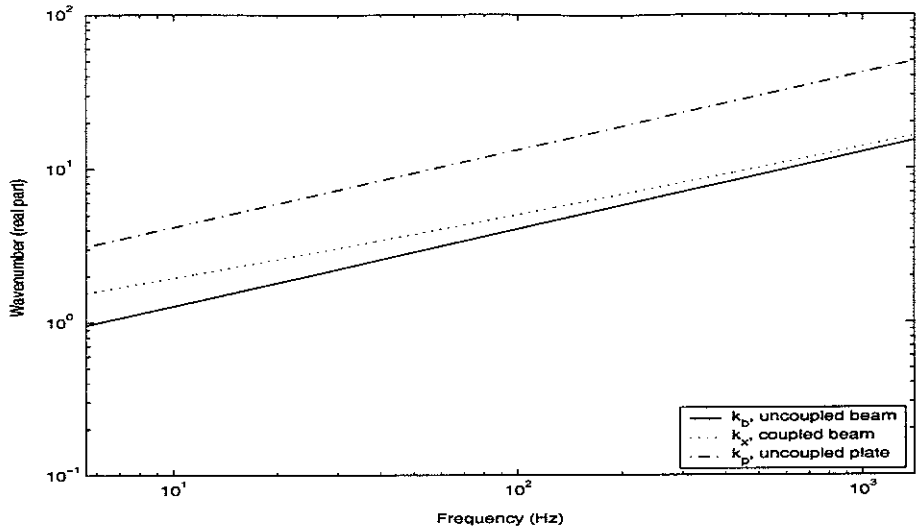

Figure 14. Wavenumber comparison of the coupled structure consisting of an infinite beam and a semi-infinite plate as in Figure 13 ($\eta_b = 0.0$, $\eta_p = 0.01$).

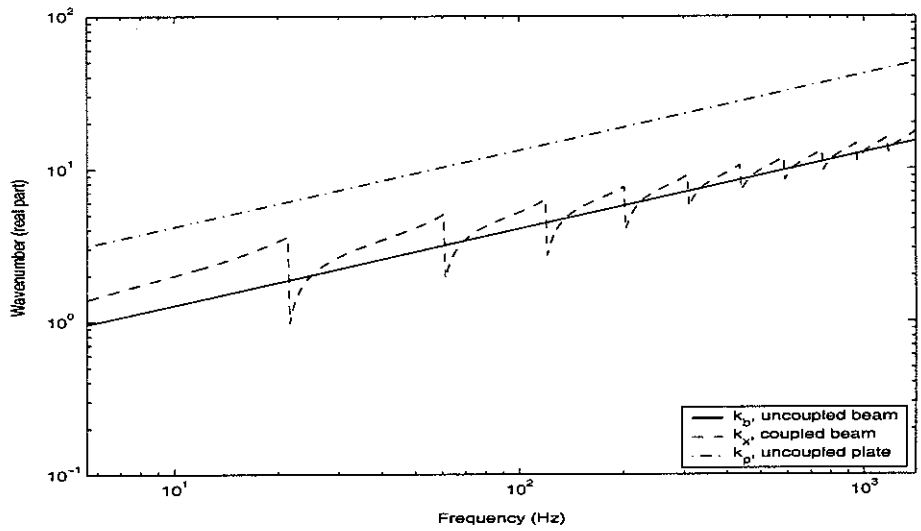

Figure 15. Wavenumber comparison of the coupled structure consisting of an infinite beam and a finite plate ($\eta_b = 0.0$, $\eta_p = 0.01$).

Note that the damping effect of the impedance results in the wavenumber $\tilde{k}_x$ in equation (3.52) being complex. This means that some energy in the beam is absorbed by the coupled plate and the beam behaves as a damped structure. Therefore, if the DLF of the beam itself is assumed to be zero, an equivalent loss factor due to the plate can be defined. For an infinite beam coupled to the plate, the equivalent loss factor (ELF) is represented by

$$\eta_e = \frac{\mathrm{Im}\left(\tilde{k}_x^{-4}\right)}{\mathrm{Re}\left(\tilde{k}_x^{-4}\right)} \tag{3.50}$$

where $\tilde{k}_x$ is the complex travelling wavenumber of the coupled beam.

It should be noted that the ELF only arises because the plate impedance acts to damp the beam [26], the DLF of the beam being assumed to be zero. Therefore, this only accounts for the net power flow from the beam to the plate. This differs from that when determining the effective CLFs, where power flows from the plate to the beam as well as from the beam to the plate, these being described separately by $\hat{\eta}_{12}$ and $\hat{\eta}_{21}$. Therefore, the net power flow related to η_e is necessarily less than that associated with η_{12}. The relationship between the ELF and the CLF can be explained by rewriting equation (2.7) as follows.

$$\eta_{12} = \frac{P_{12}^{(1)} + \omega\eta_{21}E_2^{(1)}}{\omega E_1^{(1)}} = \frac{P_{12}^{(1)}}{\omega E_1^{(1)}} + \frac{\eta_{21}E_2^{(1)}}{E_1^{(1)}}. \tag{3.51}$$

The first term on the right hand side of the equation accounts for the net power from the beam to the plate (corresponding to η_e) and therefore, one can expect $\eta_e < \hat{\eta}_{12}$ as the second term is positive and added. Physically, if a coupled structure has weak coupling, then the influence of the energy of the plate (related to the second term in equation (3.51)) is small so it can be neglected compared with the first term, and $\hat{\eta}_{12}$ becomes closer to η_e. Therefore it seems worth comparing the effective CLF and the ELF. One can see that the difference increases as the strength of coupling increases.

4. COUPLING LOSS FACTOR OF A FINITE BEAM-PLATE COUPLED STRUCTURE

4.1 Baseline model

The power balance relationship for the beam-plate coupled structure shown in Figure 3 has been studied in [2] using a Fourier technique, in which an external point force was applied at the end of the beam.

In this section, the same procedure based on the Fourier technique is used to evaluate energies and hence the CLF η_{12} for a coupled structure as in Figure 3 if the beam is regarded as the source structure. Note that although the dynamic characteristics of the effective CLF $\hat{\eta}_{12}$ are explained here, in fact in order to obtain the effective CLFs $\hat{\eta}_{12}$ and $\hat{\eta}_{21}$, it is necessary to consider both the beam-excited and the plate-excited cases simultaneously as seen in equation (2.9), and also assuming $\hat{\eta}_{ij}^{(1)} = \hat{\eta}_{ij}^{(2)}$.

In the previous analysis [2], 400 components ($n = 400$) of the Fourier series were used, which can be regarded as exact results. The number of components in the Fourier series may be changed to reduce the calculation time. For example, for the case of the beam length $L_x = 3.0\,\mathrm{m}$, 40 components are considered. The maximum difference in the narrow band results such as the energy and power, is less than 0.25%, compared with the results including 400 components for frequencies up to 1413 Hz.

The ends of the beam are assumed to be sliding and the plate is also assumed to be sliding along the edges $x = 0$, $x = L_x$ and along the coupling junction $y = 0$, while the opposite edge to the junction, $y = L_y$ is assumed to be pinned. All physical properties and the dimensions are the same as presented in section 3.4.1 except that the DLFs η_p are changed to 0.01 ($\eta_b = 0.03$).

SEA was originally formulated for random forcing, so-called 'rain-on-the-roof' forcing, and the response of the system to the rain-on-the-roof forcing is taken to be the equivalent to the average response to the point forcing over all possible excitation locations [8]. In the present study, 20 excitation points are chosen randomly on both the beam and the plate and each is used to obtain total energy of the subsystem, total power input and dissipated. The energy corresponding to each subsystem is obtained from the maximum strain energy [2].

Frequency bands such as 1/3 octave or octave bands can be chosen for estimating the CLF, and in the present report the octave band is used. This is used because it is necessary to include a sufficient number of modes, especially for the beam which is much stiffer than the plate. Also, for obtaining enough information concerning coupling, an overlapping band

technique is used, so that the data can be presented with a resolution of 1/3 octave bands. The natural frequencies of the uncoupled beam are shown in Table 2 and the number of modes of the uncoupled plate in the octave bands is presented in Table 3. The actual modes of the coupled system will differ a little from these.

Table 2. Natural frequencies of uncoupled beam ($L_x = 3.0$ m, $t_b = 5.9$ mm) in the frequency of interest 5.6 – 1413 Hz.

Mode Number	1	2	3	4	5	6	7
Natural frequency (Hz)	6.7	26.9	60.1	107.2	167.4	240.9	327.9
Mode Number	8	9	10	11	12	13	14
Natural frequency (Hz)	428.5	542.6	669.5	810.2	963.9	1131.1	1312.7

Table 3. The number of modes in each octave frequency band for the beam and the plate ($L_x = 3.0$ m, $L_y = 0.75$ m).

f_{lwr}	f_{ctr}	f_{upr}	Number of modes		f_{lwr}	f_{ctr}	f_{upr}	Number of modes	
			Beam	Plate				Beam	Plate
5.62	7.94	11.2	1	1	70.8	100	141	1	23
7.08	10	14.1	0	2	89.1	125	178	2	27
8.92	12.5	17.8	0	1	112	160	224	1	38
11.2	15.8	22.4	0	2	141	200	282	2	44
14.1	20	28.2	1	4	178	250	355	2	59
17.8	25	35.5	1	8	224	316	447	3	74
22.4	32	44.7	1	8	282	400	562	3	87
28.2	40	56.2	0	8	355	500	708	3	108
35.5	50	70.8	1	11	447	630	891	3	137
44.7	63	89.1	1	15	562	794	1122	3	180
56.2	80	112	2	17	708	1000	1413	4	225

4.2 Effective CLF, $\hat{\eta}_{12}$ (beam to plate)

4.2.1 Relationship between energy and CLF

The CLF is the constant of proportionality between the power flow and the difference between modal energies of subsystems. Accordingly, the CLF is related to the characteristics of each subsystem energy of the coupled structure. The energy of each subsystem averaged over 20 excitation positions on the beam is shown in narrow bands in Figure 16 and the corresponding energy averaged in overlapping octave bands is shown in Figure 17. It can be seen that the peaks of the octave band results such as 20 Hz correspond to those of the narrow band results. Also note that natural frequencies of the coupled beam are different from those of

the uncoupled beam. Thus, the peaks such as 10.6 and 36.1 Hz in the beam energy correspond to the coupled beam modes that are predominantly dependent on the beam behaviour.

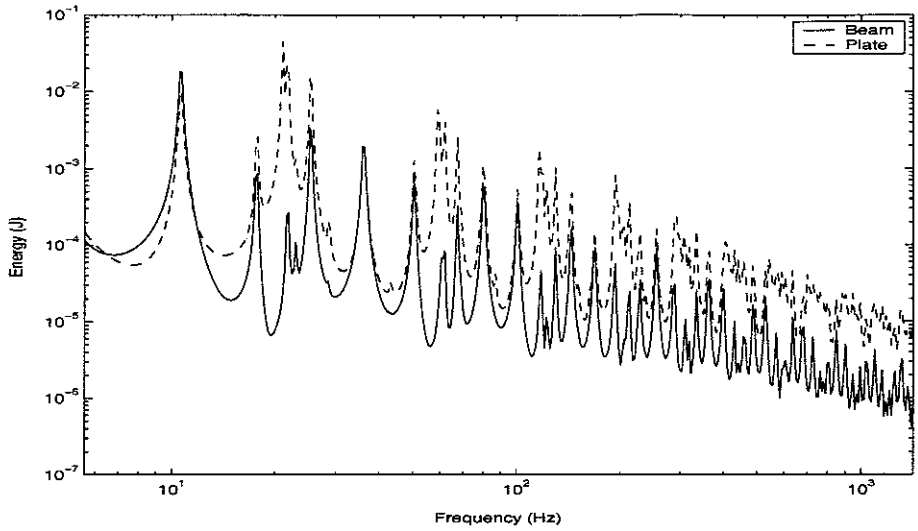

Figure 16. Total energy stored in each subsystem of the baseline model when the beam is excited ($L_x = 3.0$ m, $\eta_b = 0.03$, $\eta_p = 0.01$).

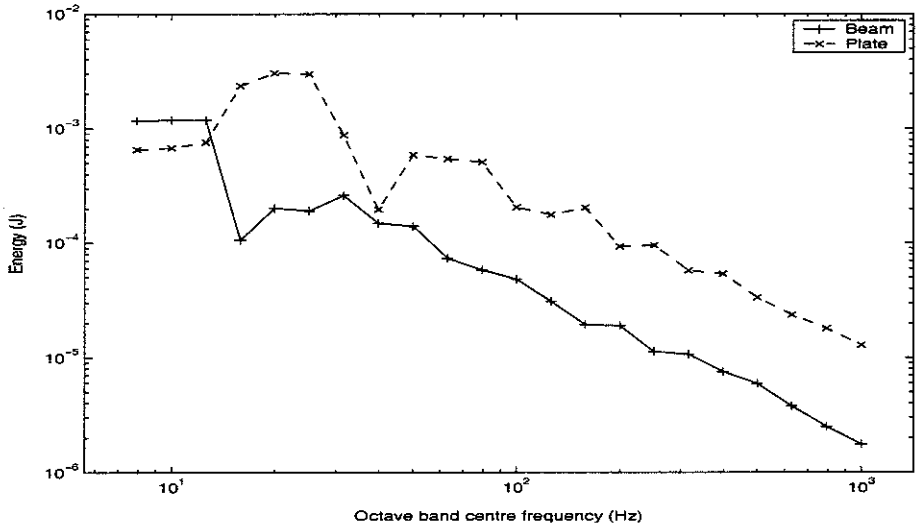

Figure 17. Total energy stored in each subsystem of the baseline model when the beam is excited ($L_x = 3.0$ m, $\eta_b = 0.03$, $\eta_p = 0.01$).

The ratio of the energy of the plate to the energy of the beam is shown in Figure 18. This energy ratio can be compared with the effective CLF $\hat{\eta}_{12}$ calculated using equation (2.9) which is shown in Figure 19. It is clear that the energy ratio shows similar trends to the effective CLF. The energy ratio is maximum when the beam has minimum energy, or when the plate has maximum energy when the resonant modes of the plate are excited by the power transferred from the beam.

Figure 19 shows that negative values of CLFs are found for frequency bands of 16, 20 and 25 Hz. This may be because there are not enough modes in the beam and correspondingly not enough energy in the beam as seen in Figure 17. In fact, there is no mode between 11 and 35 Hz for the present coupled beam and the coupled structure is dominated by the plate motion. For example, at 21 Hz, the dominant mode of the coupled structure is flexural mode of the plate where the wavelength is about $\lambda \approx 1.0$ m. Meanwhile the beam remains in rigid motion. The consequent subsystem energies that explain this can be found in Figure 16. Therefore, the small modal energy of the beam results in the negative value of the CLF. Note that SEA is based on the assumption of the modal energy relationship and it is generally recommended to have at least 5 modes in a band [9].

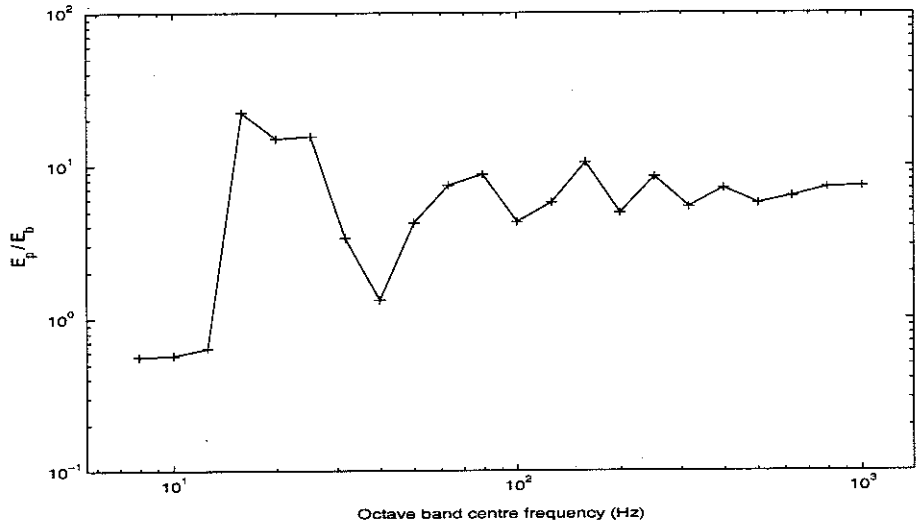

Figure 18. Ratio of the energy of the plate to the energy of the beam of the baseline model ($L_x = 3.0$ m, $\eta_b = 0.03$, $\eta_p = 0.01$).

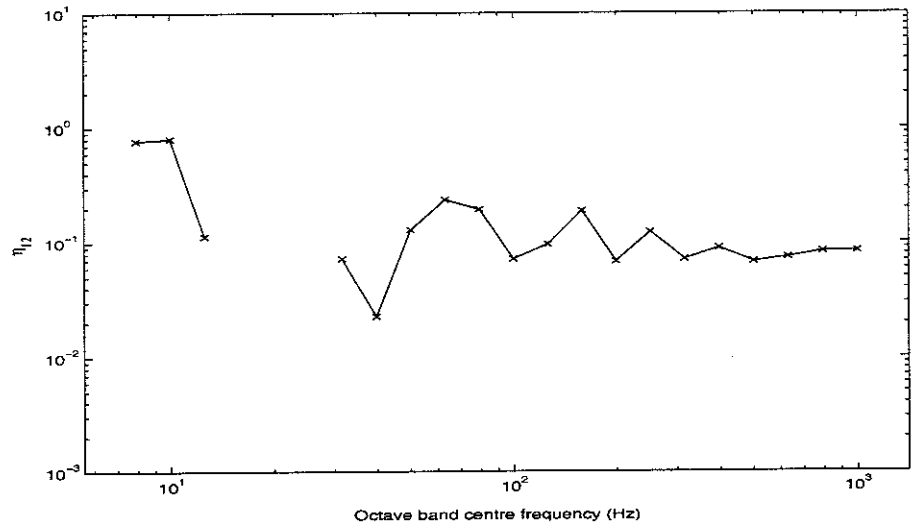

Figure 19. The effective CLFs $\hat{\eta}_{12}$ in overlapping octave bands for the baseline model as in Figure 3 ($L_x = 3.0$ m, $\eta_b = 0.03$, $\eta_p = 0.01$).

It is of interest to note that the energy level of the plate is generally higher than that of the beam. One of the general hypotheses of SEA is that 'weak coupling' is present. Although weak coupling is not defined quantitatively, it can generally be said that if the subsystems are weakly coupled then the energy of the excited subsystem (or source subsystem) is greater than that of a receiver subsystem [27]. From this point of view, it can be said that the baseline structure is strongly coupled. If the Smith criterion is used, where the coupling is considered weak when the CLF η_{12} is smaller than the DLF of the source subsystem η_1, that is $\eta_{12} < \eta_1$ [28], then the baseline model seems clearly to be in a strong coupling regime, as seen in Figure 19. Note that the DLF of the beam (source structure) $\eta_b (= \eta_1)$ is 0.03 and the effective CLF $\hat{\eta}_{12}$ is about 0.1.

The numerical analysis for the equivalent loss factor (ELF) explained in section 3.5 is carried out to compare with the effective CLF $\hat{\eta}_{12}$. In Figure 20, the effective CLF of the baseline model and the ELFs calculated using the wave method are compared. The ELFs are calculated for a situation in which the plate width is 0.75 m, which is the same as that of the baseline model, and when the plate is regarded as being semi-infinite in width.

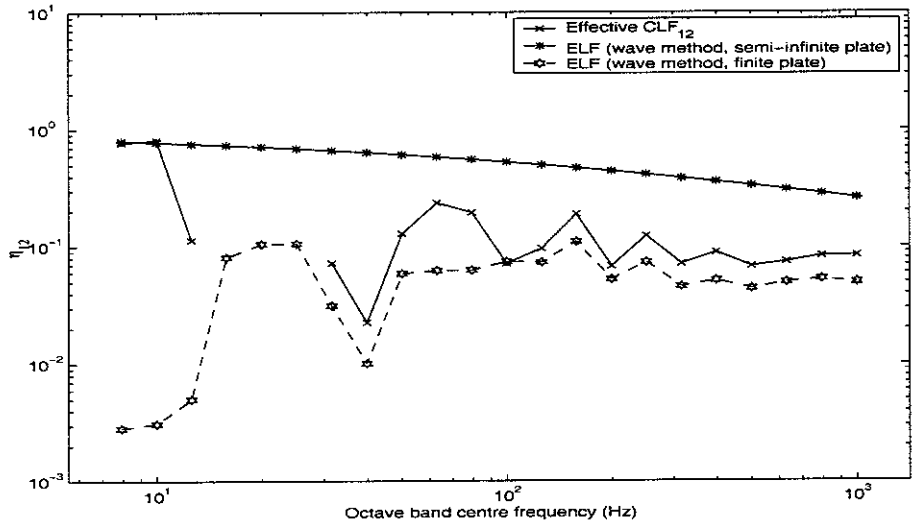

Figure 20. Comparison of the effective CLF $\hat{\eta}_{12}$ and ELF η_e of the baseline model ($\eta_b = 0.03$, $\eta_p = 0.01$ for the effective CLF and $\eta_b = 0.0$, $\eta_p = 0.01$ for the ELF η_e).

Comparing the effective CLF of the finite system and the ELF of the finite width plate case, it can be seen that the effective CLF is greater than the ELF ($\eta_{12} > \eta_e$) as explained

above. This can be confirmed if only the energy of the beam (E_1) is considered in equation (3.51), that is writing $\eta_{12} = P_{12}/(\omega E_1)$. This gives an equivalent loss factor for the beam accounting for the net power flow, which is comparable to the infinite beam wave result (3.50). The result is shown in Figure 21. In that case, it can be seen that the power ratio $P_{12}/(\omega E_1)$ (instead of the effective CLF) becomes much closer to the ELF, as expected. For the same reason, the ELF for the semi-infinite plate is larger than for the finite plate case.

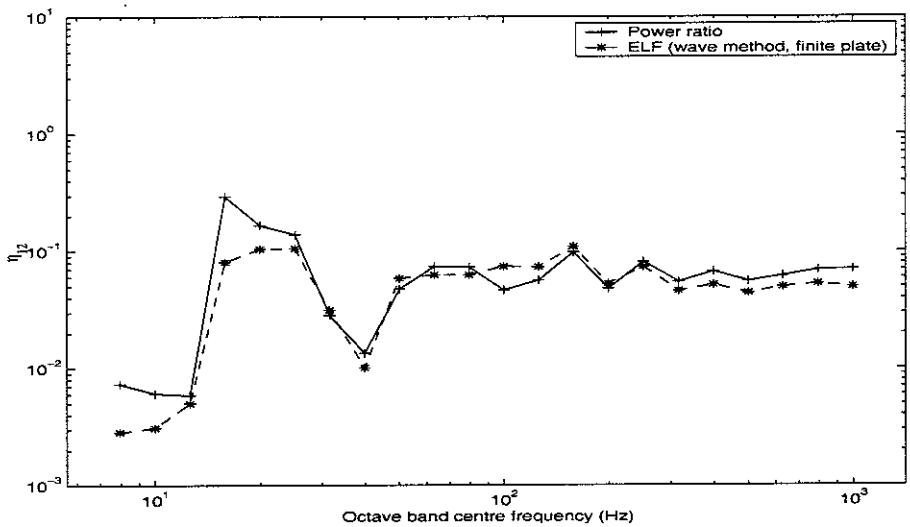

Figure 21. Comparison of the ELF η_e and the power ratio ($P_{12}/(\omega E_1)$) when only the power from the beam to the plate is considered (baseline model. $\eta_b = 0.03$, $\eta_p = 0.01$ for the power ratio and $\eta_b = 0.0$, $\eta_p = 0.01$ for the ELF η_e).

4.2.2 CLFs for different dimensions

As explained in section 4.2.1, the effective CLF $\hat{\eta}_{12}$ shows negative values at low frequencies, which is related to the number of modes of the beam. To eliminate these, the frequency band can be enlarged or the dimensions of the structure can be reconsidered so that enough number of modes can be included. The enlargement of the frequency band can cause loss of information. Thus, the dimensions of the structure were reconsidered. Initially the length of the beam L_x was changed. Figure 22 shows the results for different beam lengths. It can be seen that the effective CLFs are in close agreement for different lengths of the beam, especially at high frequencies. The modes of the beam therefore have little effect on this CLF.

Although the results show that the effective CLFs near 20 Hz still have negative values, even for a 5.0 m beam case, it can be seen that the result of the 3.0 m or 4.0 m beam

case is closer to that of the 5.0 m case than that of the 2.0 m beam. Therefore, it seems that a 3.0 m beam is suitable as the baseline model, as a beam of 4.0 m or greater requires much more calculation time.

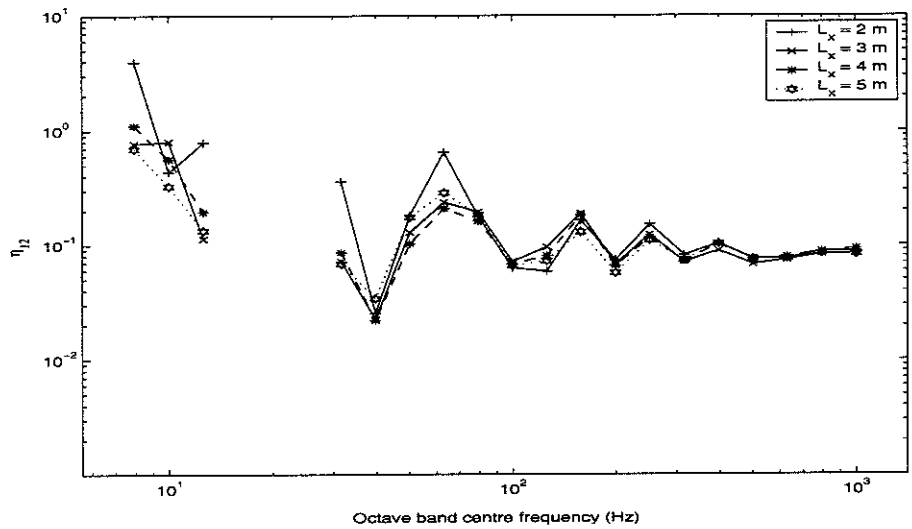

Figure 22. The effective CLFs $\hat{\eta}_{12}$ for the baseline model as in Figure 3. The length of the beam L_x is changed from 2.0 m to 5.0 m ($L_y = 0.75$ m, $\eta_b = 0.03$, $\eta_p = 0.01$).

In addition to the length of the plate, it seems appropriate to investigate the influence of the plate width L_y. Fixing the length of the beam $L_x = 3.0$ m, various widths of the plate are considered to investigate the effective CLF and the results are shown in Figure 23.

With increasing width, it can be seen that the peaks and dips tend to disappear. At this stage, it should again be noted that the behaviour of the plate is strip-like [26] where the beam carries long wavelength waves and the plate carries short wavelength waves. Therefore the dynamic characteristics of the plate can be represented by strip-like behaviour, which is not influenced by the position x along the beam but is influenced by the width. Therefore, with increasing width, it can be said that the number of resonances increases as well, which means that the CLFs are less dominated by one or a few plate strip-like resonance frequencies, and peaks and dips of the CLFs tend to disappear.

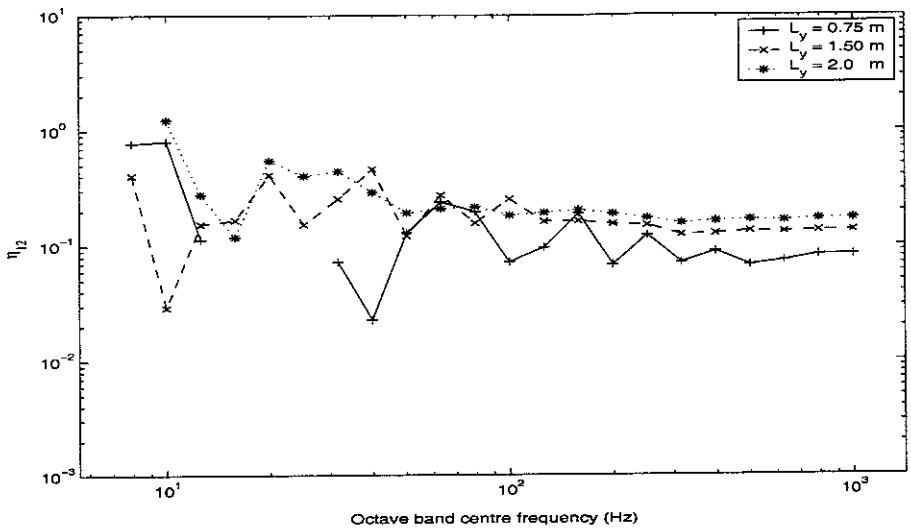

Figure 23. The effective CLFs $\hat{\eta}_{12}$ for the baseline model as in Figure 3. The width of the plate L_y is changed from 0.75 m to 2.0 m ($L_x = 3.0$ m, $\eta_b = 0.03$, $\eta_p = 0.01$).

For the case when the width is short such as $L_y = 0.75$ m, the fluctuation of the CLFs is greater, and it can be seen that the corresponding frequencies are related to the widths of the plate. Also note that the CLFs are related to the stored energy of the subsystems. As explained in section 4.2.1, the effective CLF increases when the energy of the plate increases, which corresponds to octave band centre frequencies of 63, 160, 250 and 400 Hz in the case $L_y = 0.75$ m in Figure 23. One can expect that in these frequency bands the displacement of the plate increases so that the energy of the plate is maximum. As the plate behaviour is like a beam, if the width of the plate increases by a factor of 2 ($L_y = 1.5$ m), then the corresponding wavenumber of the plate for a given mode should decrease by half compared with $L_y = 0.75$ m. Then as $\omega^2 = k_p^4 D_p / m_p''$, the corresponding resonance frequencies are a factor of $1/2^2$ for the plate of double the width. An example of this is shown in Figure 24 for the forced response at 395.7 Hz, in which the plate displacements are presented when a unit magnitude point force is applied at the end of the beam, $x = 0$. Figure 24 (a) shows the real part of the displacement for the plate width $L_y = 0.75$ m and (b) shows that for double the width, i.e. case $L_y = 1.5$ m. They show the same shape, but the frequency decreases by $1/4$ to 99.4 Hz for the latter case.

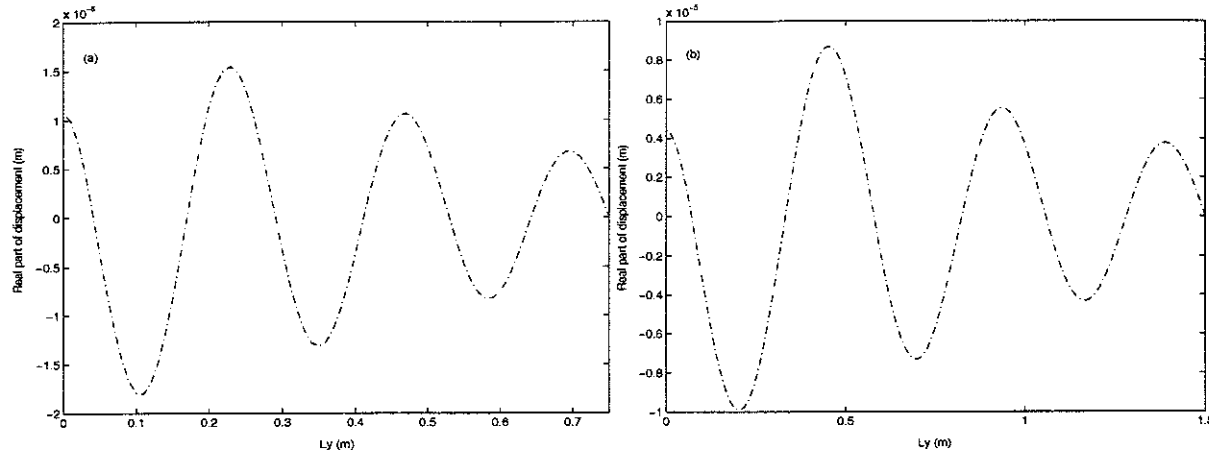

Figure 24. The displacement of the plate along the width y of the baseline model as in Figure 3. The width of the plate L_y is changed ($L_x = 3.0$ m , $\eta_b = 0.03$, $\eta_p = 0.01$, point force applied at $x = 0$ of the beam, response at $x = 0$); (a) 395.7 Hz, $L_y = 0.75$ m (b) 99.4 Hz, $L_y = 1.5$ m.

In the same manner, the frequencies of the peaks and dips in Figure 23 can again be explained. For example, the peaks in the CLFs for the case $L_y = 0.75$ m such as in the 63, 160 and 250Hz bands correspond to the same peaks in the 20, 40 and 63 Hz bands for the case $L_y = 2.0$ m.

4.2.3 Damping effect of subsystems

The effect of the damping of the receiver plate is investigated and presented in Figure 25 where the DLFs of the plate η_p are varied between 0.01 and 0.3. As the DLF of the plate increases, the effective CLF increases, because more energy is dissipated by the plate.

The effective CLFs are heavily influenced by the DLF because the structure is strongly coupled, as explained before. For a weakly coupled structure, it is expected that the CLF will be unaffected by the damping because the receiver system hardly affects the behaviour of the source subsystem. An example of this will be shown later.

Although the effective CLFs increase with increasing DLF, they converge as the plate becomes heavily damped. Comparing the effective CLFs with the ELF of the semi-infinite plate case, it can be seen that the ELF may be regarded approximately as an asymptotic result for high damping where the small difference may occur because the different values of the DLFs are used in the calculations of the ELF and the CLFs.

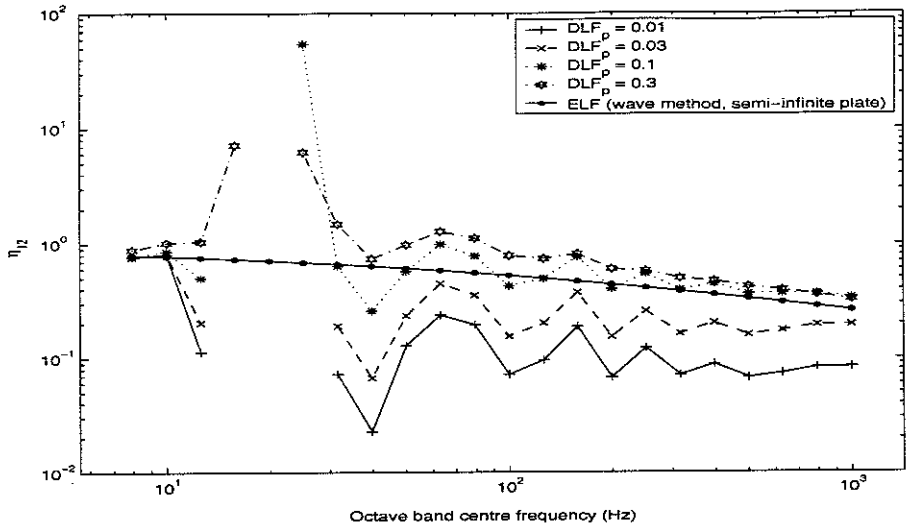

Figure 25. The effective CLFs $\hat{\eta}_{12}$ with different DLFs of the plate of the baseline model. $\eta_b = 0.0$ and $\eta_p = 0.01$ are used in wave method.

In addition, the effect of the DLF of the beam on the effective CLFs is shown in Figure 26. Again, the CLFs increase as the DLF of the beam is increased. In this case, in fact the power flow $P_{21}^{(2)}$ in equation (2.9) increases so that the effective CLF $\hat{\eta}_{12}$ increases.

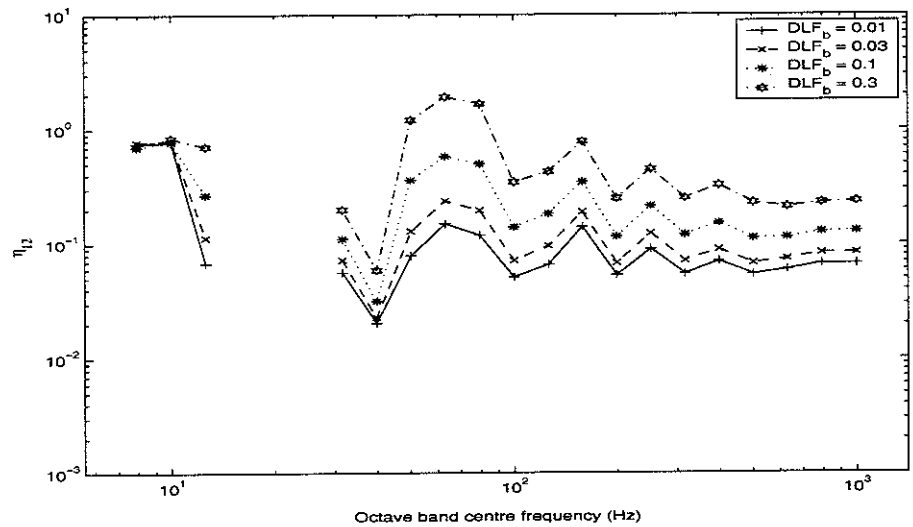

Figure 26. The effective CLFs $\hat{\eta}_{12}$ with different DLFs of the beam of the baseline model.

4.3 Effective CLF, $\hat{\eta}_{21}$ (plate to beam)

Similar to section 4.2, the effective CLFs $\hat{\eta}_{21}$ for the structure shown in Figure 3 are investigated based on the power balance relationship. Also, the CLFs based on the diffuse

field transmission coefficient are compared with these results in this section. The baseline structure is the same as presented in section 3 where the length of the beam is $L_x = 3.0$ m and the width of the plate is $L_y = 0.75$ m. The DLFs of the subsystem is $\eta_b = 0.03$ and $\eta_p = 0.01$. However the CLFs based on the transmission coefficient are obtained assuming that $\eta_b = 0.03$ and $\eta_p = 0.0$ where the influence of the difference in the DLF of the plate is expected to be negligible.

4.3.1 Baseline model

The effective CLF $\hat{\eta}_{21}$ of the baseline model is shown in Figure 27. It can be seen that the effective CLF $\hat{\eta}_{21}$ is smaller than $\eta_2 (= \eta_p = 0.01)$, especially above 100 Hz, which suggests that $\hat{\eta}_{21}$ represents a weakly coupled situation.

Also in the same figure the effective CLF $\hat{\eta}_{21}$ is compared with the low bound based on the diffuse field transmission coefficient. It can be seen that there is a significant difference between them. The diffuse field estimate is generally known to be accurate only for weak coupling for example in a plate coupled structure [6]. Although the present case can be considered to be weakly coupled based on Smith's criteria, it seems that the diffuse field bound is not appropriate to describe this coupling situation. However, it is expected that the difference reduces as the coupling becomes weaker, which will be shown later.

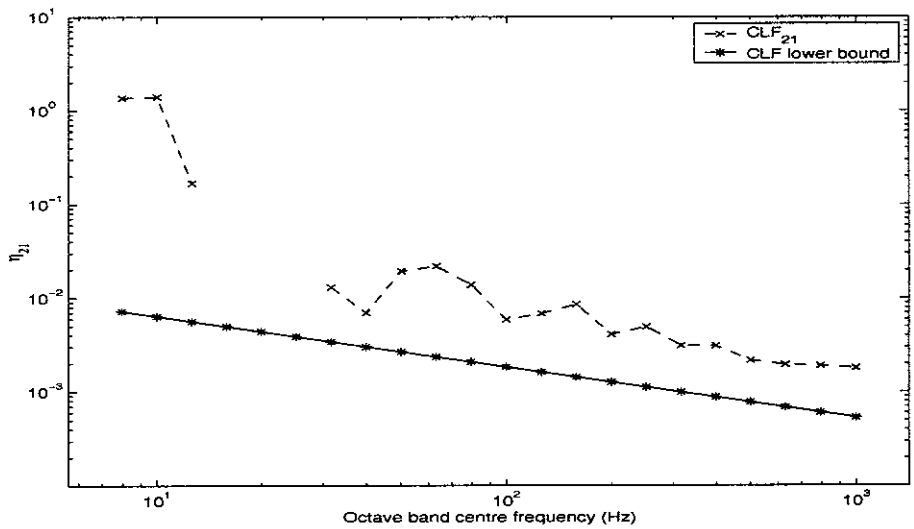

Figure 27. The effective CLFs $\hat{\eta}_{21}$ for the baseline model ($L_x = 3.0$ m, $\eta_b = 0.03$, $\eta_p = 0.01$).

4.3.2 Damping effect of subsystems

The DLF of the beam η_b is varied between 0.01 and 0.3 and the corresponding effective CLF are presented in Figure 28. The CLFs increase as the DLF increases. It can be said that more energy is transmitted to the beam as the DLF increases, which means the coupling of the structure becomes stronger as the DLF of the beam is increased. Comparing the effective CLFs with the CLF lower bound based on the diffuse field assumption, it can be seen that there is reasonably good agreement for $\eta_b = 0.3$. However as the damping is reduced, the effective CLF reduce only slightly whereas the lower bound reduces in proportion to η_b (see Figure 10). Hence, it is found that the lower bound can be used as an asymptotic representation only for a heavily damped beam, as shown in Figure 28.

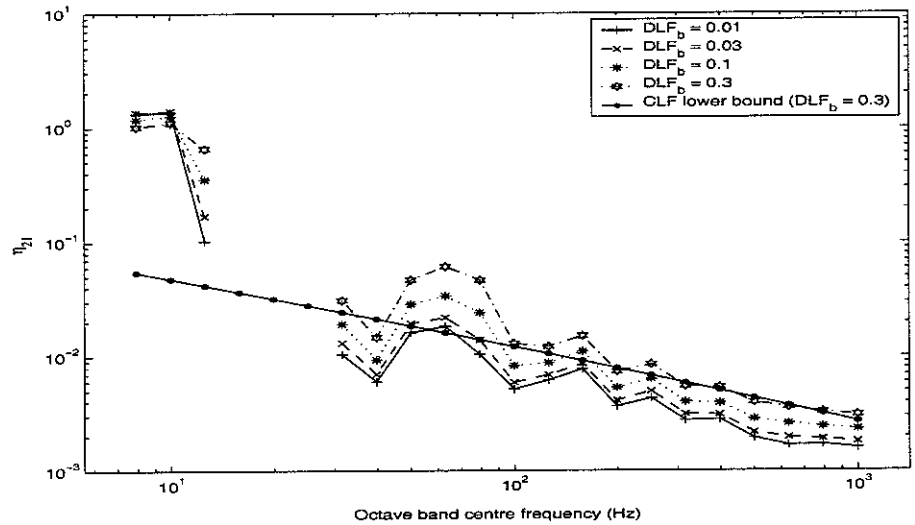

Figure 28. The effective CLFs $\hat{\eta}_{21}$ with different DLFs of the beam for the baseline model ($L_x = 3.0$ m . $\eta_p = 0.01$ for the effective CLFs and $\eta_p = 0.0$ for DLF lower bound used respectively).

In addition, the influence of the plate damping is shown in Figure 29. The change in the CLF is much greater here than for similar values of the beam damping shown in Figure 28.

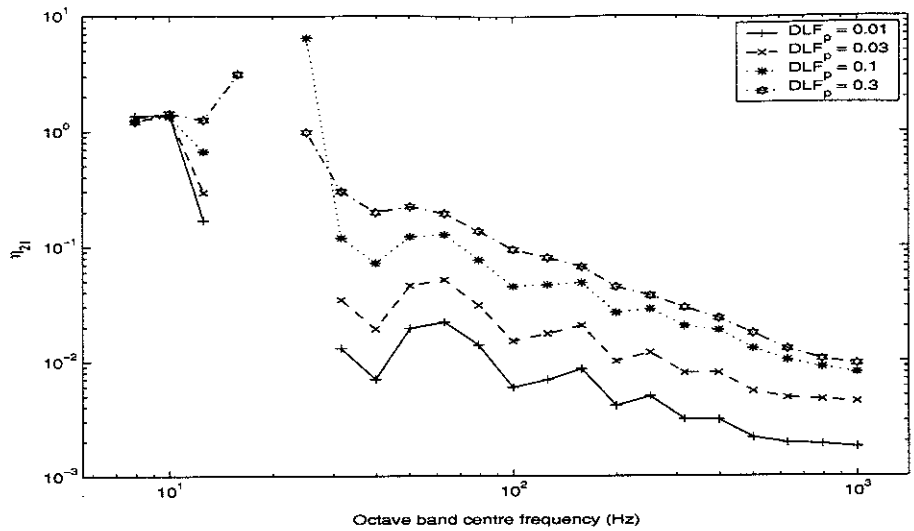

Figure 29. The effective CLFs $\hat{\eta}_{21}$ with different DLFs of the plate for the baseline model ($L_x = 3.0$ m, $\eta_b = 0.03$).

Recalling the results of the effective CLF $\hat{\eta}_{12}$ (beam-to plate) in section 4.2, it can be said that the CLFs $\hat{\eta}_{12}$ and $\hat{\eta}_{21}$ both increase with increasing damping of both the beam and the plate.

5. EFFECT OF HEIGHT/THICKNESS OF BEAM

In most SEA applications, the prediction is known to be accurate for weak coupling [27] and often, a weakly coupled structure can be assumed. In the previous section, the effective CLF has been found not to agree particularly well with the ELF or diffuse field lower bound. It is suspected that these discrepancies may be due to the presence of rather strong coupling. Therefore, it is worth comparing the results where the coupling situations are changed. In this section, the baseline model shown in Figure 3 is slightly modified in order to realise weaker coupling. Although the various dimensions of each subsystem could be adjusted, the height and the thickness of the beam are considered here. As explained before, for weak coupling, it is expected that the source structure has more energy than the receiver structure. Therefore, numerical analysis is carried out when taller or thicker beams are used.

5.1 Effective CLF, $\hat{\eta}_{12}$ (beam-to-plate) and comparison with the ELF

Firstly, the height of the coupled beam used in Figure 3 is changed from 68 mm to 180 mm and then 360 mm, which are about 3 and 5 times greater than that of the baseline model. Other parameters are given in Table 1. The corresponding effective CLFs are presented in Figure 30. As expected, it can be seen that the CLFs generally decrease as the beam height increases, which means more energy is dissipated in the beam than in the plate. Remembering the DLF of the beam is 0.03 and Smith's criteria, it seems that a beam of height 360 mm can be considered to be weakly coupled, as $\eta_{12} < \eta_b$ at least above 100 Hz. For this case, the wavenumbers of the beam are compared in Figure 31. The beam wavenumber for a beam of height 360 mm is a factor of 2.3 smaller than that of the baseline model having a height of 68 mm.

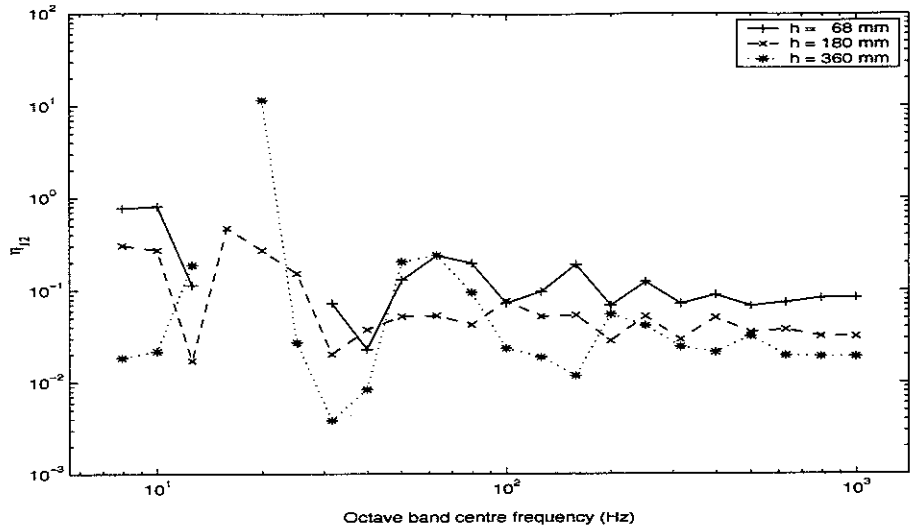

Figure 30. The effective CLFs $\hat{\eta}_{12}$ with different heights of the beam ($t_b = 5.9\,\text{mm}$, $\eta_b = 0.03$, $\eta_p = 0.01$).

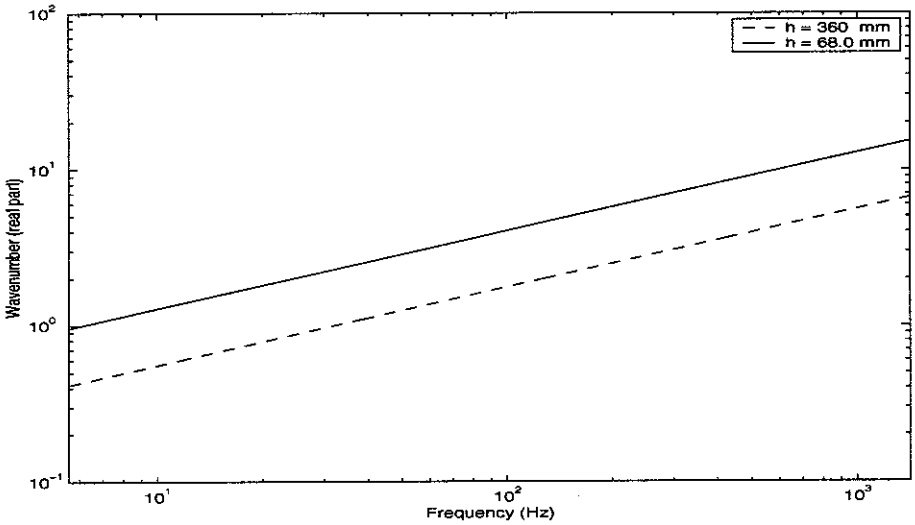

Figure 31. The travelling wavenumber of the beam k_b for two different heights (68 mm and 360 mm).

As explained in section 3.5, it is expected that the ELF based on the wave method should provide an asymptotic estimate of the CLFs, especially when the coupled structure can be considered to be weakly coupled. Results are presented in Figure 32. Equivalent results for the baseline structure were given in Figure 20. Note that the beam is undamped, i.e. $\eta_b = 0.0$ so as to consider only the effect of the plate in the wave method.

It can be seen that the ELF based on the semi-infinite plate becomes closer to the CLFs in the case of a 360 mm beam height.

The ELF based on the finite plate shows better results for both cases than for the baseline model. Generally the ELFs based on the finite plate seem comparable to the CLFs although the 180 mm case shows a better result than the 360 mm case.

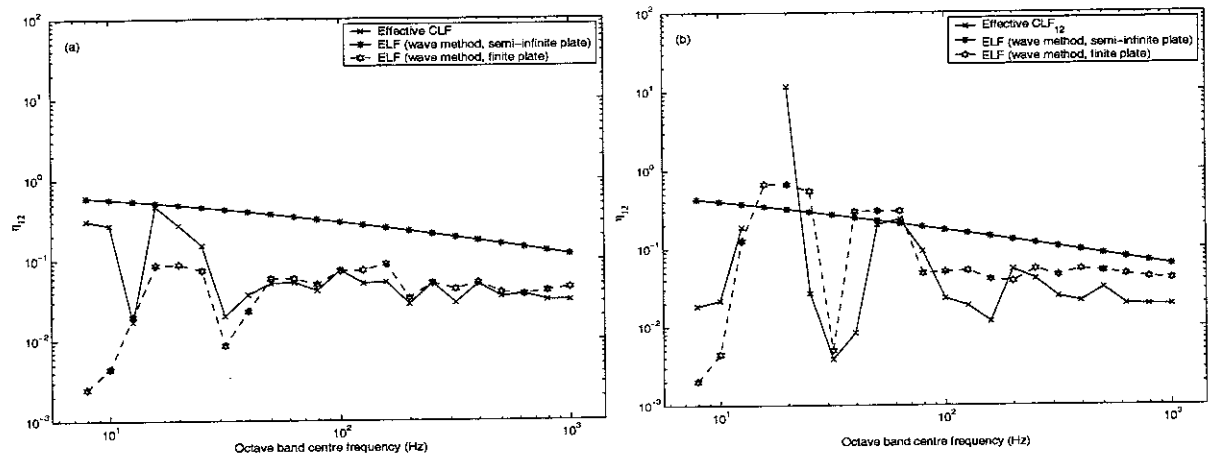

Figure 32. The effective CLFs $\hat{\eta}_{12}$ and the corresponding ELF for different beam heights ($t_b = 5.9\,\text{mm}$, $\eta_b = 0.03$, $\eta_p = 0.01$); (a) $h = 180$ mm (b) $h = 360$ mm.

Changing the thickness of the beam produces the effective CLFs shown in Figure 33 where the thickness is changed from 5.9 mm to 200 mm and 400 mm. Although such thicknesses are very large, they are treated here simply as mathematical changes without considering implications for the validity of modelling it as a beam. Note that the wavenumber of the beam is unaffected by its width, but its mass is increased. It can be seen that the CLFs in both cases decrease, mostly by more than a factor of 10, except in the low frequency region. It can be thus seen that for these thicker beams the plate can be regarded as weakly coupled.

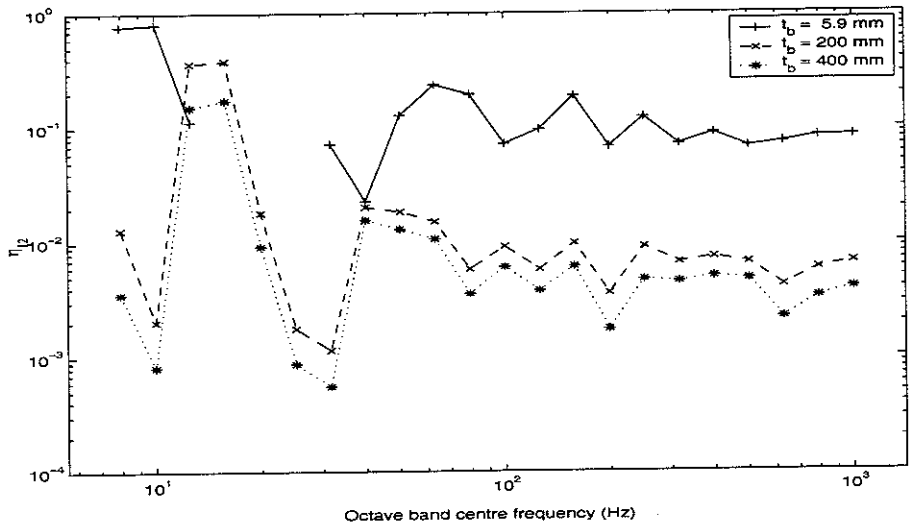

Figure 33. The effective CLFs $\hat{\eta}_{12}$ with different thicknesses of the beam ($h = 68\,\text{mm}$, $\eta_b = 0.03$, $\eta_p = 0.01$).

The asymptotic ELFs are again compared with the CLFs for the cases of 200 mm and 400 mm thickness in Figure 34. It can be seen that the ELFs again provide good asymptotic approximations here.

Also, the ELFs based on the finite plate are shown in the same figures. The results show generally good agreement with the effective CLFs except at low frequencies.

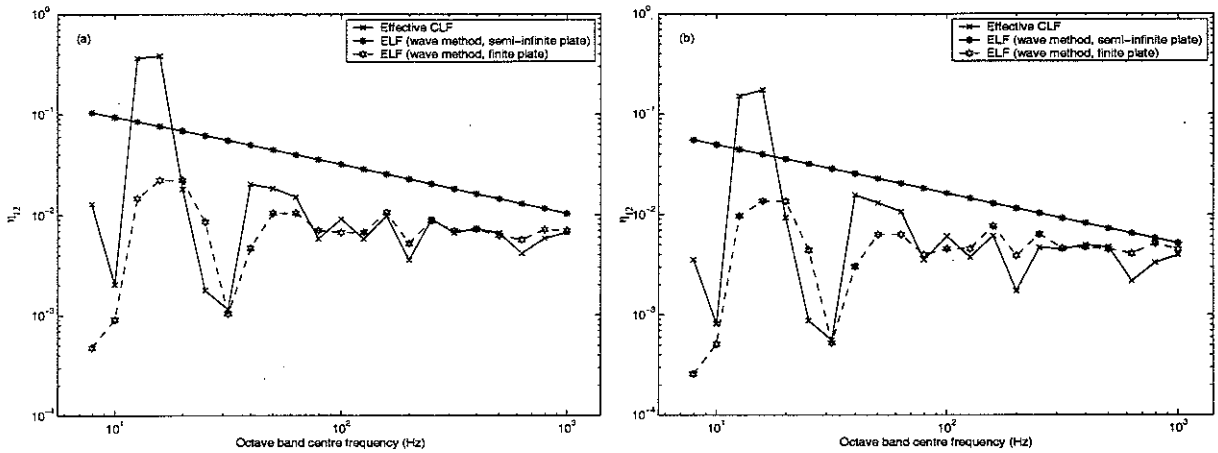

Figure 34. The effective CLFs $\hat{\eta}_{12}$ and the corresponding ELF with different thicknesses of the beam ($h = 68$ mm, $\eta_b = 0.03$, $\eta_p = 0.01$); (a) $t_b = 200$ mm (b) $t_b = 400$ mm.

Finally, both a height of 360 mm and a thickness of 400 mm are considered simultaneously and the corresponding results are shown in Figure 35. Considering the results of Figures 30 and 33, it is clear that both height and thickness have an influence on the results. As the damping of the plate increases, the effective CLFs converge to a certain value, which may indicate the asymptotic values of the CLF of the coupled structure.

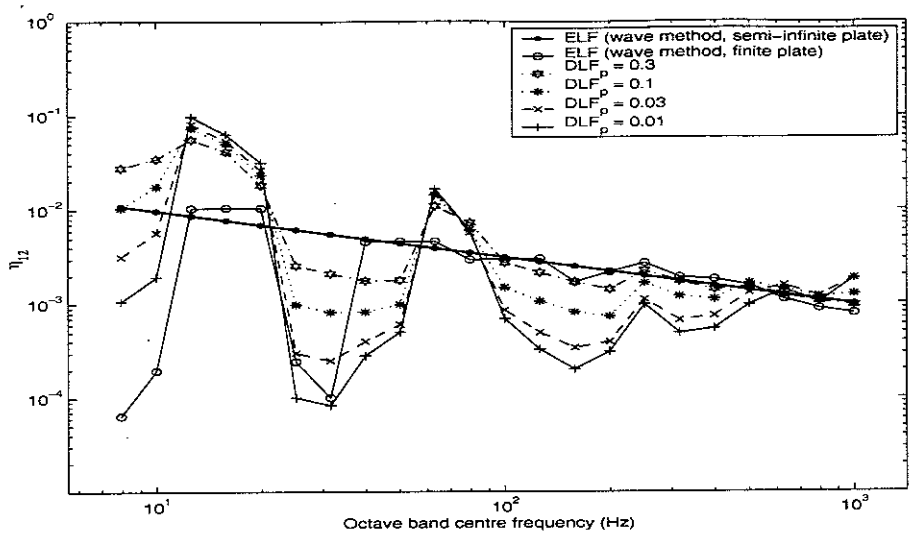

Figure 35. The effective CLFs $\hat{\eta}_{12}$ with different DLFs of the plate ($h = 360\text{mm}$, $t_b = 400\text{mm}$). $\eta_b = 0.03$ is used in SEA. $\eta_b = 0.00$ and $\eta_p = 0.01$ are used in wave method.

It is worth comparing again the asymptotic ELF obtained from the wave method, also shown in the same figure. Recalling the result of the baseline model (Figure 25), the ELF of the semi-infinite plate case can be regarded as an asymptotic representation for the effective CLFs $\hat{\eta}_{12}$.

For the ELFs based on the finite plate, the curve is close to the asymptotic ELF except at low frequencies. However, it can be seen that there are some differences between the ELF based on the finite plate and the CLF $\hat{\eta}_{12}$.

Also, the difference may occur for a coupled structure assumed to be strongly coupled as seen in Figure 20, which is normally considered in real applications. Therefore, although the ELF based on the wave method can be considered as an alternative of the CLF, it should be noted that that there is some limit on the use of the ELFs to represent the exact CLF.

5.2 Effective CLF, $\hat{\eta}_{21}$ (plate-to-beam) and comparison with the diffuse field lower bound results

In section 3.4.2, the effect of the different height and thickness of the beam on the diffuse field transmission coefficient was presented. In this section, the effective CLFs $\hat{\eta}_{21}$ based on the power balance equation are shown to investigate the influence of the height and the thickness of the beam for comparison with the diffuse field results.

Firstly, the height of the beam is changed to 180 and 360 mm and the corresponding $\hat{\eta}_{21}$ are shown in Figure 36. Similar to $\hat{\eta}_{12}$, the effective CLF $\hat{\eta}_{21}$ decreases with increasing heights.

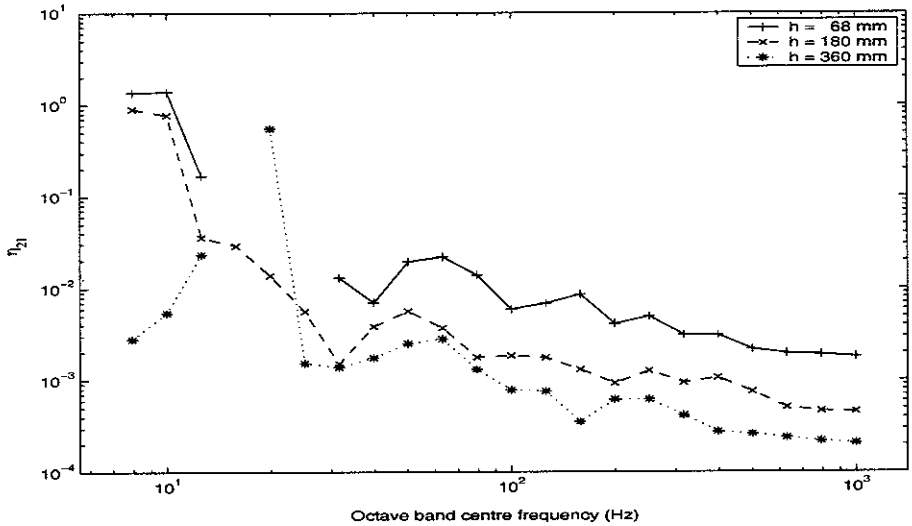

Figure 36. The effective CLFs $\hat{\eta}_{21}$ with different beam heights ($t_b = 5.9$ mm, $\eta_p = 0.01$, $\eta_b = 0.03$).

The diffuse field lower bounds are compared with the effective CLFs in Figure 37. One can see that the difference between them reduces with increasing beam height (also see Figure 27).

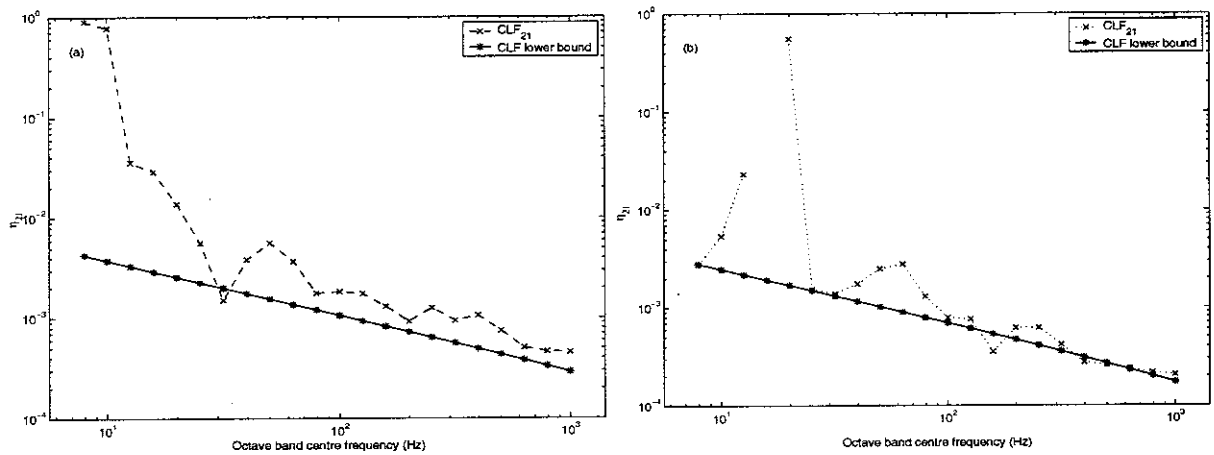

Figure 37. Comparison of the effective CLFs $\hat{\eta}_{21}$ and corresponding lower bounds for $\hat{\eta}_{21}$ based on the transmission coefficient $\tau_{21,d}$ of the baseline model ($\eta_p = 0.01$ and $\eta_b = 0.03$ for the effective CLFs $\hat{\eta}_{21}$ and $\eta_p = 0.0$ for $\tau_{21,d}$ used respectively); (a) $h = 180$ mm (b) $h = 360$ mm.

Also, the effective CLF $\hat{\eta}_{21}$ is investigated when the beam thickness is changed from 5.9 mm to 200 and 400 mm and shown in Figure 38. As expected, $\hat{\eta}_{21}$ decreases with increasing thickness.

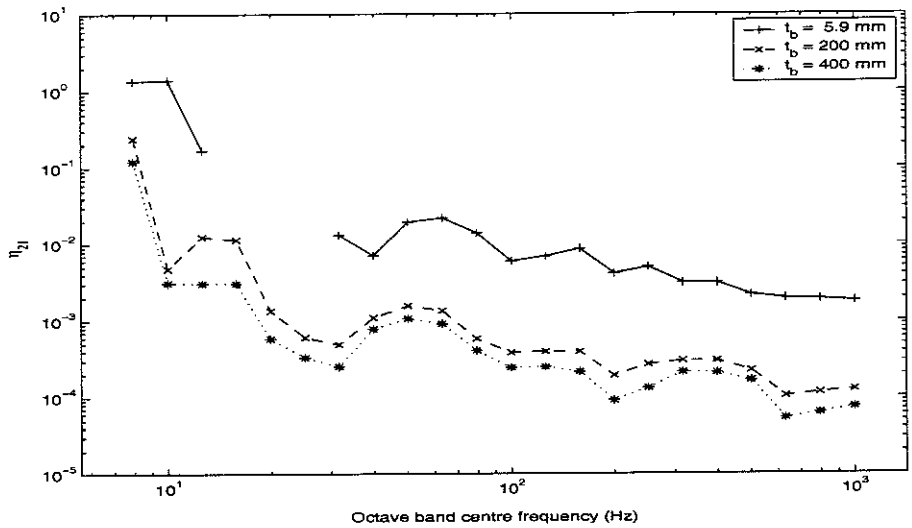

Figure 38. The effective CLFs $\hat{\eta}_{21}$ with different beam thicknesses ($t_b = 60$ mm, $\eta_p = 0.01$, $\eta_b = 0.03$).

Comparing the effective CLF and the diffuse field lower bounds, the difference is much smaller than that for the baseline model, as shown in Figure 39. Therefore, it can be said that the diffuse field results can be an appropriate asymptotic representation for a weakly coupled structure.

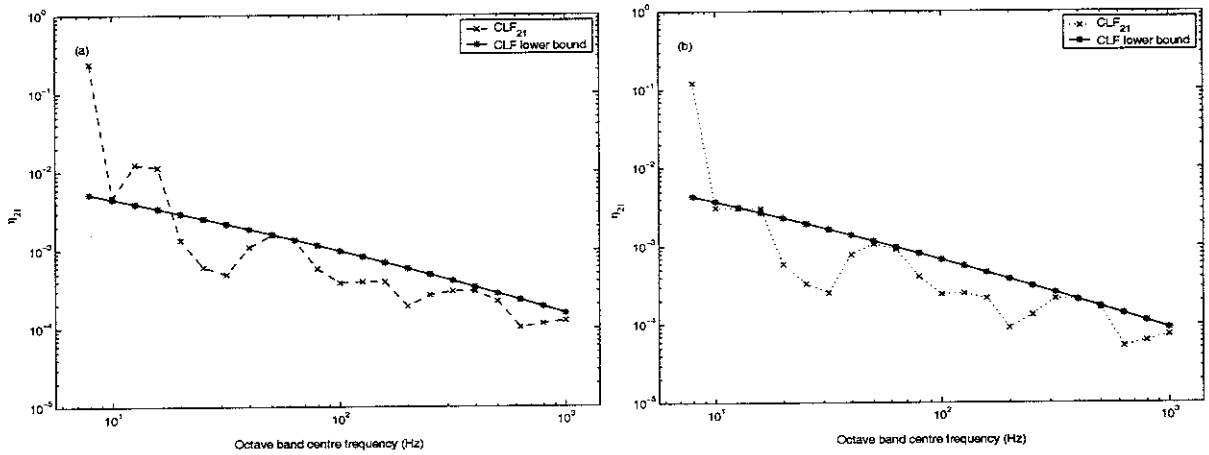

Figure 39. Comparison of the effective CLFs $\hat{\eta}_{21}$ and corresponding lower bounds for $\hat{\eta}_{21}$ based on the transmission coefficient $\tau_{21,d}$ of the baseline model ($\eta_p = 0.01$ and $\eta_b = 0.03$ for the effective CLFs $\hat{\eta}_{21}$ and $\eta_p = 0.0$ for $\tau_{21,d}$ used respectively); (a) $t_b = 200$ mm (b) $t_b = 400$ mm.

The results of $\hat{\eta}_{21}$ where both the height and the thickness are modified are shown in Figure 40. Similar to $\hat{\eta}_{12}$, $\hat{\eta}_{21}$ increases with increasing DLF of the plate and it can be seen that the diffuse field 'lower bound' gives an asymptotic representation of the effective CLFs.

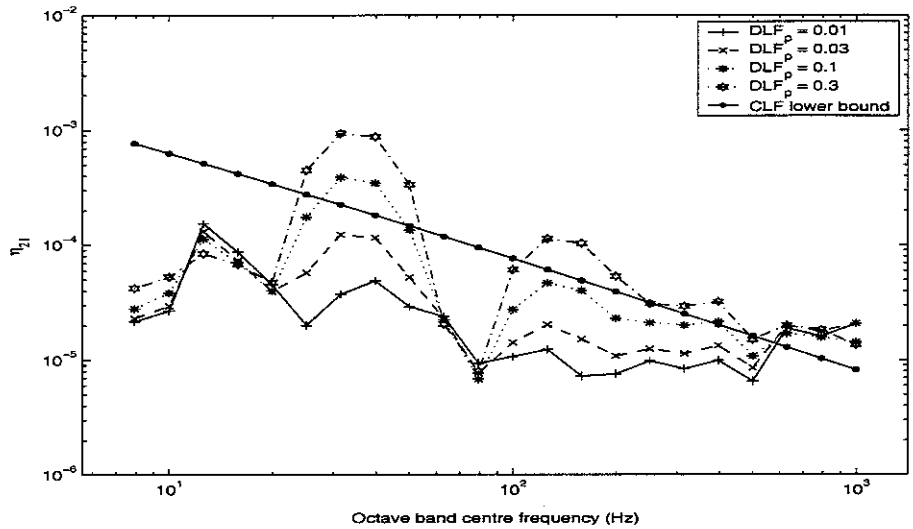

Figure 40. The effective CLFs $\hat{\eta}_{21}$ with different DLFs of the plate ($h = 360\text{mm}$, $t_b = 400\text{mm}$. $\eta_b = 0.03$ for the effective CLFs $\hat{\eta}_{21}$ and $\eta_p = 0.0$ for $\tau_{21,d}$ used respectively).

5.3 Consistency for coupled structures based on power balance

The consistency relationship was explained previously in section 2.3. In this section, the simulated numerical results are shown based on the modal density and the effective CLFs obtained using the power balance equations presented in section 2.1.

Firstly, the modal density of the baseline model (equations (2.14) and (2.17)) is presented in Figure 41. Then, using the modal densities of the subsystems and the effective CLFs, one can examine the consistency relationship. The consistency relationships are shown in terms of the ratio of $n_1\eta_{12}$ to $n_2\eta_{21}$ (see equation (2.10)), as this would produce a ratio of 1 if consistency holds.

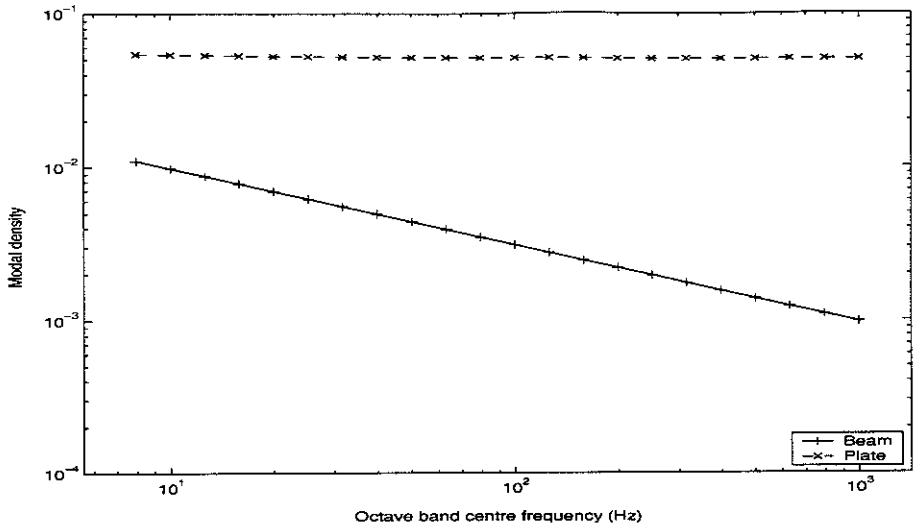

Figure 41. Asymptotic modal density $n(\omega)$ of subsystems of the baseline model as Figure 3.

The results for the baseline model are shown in Figure 42. For the present case of the baseline model, it can be said that the consistency relationship holds except at very low frequencies.

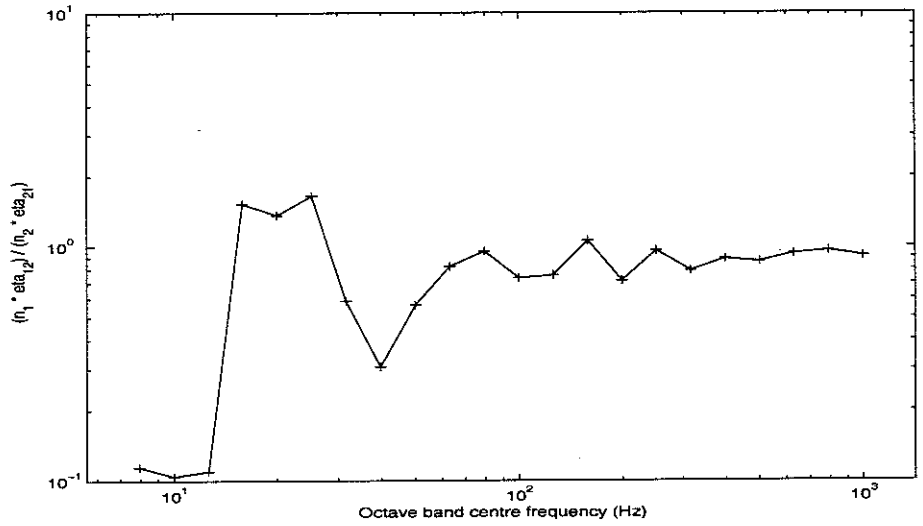

Figure 42. $n_1\eta_{12}/n_2\eta_{21}$ for the baseline model ($\eta_b = 0.03$, $\eta_p = 0.01$)

The consistency relationships for different beam dimensions are also considered and examined. The 360 mm height and the 400 mm thickness of the beam are considered separately and then simultaneously. The ratios $n_1\eta_{12}/n_2\eta_{21}$ are shown in Figure 43.

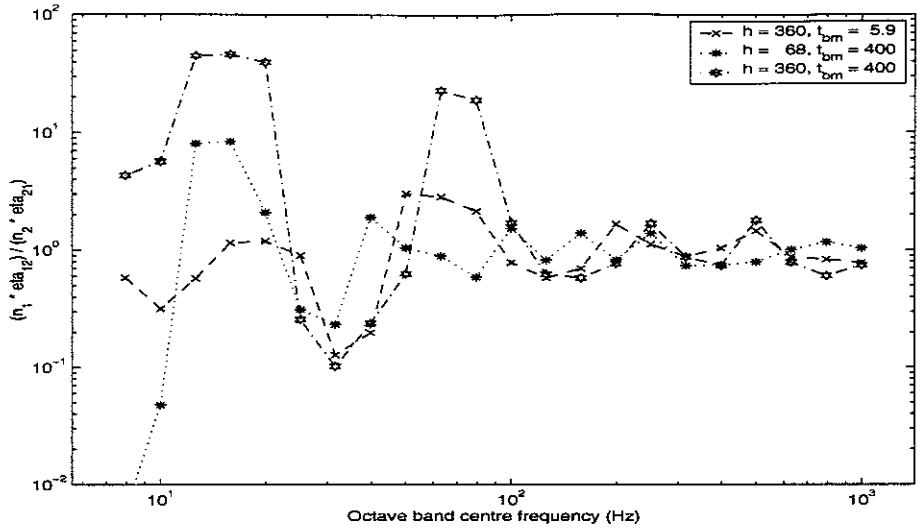

Figure 43. $n_1\eta_{12}/n_2\eta_{21}$ with different beam heights and thicknesses ($\eta_b = 0.03$ and $\eta_p = 0.01$ are used).

It seems that the consistency ratio becomes worse, especially comparing the baseline model and the 360 mm height and 400 mm thickness model. This is because as the height or the thickness increases, the number of modes of the coupled beam decreases. The first three natural frequencies of the corresponding uncoupled beams are shown in Table 4. The modes in the coupled structure are slightly different from these but one can expect that the larger beams have fewer modes than the baseline model.

Table 4. The first three natural frequencies of uncoupled beam ($L_x = 3.0$ m).

Mode Number		1	2	3
Natural frequency (Hz)	Baseline model	6.7	26.9	60.1
	$h = 360$mm	35.4	141.8	319.0
	$t_b = 400$mm	6.7	26.9	60.1

As the number of modes of the coupled beam decreases, the finite system is more sensitive to the modal behaviour of the beam and the assumptions of high modal density and high modal overlap are incorrect for the larger beams. Correspondingly, the energy of the beam is mainly dependent on a few modes as the dimensions increase, and this results in fluctuations such as seen in Figure 43. Conversely the energy of the beam in the baseline model is dependent on more modes. This can be seen from Figure 16 where the energy is relatively evenly distributed with frequency. Therefore, the fluctuations of the consistency result for the baseline model are smaller as shown in Figure 42.

Although there are some fluctuations at low frequencies, it can be seen that ratio $n_1\eta_{12}/n_2\eta_{21}$ gradually converges with increasing frequency so that the ratio tends to unity. Therefore, it seems that the consistency relationship holds for the various coupling situations such as shown in the present report.

6. ENERGY PREDICTION FOR A BEAM-PLATE-BEAM STRUCTURE

6.1 Power balance relationships for a beam-plate-beam coupled structure

In previous sections the coupling loss factors for a single beam coupled to a plate were investigated. As it is normally assumed that the interaction between two subsystems is not affected by the presence of a third subsystem [29], using the coupling loss factors obtained from the single beam structure, it would seem possible to predict using SEA the energy of each subsystem of a beam-plate-beam coupled structure shown in Figure 44. As the Fourier technique can also be applied to predict the response of the two-beam coupled structure this is used to give an 'exact' result for comparison. The two beams are chosen to have different dimensions initially.

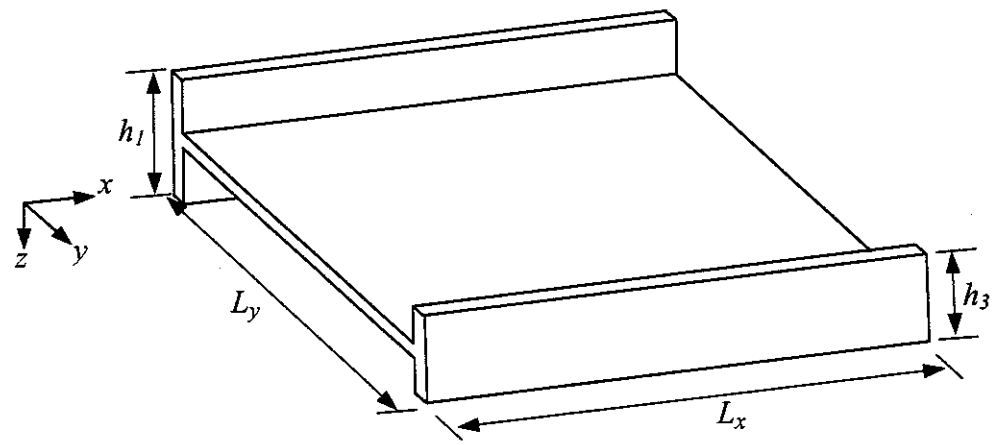

Figure 44. A built-up structure consisting of two finite beams attached to a rectangular plate.

To predict the energy of a subsystem, firstly it is necessary to identify the power balance relationship in terms of a SEA model. The power balance relationships for the coupled structure consisting of three subsystems are shown in Figure 45 and the corresponding power balance equations for the different excitation cases can be derived. In this section to avoid confusion in the notation, beam 1 is named subsystem 1, the plate is named subsystem 2 and the second beam is named subsystem 3 (or beam 3).

Note that there is no direct power transfer between subsystem 1 and subsystem 3 in the figure. For the present study, it is assumed that the coupling between subsystem 1 (beam

1) and subsystem 3 (beam 3), so-called 'indirect coupling', is negligible so that the coupling loss factors η_{13} and η_{31} are zero, although it is not always true.

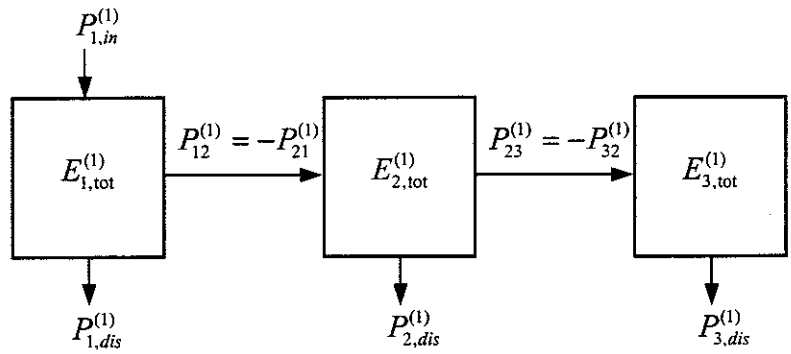

(a) Power input to subsystem 1

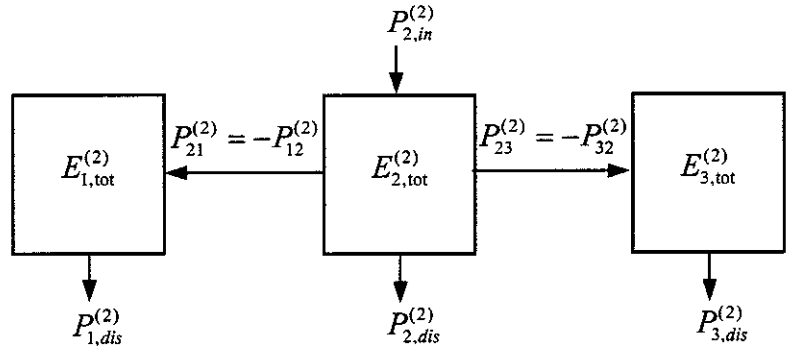

(b) Power input to subsystem 2

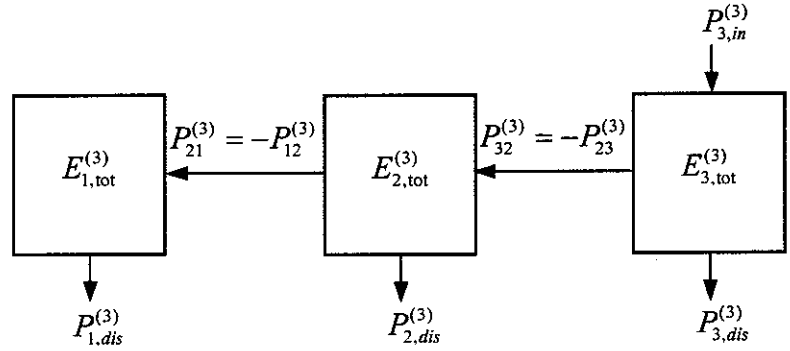

(c) Power input to subsystem 3

Figure 45. Power balance between subsystems of the coupled structure as in Figure 44.

If an external force is applied to subsystem 1 as in Figure 45 (a), using the ensemble notation '-', the power balance equations are

$$\bar{P}_{1,in}^{(1)} = \bar{P}_{1,dis}^{(1)} + \bar{P}_{12}^{(1)}. \tag{6.1a}$$

$$\overline{P}_{12}^{(1)} = \overline{P}_{2,dis}^{(1)} + \overline{P}_{23}^{(1)}. \tag{6.1b}$$

$$\overline{P}_{23}^{(1)} = P_{3,dis}^{(1)}. \tag{6.1c}$$

where $\overline{P}_{ij}$ is the net transferred power between subsystem i and j and $\overline{P}_{i,dis}$ is the net dissipated power by subsystem i. The superscript indicates which subsystem is being excited. Similarly, if the force is applied to subsystem 2 as in Figure 45 (b), then the power balance equations are

$$\overline{P}_{2,in}^{(2)} = \overline{P}_{2,dis}^{(2)} + \overline{P}_{21}^{(2)} + \overline{P}_{23}^{(2)}. \tag{6.2a}$$

$$\overline{P}_{21}^{(2)} = \overline{P}_{1,dis}^{(2)}. \tag{6.2b}$$

$$\overline{P}_{23}^{(2)} = P_{3,dis}^{(2)}. \tag{6.2c}$$

Also, if the force is applied to subsystem 3 as in Figure 45 (c), then the power balance equations are

$$\overline{P}_{3,in}^{(3)} = \overline{P}_{3,dis}^{(3)} + \overline{P}_{32}^{(3)}. \tag{6.3a}$$

$$\overline{P}_{32}^{(3)} = \overline{P}_{2,dis}^{(3)} + \overline{P}_{21}^{(3)}. \tag{6.3b}$$

$$\overline{P}_{21}^{(3)} = P_{1,dis}^{(3)}. \tag{6.3c}$$

Introducing the relationship between the dissipated power and stored energies i.e. $\overline{P}_{i,dis} = \eta_i \omega \overline{E}_i$, with η_i the internal loss factors, and $\overline{P}_{ij} = \eta_{ij}\omega\overline{E}_i - \eta_{ji}\omega\overline{E}_j$, with η_{ij} the coupling loss factors, then the power balance equations corresponding to equations (6.1) - (6.3) can be expressed as follows.

$$\overline{P}_{1,in}^{(1)} = \omega\left[\left(\eta_1^{(1)} + \eta_{12}^{(1)}\right)\overline{E}_1^{(1)} - \eta_{21}^{(1)}\overline{E}_2^{(1)}\right]. \tag{6.4a}$$

$$0=\omega\left[-\eta_{12}^{(1)}\bar{E}_1^{(1)}+\left(\eta_2^{(1)}+\eta_{21}^{(1)}+\eta_{23}^{(1)}\right)\bar{E}_2^{(1)}-\eta_{32}^{(1)}\bar{E}_3^{(1)}\right]. \tag{6.4b}$$

$$0=\omega\left[\left(\eta_3^{(1)}+\eta_{32}^{(1)}\right)\bar{E}_3^{(1)}-\eta_{23}^{(1)}\bar{E}_2^{(1)}\right]. \tag{6.4c}$$

$$\bar{P}_{2,in}^{(2)}=\omega\left[-\eta_{12}^{(2)}\bar{E}_1^{(2)}+\left(\eta_2^{(2)}+\eta_{21}^{(2)}+\eta_{23}^{(2)}\right)\bar{E}_2^{(2)}-\eta_{32}^{(2)}\bar{E}_3^{(2)}\right]. \tag{6.5a}$$

$$0=\omega\left[\left(\eta_1^{(2)}+\eta_{12}^{(2)}\right)\bar{E}_1^{(2)}-\eta_{21}^{(2)}\bar{E}_2^{(2)}\right]. \tag{6.5b}$$

$$0=\omega\left[\left(\eta_3^{(2)}+\eta_{32}^{(2)}\right)\bar{E}_3^{(2)}-\eta_{23}^{(2)}\bar{E}_2^{(2)}\right]. \tag{6.5c}$$

$$\bar{P}_{1,in}^{(1)}=\omega\left[\left(\eta_3^{(3)}+\eta_{32}^{(3)}\right)\bar{E}_3^{(3)}-\eta_{23}^{(3)}\bar{E}_2^{(3)}\right]. \tag{6.6a}$$

$$0=\omega\left[-\eta_{12}^{(3)}\bar{E}_1^{(3)}+\left(\eta_2^{(3)}+\eta_{21}^{(3)}+\eta_{23}^{(3)}\right)\bar{E}_2^{(3)}-\eta_{32}^{(3)}\bar{E}_3^{(3)}\right]. \tag{6.6b}$$

$$0=\omega\left[\left(\eta_1^{(3)}+\eta_{12}^{(3)}\right)\bar{E}_1^{(3)}-\eta_{21}^{(3)}\bar{E}_2^{(3)}\right]. \tag{6.6c}$$

In equations (6.4) - (6.6), powers and energies are time-averaged quantities, η_1, η_2 and η_3 are the damping loss factors of the corresponding subsystems and $\hat{\eta}_{12}$, $\hat{\eta}_{21}$, $\hat{\eta}_{23}$ and $\hat{\eta}_{32}$ are the coupling loss factors estimated from any of the aforementioned approaches.

6.2 Effective CLF

As explained earlier in section 2.2, the effective coupling loss factors (CLFs) are obtained instead of the exact CLFs based on an average over an ensemble of realisations. Assuming $\hat{\eta}_{ij}^{(i)}=\hat{\eta}_{ij}^{(j)}$, the effective CLFs can be obtained from equations (6.4) - (6.6). Introducing a matrix form results in equation (6.7).

$$\omega^{-1}\begin{bmatrix} P_{1,in}^{(1)} & 0 & 0 \\ 0 & P_{2,in}^{(2)} & 0 \\ 0 & 0 & P_{3,in}^{(3)} \end{bmatrix} = \begin{bmatrix} \eta_1 + \hat{\eta}_{12} & -\hat{\eta}_{12} & 0 \\ -\hat{\eta}_{21} & \eta_2 + \hat{\eta}_{21} + \hat{\eta}_{23} & -\hat{\eta}_{23} \\ 0 & -\hat{\eta}_{32} & \eta_3 + \hat{\eta}_{32} \end{bmatrix} \begin{bmatrix} E_1^{(1)} & E_1^{(2)} & E_1^{(3)} \\ E_2^{(1)} & E_2^{(2)} & E_2^{(3)} \\ E_3^{(1)} & E_3^{(2)} & E_3^{(3)} \end{bmatrix}, \tag{6.7}$$

and more simply

$$\omega^{-1}\mathbf{P} = [\eta]\mathbf{E} \tag{6.8}$$

where

$$\mathbf{P} = \begin{bmatrix} P_{1,in}^{(1)} & 0 & 0 \\ 0 & P_{2,in}^{(2)} & 0 \\ 0 & 0 & P_{3,in}^{(3)} \end{bmatrix}, \tag{6.9}$$

$$\mathbf{E} = \begin{bmatrix} E_1^{(1)} & E_1^{(2)} & E_1^{(3)} \\ E_2^{(1)} & E_2^{(2)} & E_2^{(3)} \\ E_3^{(1)} & E_3^{(2)} & E_3^{(3)} \end{bmatrix}, \tag{6.10}$$

$$[\eta] = \begin{bmatrix} \eta_1 + \hat{\eta}_{12} & -\hat{\eta}_{12} & 0 \\ -\hat{\eta}_{21} & \eta_2 + \hat{\eta}_{21} + \hat{\eta}_{23} & -\hat{\eta}_{23} \\ 0 & -\hat{\eta}_{32} & \eta_3 + \hat{\eta}_{32} \end{bmatrix}. \tag{6.11}$$

6.3 Prediction of subsystem energy

In equation (6.11), one can see that the matrix contains only the effective CLFs between subsystems 1 and 2 or subsystems 2 and 3 as it is assumed that there is no coupling between subsystem 1 and 3. These CLFs have already obtained from a beam-plate system. Therefore the energies E can be predicted using the CLFs earlier.

$$\mathbf{E} = \omega^{-1}[\eta]^{-1}\mathbf{P}. \tag{6.12}$$

In fact, in order to obtain the energy terms it is necessary to know the input powers of the beam-plate-beam coupled structure. However, by scaling the total input power to unity, the energy normalised by the input power can be found from the coupling loss factors of the beam-plate coupled structure where excitation is applied separately to one of the subsystems and solving equation (6.7) for the known power input and coupling matrix.

6.4 Numerical analysis

In this section, using the effective CLFs obtained based on the beam-plate structure, the energies normalised by the total input powers of the beam-plate-beam structure as in Figure 44 are predicted and examined. The dimensions of the beams in the corresponding beam-plate-beam coupled structure are shown in Table 4 and the other dimensions are the same as shown in Table 1 for the beam-plate structure. The height of beam 3 is arbitrarily chosen so that it has different wavenumbers from beam 1 ($h_1 = 68\text{mm}$ and $h_3 = 50\text{mm}$), and it is expected that their modal behaviours are different. The uncoupled wavenumber of the 50 mm height beam is 17 % greater than that of the 68 mm height beam.

Table 4. Dimensions of the built-up structure shown in Figure 44.

	Beam 1 (subsystem 1)	Beam 3 (subsystem 3)
Height of the beam, h (mm)	68.0	50.0
Thickness, t (mm)	5.9	5.9
Loss factor of the beam, η_b	0.03	0.03
Beam length, L_x (m)	3.0	
Plate width, L_y (m)	0.75	
Loss factor of the plate, η_p	0.01	

The effective CLFs of the coupled structure consisting of a single beam and a plate are obtained using the same procedure explained previously in section 2. That is, the numerical calculation for the effective CLFs of a coupled structure where the beam height is 68 mm is carried out using the Fourier transform approach and then a 50 mm height beam case is considered. Then these effective CLFs are used to predict the normalised energy using equation (6.12) where excitation is applied to one of the subsystems. It is necessary to mention that the boundary conditions for the opposite edge of the plate coupled to a single beam is assumed to be a pinned condition as before, while the edges of a plate coupled to two beams are sliding. Although their boundary conditions are not the same, it is assumed that the effect of the boundary condition is small, especially at high frequencies.

For comparison with the SEA predicted normalised energies, the comparable normalised energies are obtained directly from the beam-plate-beam structure using the

Fourier technique. The responses are averaged over 20 point excitations separately applied to one of the subsystems only. The analytical solution for the motion of such a beam-plate-beam structure where a beam is excited is described in [2] and the solution for the plate-excited case is given in appendix B.

Firstly, the normalised energies when subsystem 1 (beam 1) is excited are shown in Figure 46. The same symbols in the lines are used to distinguish each subsystem. The thick lines indicate results obtained directly from the Fourier approach while the thin lines are obtained from the SEA model.

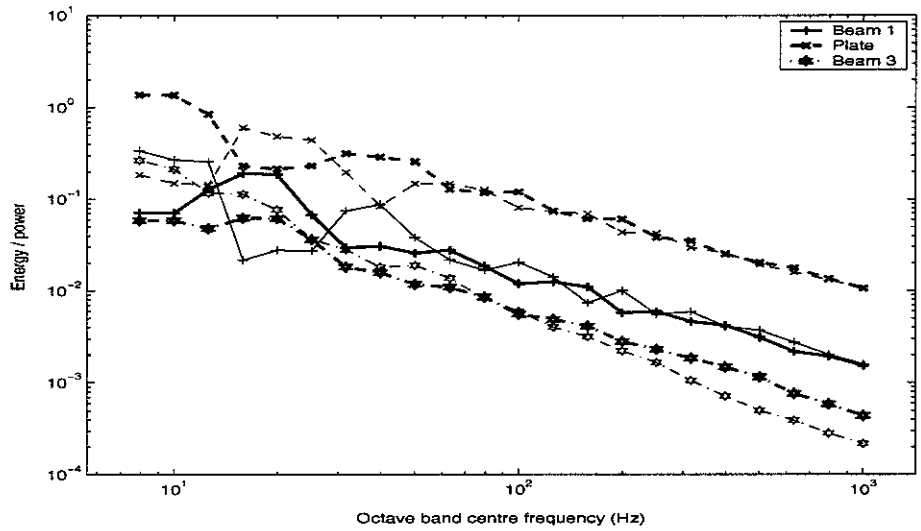

Figure 46. Energies normalised by total input power ($h_1 = 68\text{mm}$, $h_3 = 50\text{mm}$. Beam 1 excited). Thick lines are obtained directly from the beam-plate-beam structure and thin lines are the predicted results based on the effective CLFs and solving the SEA model.

Significant differences are found at low frequencies. One can recall that the effective CLFs of the single beam structure show negative values around 20 Hz (see section 4.2) and it can be said that the corresponding effective CLFs are not appropriate for the prediction of energy. However, the energies of each subsystem are in good agreement at higher frequency, especially for beam 1 and the plate. There is some difference for the energy of beam 3. Note that this is the case when beam 1 is excited and this has higher response at high frequencies than the other beam.

For the plate-excited case, the corresponding results are shown in Figure 47. It can be seen that they are generally in good agreement for all subsystems. The plate has the greatest response and the two beams, although slightly dissimilar, are significantly lower in response and not differing very much. This is probably the case of best agreement using the SEA model and the exact beam-plate-beam analysis.

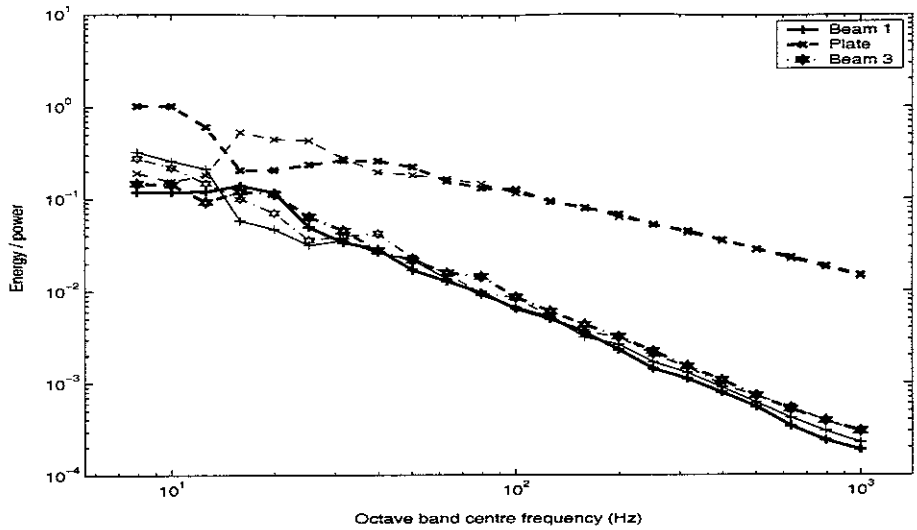

Figure 47. Energies normalised by total input power ($h_1 = 68\text{mm}$, $h_3 = 50\text{mm}$. Plate excited). Thick lines are obtained directly from the beam-plate-beam structure and thin lines are the predicted results based on the effective CLFs and solving the SEA model.

The case for excitation on beam 3 is shown in Figure 48. The normalised energies are generally in good agreement for beam 3 and the plate. However there is a big difference between the SEA prediction and the exact result for the non-excited beam (beam 1).

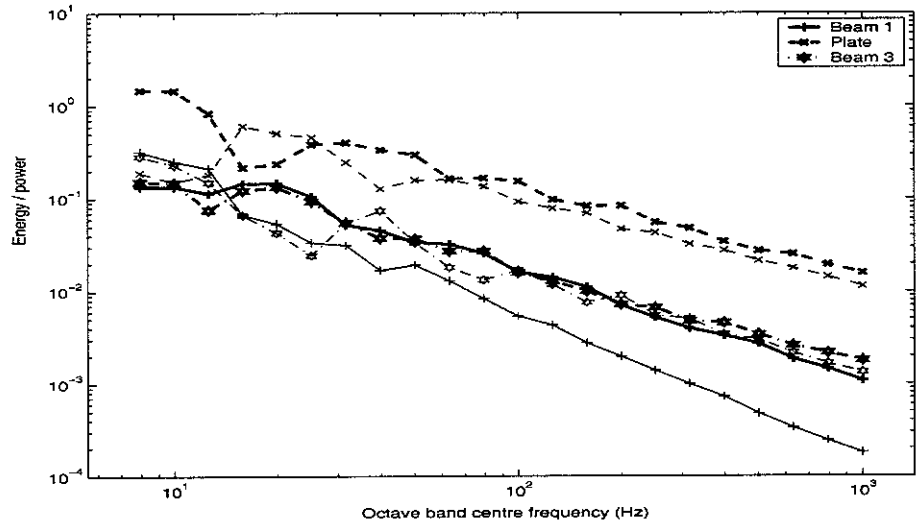

Figure 48. Energies normalised by total input power ($h_1 = 68\text{mm}$, $h_3 = 50\text{mm}$. Beam 3 excited). Thick lines are obtained directly from the beam-plate-beam structure and thin lines are the predicted results based on the effective CLFs and solving the SEA model.

From Figures 46 - 48, one can see that the differences between the SEA and exact predictions for the normalised energies are greatest when the response of the non-excited beam subsystem is calculated for excitation on the other beam. Otherwise, for the case when the plate is excited, they show very good agreement.

This may be due to the indirect coupling between beam 1 and beam 3. Although they are not coupled physically, in fact it seems true that there is a coupling so that power flow occurs between two indirectly coupled beams. This is referred to as a 'tunnelling effect' by Heron [11].

Further investigation of this effect is carried out. It is expected that the indirect coupling is maximum when both beams have similar modal energies [30]. To realise this situation, the height of beam 3 is modified to 67 mm, which is close to that of beam 1 but not identical. Firstly, the results for excitation on beam 1 are shown in Figure 49. It can be seen that the difference in the normalised energy of beam 3 is greater than that shown in Figure 46. Moreover, the response of beam 1 is slightly lower than that predicted by the SEA model.

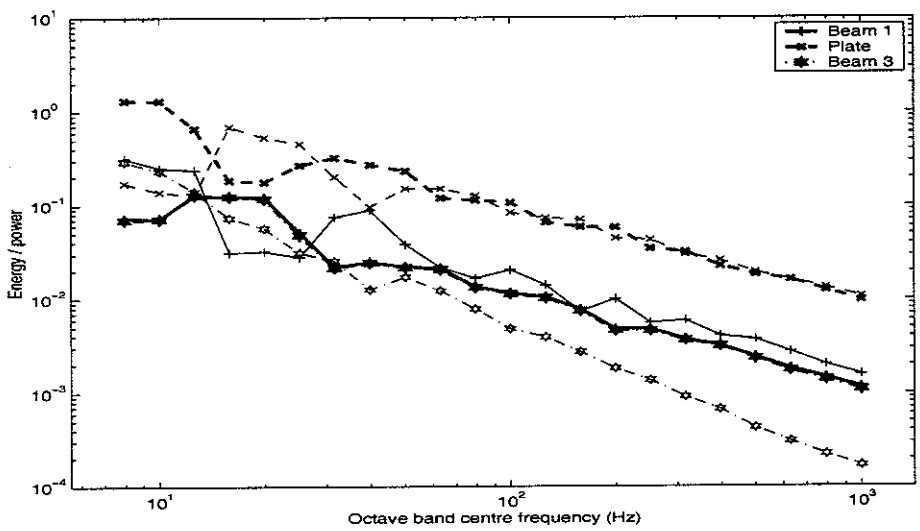

Figure 49. Energies normalised by total input power ($h_1 = 68\,\text{mm}$, $h_3 = 67\,\text{mm}$. Beam 1 excited). Thick lines are obtained directly from the beam-plate-beam structure and thin lines are the predicted results based on the effective CLFs and solving the SEA model.

However, if the plate is excited, good agreement is found between the results predicted using the CLFs and SEA and those directly obtained from the beam-plate-beam Fourier analysis as shown in Figure 50.

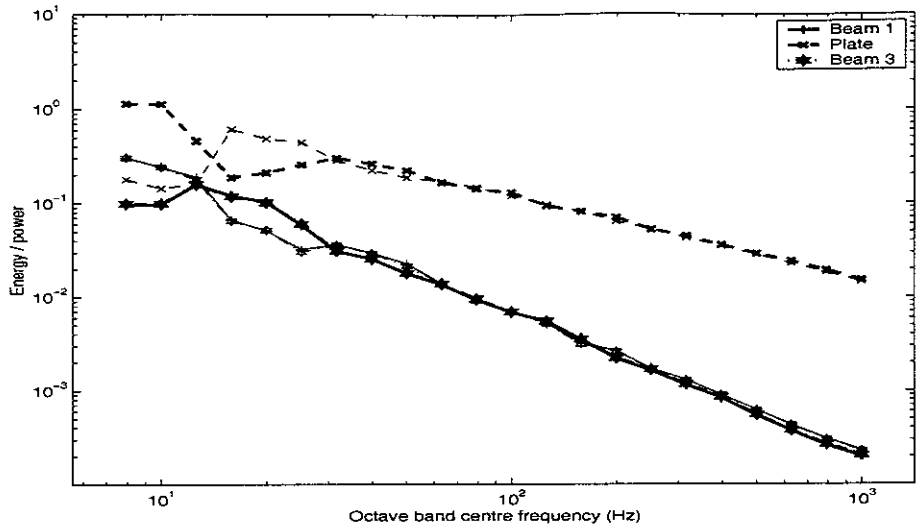

Figure 50. Energies normalised by total input power ($h_1 = 68\,\text{mm}$, $h_3 = 67\,\text{mm}$. Plate excited). Thick lines are obtained directly from the beam-plate-beam structure and thin lines are the predicted results based on the effective CLFs and solving the SEA model.

Finally, the results for excitation on beam 3 are shown in Figure 51. One can see that the difference for the response of beam 1 again increases as frequency increases.

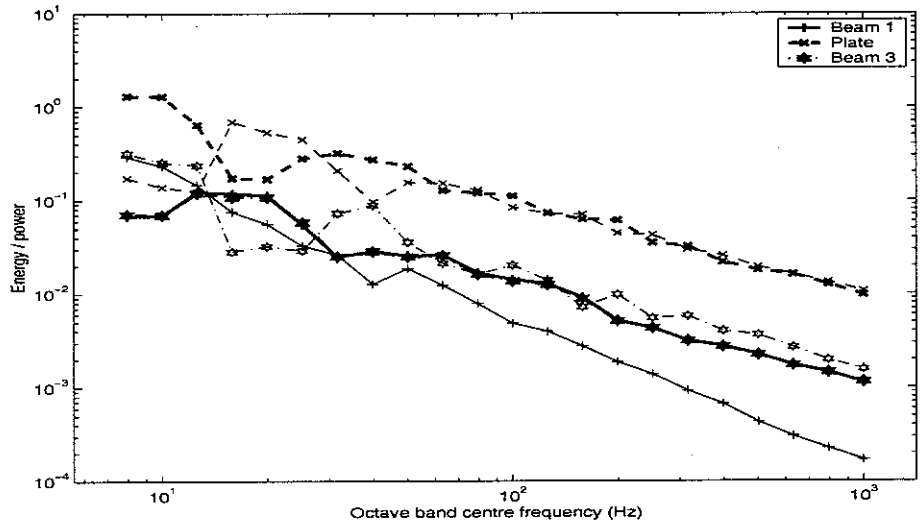

Figure 51. Energies normalised by total input power ($h_1 = 68\,\text{mm}$, $h_3 = 67\,\text{mm}$. Beam 3 excited). Thick lines are obtained directly from the beam-plate-beam structure and thin lines are the predicted results based on the effective CLFs and solving the SEA model.

Therefore, from Figures 49 - 51, it can be inferred that the indirect coupling effect plays an important role for such a beam-plate-beam coupled structure. To get accurate results using the

SEA model it is insufficient to use only the direct effective CLFs calculated between a plate and a beam. The problem may also be a consequence of SEA's inability accurately to predict the response of waveguide structures, and this is effectively what the motion in the beam can be considered as possessing.

7. CONCLUSIONS

Based on the power balance equations, the effective coupling loss factor (CLF) of a beam-plate coupled structure is investigated in terms of the SEA framework, when the external forces are applied to the beam and the plate respectively. The power and energy of the subsystems are obtained from the Fourier technique previously presented [2]. Although the actual CLF is defined in terms of an ensemble average, the frequency average technique is used here instead of the ensemble average. The CLFs are presented in overlapping octave frequency bands.

For the baseline model used previously [2], the effective CLFs $\hat{\eta}_{12}$ and $\hat{\eta}_{21}$ are obtained and analysed in terms of energy. It seems that the baseline model behaves as a strongly coupled system, particularly for power flow from the beam to the plate. The height and thickness of the beam have also been varied to realise a more weakly coupled situation.

The power transmission coefficient τ_θ (plate-to-beam) is found using a wave transmission approach, based on the assumption of a semi-infinite structure. Then, using the transmission coefficient and the assumption of a diffuse field in the plate, a lower bound is obtained for the CLF η_{21} of the equivalent finite plate and beam coupled structure.

An equivalent loss factor (ELF) based on the wave method is introduced as an alternative representation of the CLF η_{12}. When the structure can be assumed to be weakly coupled, it is shown that the ELFs based on the semi-infinite plate are comparable with the effective CLF η_{12}, and the diffuse field lower bound for the CLF can be used as an asymptotic representation of the effective CLF η_{21}. However where stronger coupling is present the asymptotic ELF based on the semi-infinite plate is an overestimate of $\hat{\eta}_{12}$ and the diffuse field result is an underestimate of $\hat{\eta}_{21}$. Concerning the ELF estimate based on the finite plate, it seems to have some limitation in representing the effective CLF $\hat{\eta}_{12}$ regardless of the coupling strength.

The effect of the damping in the subsystem is studied. For both $\hat{\eta}_{12}$ and $\hat{\eta}_{21}$, it is shown that the CLFs increase as the dissipation loss factor (DLF) of both the source and receiver structure increases.

The consistency relationship is investigated. For this, the asymptotic modal densities of the subsystem such as the beam and the plate are used when the corresponding boundary conditions are considered. It is shown that the consistency relationship generally holds,

independent of coupling situations. With the increased height and thickness of the beam, the consistency relationship becomes worse. This is because, as the dimensions of the beam increase, the number of modes of the coupled beam decreases.

An attempt was made to predict the subsystem energy of the beam-plate-beam structure using the effective CLFs previously obtained from the beam-plate structure. The energy normalised by input power was compared with that directly obtained from the Fourier approach. They were generally in good agreement at high frequencies for the plate-excited situation. However, when one beam is excited, the normalised energy of the other beam shows some discrepancy. It seems that this may occur due to the indirect coupling effect between the two beams. The discrepancy is largest when the beams are similar.

For future study, an analytical approach will be developed to obtain the response of a fully framed structure. Then results obtained in the present report might be applied to the analysis of the dynamic characteristics of the framed structure and indicate the usefulness or restrictions of applying SEA to such a problem. Also the problem of the wave approach highlighted previously will be re-examined and considered for approximate calculations of the framed structure.

References

1. J. W. Yoo, D. J. Thompson and N. S. Ferguson 2003 *ISVR Memorandom No*: **905**. Structural analysis of a symmetric structure consisting of two beams and a plate based on a wave approach.

2. J. W. Yoo, D. J. Thompson and N. S. Ferguson 2003 *ISVR Memorandom No*: **927**. A Fourier technique for the analysis of beam-plate coupled structure.

3. M. S. Kompella and B. J. Bernhard 1993 In Proc. SAE noise and vibration Conf. Warrendale U.S.A: Society of Automotive Engineers. Measurement of the statistical variation of structural-acoustic characteristics of automotive vehicles.

4. R. H. Lyon and R. G. DeJong 1995 *Theory and Application of Statistical Energy Analysis*. Boston: Butterworth-Heinemann.

5. B. R. Mace 1992 *Journal of Sound and Vibration* **154**, 289-319. Power flow between two continuous one-dimensional subsystems: a wave solution.

6. B. R. Mace and J. Rosenberg 1995 *Proceedings of Inter-Noise '95* 1271-1274. Energy flow between two coupled plate: finite element and statistical energy analyses.

7. R. G. DeJong 1997 in *Proceedings of IUTAM symposium on Statistical Energy Analysis*, 71-82. An approach to the Statistical Energy Analysis of strongly coupled systems.

8. E. C. N. Wester and B. R. Mace 1996 *Journal of Sound and Vibration* **193**, 793-822. Statistical energy analysis of two edge-coupled rectangular plate: ensemble averages.

9. F. J. Fahy and A. D. Mohammed 1992 *Journal of Sound and Vibration* **158**, 45-67. A study of uncertainty in applications of SEA to coupled beam and plate systems, part 1: computational experiment.

10. R. S. Langley and K. H. Heron 1990 *Journal of Sound and Vibration* **143**, 241-253. Elastic wave transmission through plate/beam junction.

11. K. H. Heron 1994 Philosophical Transactions of the Royal Society of London, series A, volume 346, 429-554. Advanced statistical energy analysis.

12. L. Ji 2003 *Ph.D. Thesis, University of Southampton.* Mid-frequency vibration analysis of built-up structures.

13. R. M. Grice and R. J. Pinnington 1999 *Journal of Sound and Vibration* **230**, 825-849. A method for the vibrational analysis of built-up structures, part 1: Introduction and analytical analysis of the plate-stiffened beam.

14. R. M. Grice and R. J. Pinnington 1999 *Journal of Sound and Vibration* **230**, 851-875. A method for the vibrational analysis of built-up structures, part 2: Analysis of the plate-stiffened beam using a combination of finite element analysis and analytical impedances.

15. R. S. Langley and P. Bremner 1999 *Journal of Acoustical Society of America*, **105**, 1657-1671. A hybrid method for the vibration analysis of complex structural-acoustic systems.

16. W. S. Park 2003 *Ph.D. Thesis, University of Southampton.* The sources of variability in statistical energy analysis coupling of two rectangular plates.

17. R. J. M. Craik, J. A. Steel and D. I. Evans 1991 *Journal of Sound and Vibration* **144**, 95-107. Statistical energy analysis of structure-borne sound transmission at low frequencies.

18. A. D. Mohammed 1990 *Ph.D. Thesis, University of Southampton.* A study of uncertainty in applications of Statistical Energy Analysis.

19. G. Fraser 1998 *Ph.D. Thesis, Heriot-Watt University.* Structure-borne sound in motor vehicles using Statistical Energy Analysis.

20. R. S. Langley 1992 *Journal of Sound and Vibration* **159**, 483-502. A wave intensity technique for the analysis of high frequency vibrations.

21. R. S. Langley 1994 *Journal of Sound and Vibration* **169**, 297-317. Elastic Wave Transmission Coefficients and Coupling Loss Factors for Structural Junctions Between Curved Panels.

22. D. A. Bies and S. Hamid 1980 *Journal of Sound and Vibration* **70**, 187-204. *In situ* determination of loss and coupling loss factors by the power injection method.

23. B. R. Mace 1994 *Journal of Sound and Vibration* **178**, 95-112. On the statistical analysis hypothesis of coupling power proportionality and some implications of its failure.

24. G. Xie, D. J. Thompson and C. J. C. Jones 2004 *Journal of Sound and Vibration.* Mode Count and modal density of structural systems: relationships with boundary conditions (in press).

25. L. Cremer, M. Heckl and E. E. Ungar 1988 *Structure-borne Sound.* Berlin: Springer Verlag; 2nd edition.

26. J. W. Yoo, N. S. Ferguson and D. J. Thompson 2002 *ISVR Memorandom No*: **888**. Structural analysis of a combined beam and plate structure using a wave approach.

27. ESDU 99009. An introduction to statistical energy analysis.

28. P. W. Smith Jr. 1979 *Journal of Acoustical Society of America*, **65**, 695-698. Statistical models of coupled dynamical systems and the transition from weak to strong coupling.

29. B. R. Mace 2002 "*ISVR Short Course Lecture Notes on High frequency modelling of structural vibration*", ISVR, University of Southampton.

30. B. R. Mace 2001 "*Lecture Notes on ISVR Advanced Course in Acoustic, Noise and Vibration*", ISVR, University of Southampton.

APPENDICES

Appendix A. Nomenclature

A	wave amplitude in a beam (m)
B	wave amplitude in a plate (m)
D	beam stiffness (Nm^2); plate stiffness (Nm)
E	Young's modulus of elasticity (N/m^2); energy
L	length of a structure
L_x	length of a beam (m)
L_y	width of a plate (m)
L_{tot}	perimeter of a structure
$N(\omega)$	number of mode below a particular frequency
P	power
S	area of a structure
c	$\cos\theta$
c_g	group velocity
f	frequency (Hz)
f_1	force function
h	height of a beam
i	$\sqrt{-1}$
k	wavenumber
k_b	uncoupled beam wavenumber
k_p	uncoupled free wavenumber in a plate
k_x	coupled travelling trace wavenumber of a beam
k_y	trace wavenumber in a plate
m	mode number
m_b'	mass per unit length of a beam (kg/m)
m_p''	mass per unit area of a plate (kg/m^2)

n	mode number
$n(\omega)$	modal density function
$\tilde{r}$	ratio of wave amplitude
s	$\sin\theta$
t	thickness (m)
w	displacement (m)
x, y, z	co-ordinates
δ	constant
ε	phase change; energy per unit area of a structure
η	dissipation loss factor (-)
η_e	equivalent loss factor, based on wavenumber
η_{ij}	ensemble average coupling loss factor
$\hat{\eta}_{ij}$	effective coupling loss factor
θ	angle
ν	Poisson's ratio
ξ	non-dimensional wavenumber ($=k_b/k_p$)
ρ	density (kg/m^3)
ρ_θ	power reflection coefficient ($=\lvert\tilde{r}\rvert^2$)
ρ_d	power reflection coefficient for a diffuse field
τ_θ	power transmission coefficient
$\tau_{ij,d}$	power transmission coefficient for a diffuse field
ϕ	phase change
μ	$m_p''/\left(m_b' k_p\right)$
ω	radian frequency (rad/s)
Δ	constant
Γ	constant

Appendix B. Motion of a beam-plate-beam structure when a plate is excited

B.1 Motion of the coupled structure

The coupled structure consisting of two infinite beams and an infinitely long finite width plate can be analysed using a Fourier transform technique. The corresponding subsystems of such a structure and their force relationships are shown in Figure B.1. Harmonic motion at frequency ω is assumed and the beams are assumed to be infinitely stiff to torsion along $y_1 = 0$ and $y_2 = L_2$.

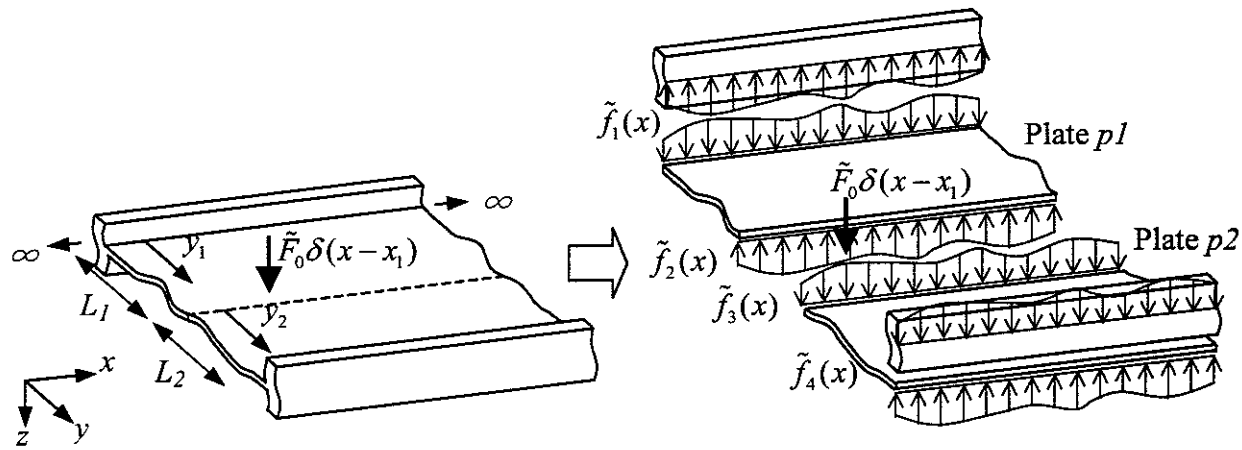

Figure B.1. A built-up structure consisting of infinite two beams attached to an infinitely long finite width plate and the force relationship between them.

The external point force is only acting on the plate located at $y_1 = L_1$ and the force is defined by $\tilde{F}_0\delta(x-x_1)\delta(y-L_1)$ where δ is the Dirac delta function. When the infinitely long finite width plate and the infinite beam (beam $b1$) are joined along the line $y_1 = 0$, a force per unit length $f_1(x)$ acts between them as shown in Figure B.1. Now considering all forces related to beam $b1$, the motion of this beam with damping becomes

$$\tilde{D}_b \frac{\partial^4 \tilde{w}_{b1}(x)}{\partial x^4} - m'_{b1}\omega^2 \tilde{w}_{b1}(x) = -\tilde{f}_1(x) \qquad \text{(B.1)}$$

where subscript $b1$ stands for the beam $b1$, $\tilde{D}_b$ is its complex bending stiffness and m'_{b1} is its mass per unit length. In the same manner, the equation of motion for the other beam (beam $b2$) is

$$\tilde{D}_b \frac{\partial^4 \tilde{w}_{b2}(x)}{\partial x^4} - m'_{b2}\omega^2 \tilde{w}_{b2}(x) = \tilde{f}_4(x). \tag{B.2}$$

The spatial Fourier transforms of equation (B.1) and (B.2) give respectively

$$\tilde{D}_b k_x^4 \tilde{W}_{b1}(k_x) - m'_{b1}\omega^2 \tilde{W}_{b1}(k_x) = -\tilde{F}_1(k_x). \tag{B.3}$$

$$\tilde{D}_b k_x^4 \tilde{W}_{b2}(k_x) - m'_{b2}\omega^2 \tilde{W}_{b2}(k_x) = \tilde{F}_4(k_x) \tag{B.4}$$

where $\tilde{W}_{b1}(k_x)$ and $\tilde{W}_{b2}(k_x)$ are the Fourier transformed displacement of beams $b1$ and $b2$ respectively and $\tilde{F}_1(k_x)$ and $\tilde{F}_4(k_x)$ are the Fourier transforms of $\tilde{f}_1(x)$ and $\tilde{f}_4(x)$ respectively.

Also, the equation of motion of the free plate with damping is

$$\tilde{D}_p \left(\frac{\partial^4 \tilde{w}_p(x,y)}{\partial x^4} + 2\frac{\partial^4 \tilde{w}_p(x,y)}{\partial x^2 \partial y^2} + \frac{\partial^4 \tilde{w}_p(x,y)}{\partial y^4} \right) - m''_p \omega^2 \tilde{w}_p(x,y) = 0, \tag{B.5}$$

where $\tilde{D}_p$ is its complex bending stiffness and m''_p is its mass per unit area of the plate. The corresponding Fourier transform of equation (B.5) is

$$\tilde{D}_p \left\{ k_x^4 \tilde{W}_p(k_x,y) - 2k_x^2 \frac{\partial^2 \tilde{W}_p(k_x,y)}{\partial y^2} + \frac{\partial^4 \tilde{W}_p(k_x,y)}{\partial y^4} \right\} - m'_p \omega^2 \tilde{W}_p(k_x,y) = 0. \tag{B.6}$$

where $\tilde{W}_p(k_x,y)$ is the Fourier transformed displacement of the plate. If harmonic waves in the plates are assumed, the wavenumber relationship can be defined. For waves of the form $e^{k_y y} e^{ik_x x}$ the wave propagating or decaying away from the junction of beam $b1$ and the plate is defined as

$$k_y = -\sqrt{k_x^2 - \tilde{k}_p^2} = \tilde{k}_{y1}, \tag{B.7a}$$

$$k_y = -\sqrt{k_x^2 + \tilde{k}_p^2} = \tilde{k}_{y2}. \tag{B.7b}$$

where $\tilde{k}_p$ is the plate free wavenumber. Meanwhile, the positive square roots are assumed for waves travelling towards the junction and are found to be

$$k_y = \sqrt{k_x^2 - \tilde{k}_p^2} = \tilde{k}_{y3}, \tag{B.7c}$$

$$k_y = \sqrt{k_x^2 + \tilde{k}_p^2} = \tilde{k}_{y4}. \tag{B.7d}$$

If $|k_x| < |\tilde{k}_p|$, then wavenumbers $\tilde{k}_{y1}$ and $\tilde{k}_{y3}$ are considered as travelling waves, and $\tilde{k}_{y2}$ and $\tilde{k}_{y4}$ are considered as nearfield waves. Conversely, if $|k_x| > |\tilde{k}_p|$, then all of them behave as nearfield waves.

Then the motion of plate $p1$ can be written as

$$\tilde{W}_{p1}(k_x, y_1) = \tilde{B}_1 e^{\tilde{k}_{y1} y_1} + \tilde{B}_2 e^{\tilde{k}_{y2} y_1} + \tilde{B}_3 e^{\tilde{k}_{y3} y_1} + \tilde{B}_4 e^{\tilde{k}_{y4} y_1} \tag{B.8}$$

and for plate $p2$,

$$\tilde{W}_{p2}(k_x, y_2) = \tilde{C}_1 e^{\tilde{k}_{y1} y_2} + \tilde{C}_2 e^{\tilde{k}_{y2} y_2} + \tilde{C}_3 e^{\tilde{k}_{y3} y_2} + \tilde{C}_4 e^{\tilde{k}_{y4} y_2} \tag{B.9}$$

Note that different local coordinate systems are used in equations (B.8) and (B.9) in describing the motion of the plate i.e. $y_1 (\equiv y)$ for plate $p1$ and $y_2 (\equiv y - L_1)$ for plate $p2$.

The response of the beams and the plates can be obtained based on application of the appropriate boundary conditions.

(i) Continuity equation for beam $b1$ and plate $p1$; equal displacement to the plate at $y_1 = 0$ of plate $p1$

$$\tilde{W}_{p1}(k_x, y_1)\big|_{y_1=0} = \tilde{W}_{b1}(k_x) \tag{B.10}$$

$$\tilde{B}_1 + \tilde{B}_2 + \tilde{B}_3 + \tilde{B}_4 - \tilde{W}_{b1}(k_x) = 0. \tag{B.11}$$

(ii) Sliding condition; beam $b1$ is assumed infinitely stiff to torsion along $y_1 = 0$ of plate $p1$

$$\left.\frac{\partial \tilde{W}_{p1}(k_x, y_1)}{\partial y_1}\right|_{y_1=0} = 0 \tag{B.12}$$

$$\left.\frac{\partial \tilde{W}_{p1}(k_x, y_1)}{\partial y_1}\right|_{y_1=0} = \tilde{B}_1\tilde{k}_{y1} + \tilde{B}_2\tilde{k}_{y2} + \tilde{B}_3\tilde{k}_{y3} + \tilde{B}_4\tilde{k}_{y4} = 0. \tag{B.13}$$

(iii) Force equilibrium condition; the force on plate $p1$ are equal and opposite to the respective force on beam $b1$

$$\tilde{D}_p\left[\frac{\partial^3 \tilde{W}_{p1}(k_x, y_1)}{\partial y_1^3} - k_x^2(2-\nu)\frac{\partial \tilde{W}_{p1}(k_x, y_1)}{\partial y_1}\right]_{y_1=0} = \tilde{F}_1(k_x) \tag{B.14}$$

Combining equations (B.3) and (B.14) results in

$$-\tilde{D}_p\left[\frac{\partial^3 \tilde{W}_{p1}(k_x, y_1)}{\partial y_1^3} - k_x^2(2-\nu)\frac{\partial \tilde{W}_{p1}(k_x, y_1)}{\partial y_1}\right]_{y_1=0} = \left(\tilde{D}_b k_x^4 - m'_{b1}\omega^2\right)\tilde{W}_{b1}(k_x). \tag{B.15}$$

Therefore,

$$\begin{aligned}&\tilde{D}_p\left[\begin{aligned}&\tilde{B}_1\left\{\tilde{k}_{y1}^3 - k_x^2(2-\nu)\tilde{k}_{y1}\right\} + \tilde{B}_2\left\{\tilde{k}_{y2}^3 - k_x^2(2-\nu)\tilde{k}_{y2}\right\}\\ &+\tilde{B}_3\left\{\tilde{k}_{y3}^3 - k_x^2(2-\nu)\tilde{k}_{y3}\right\} + \tilde{B}_4\left\{\tilde{k}_{y4}^3 - k_x^2(2-\nu)\tilde{k}_{y4}\right\}\end{aligned}\right]\\ &+\left(\tilde{D}_b k_x^4 - m'_{b1}\omega^2\right)\tilde{W}_{b1}(k_x) = 0\end{aligned} \tag{B.16}$$

(iv) Continuity equation for plate $p1$ and plate $p2$; equal displacement at junction $y_1 = L_1$ of plate $p1$ and $y_2 = 0$ of plate $p2$

$$\left.\tilde{W}_{p1}(k_x, y_1)\right|_{y_1=L_1} = \left.\tilde{W}_{p2}(k_x, y_2)\right|_{y_2=0} \tag{B.17}$$

$$\tilde{B}_1 e^{\tilde{k}_{y1}L_1} + \tilde{B}_2 e^{\tilde{k}_{y2}L_1} + \tilde{B}_3 e^{\tilde{k}_{y3}L_1} + \tilde{B}_4 e^{\tilde{k}_{y4}L_1} - \tilde{C}_1 - \tilde{C}_2 - \tilde{C}_3 - \tilde{C}_4 = 0 \tag{B.18}$$

(v) Continuity equation for plate $p1$ and plate $p2$; equal rotational displacement at junction $y_1 = L_1$ of plate $p1$ and $y_2 = 0$ of plate $p2$

$$\left.\frac{\partial \tilde{W}_{p1}(k_x, y_1)}{\partial y_1}\right|_{y_1=L_1} = \left.\frac{\partial \tilde{W}_{p2}(k_x, y_2)}{\partial y_2}\right|_{y_2=0} \tag{B.19}$$

$$\tilde{B}_1\tilde{k}_{y1}e^{\tilde{k}_{y1}L_1} + \tilde{B}_2\tilde{k}_{y2}e^{\tilde{k}_{y2}L_1} + \tilde{B}_3\tilde{k}_{y3}e^{\tilde{k}_{y3}L_1} + \tilde{B}_4\tilde{k}_{y4}e^{\tilde{k}_{y4}L_1} - \tilde{C}_1\tilde{k}_{y1} - \tilde{C}_2\tilde{k}_{y2} - \tilde{C}_3\tilde{k}_{y3} - \tilde{C}_4\tilde{k}_{y4} = 0 \tag{B.20}$$

(vi) Moment equilibrium condition; the moments acting on plates $p1$ and $p2$ are equal at junction $y_1 = L_1$

$$\tilde{M}_{p1}(k_x, y_1)\big|_{y_1=L_1} = \tilde{M}_{p2}(k_x, y_2)\big|_{y_2=0} \tag{B.21}$$

where $\tilde{M}_p(k_x, y_i)$ is the Fourier transform of the moment per unit length $\tilde{M}_p(x, y_i)$ acting on edges of a plate and given by

$$\tilde{M}_p(k_x, y_i) = \tilde{D}_p\left[\frac{\partial^2 \tilde{W}_p(k_x, y_i)}{\partial y_i^2} - k_x^2 \nu \tilde{W}_p(k_x, y_i)\right],\ i = 1,2. \tag{B.22}$$

Therefore,

$$\begin{aligned}&\tilde{D}_p\left[\tilde{B}_1\left(\tilde{k}_{y1}^2 - k_x^2\nu\right)e^{\tilde{k}_{y1}L_1} + \tilde{B}_2\left(\tilde{k}_{y2}^2 - k_x^2\nu\right)e^{\tilde{k}_{y2}L_1} + \tilde{B}_3\left(\tilde{k}_{y3}^2 - k_x^2\nu\right)e^{\tilde{k}_{y3}L_1} + \tilde{B}_4\left(\tilde{k}_{y4}^2 - k_x^2\nu\right)e^{\tilde{k}_{y4}L_1}\right] \\ &-\tilde{D}_p\left[\tilde{C}_1\left(\tilde{k}_{y1}^2 - k_x^2\nu\right) + \tilde{C}_2\left(\tilde{k}_{y2}^2 - k_x^2\nu\right) + \tilde{C}_3\left(\tilde{k}_{y3}^2 - k_x^2\nu\right) + \tilde{C}_4\left(\tilde{k}_{y4}^2 - k_x^2\nu\right)\right] = 0.\end{aligned} \tag{B.23}$$

(vii) Force equilibrium condition; the forces acting at junction $y_1 = L_1$ of plate $p1$ and $y_2 = 0$ of plate $p2$ should be in equilibrium with the applied external force as shown in Figure B.1.

$$-\tilde{F}_2(k_x, y_1)\big|_{y_1=L_1} + \tilde{F}_3(k_x, y_2)\big|_{y_2=0} = \tilde{F}_0(k_x) \tag{B.24}$$

where $\tilde{F}_2(k_x, y_1)$, $\tilde{F}_3(k_x, y_2)$ and $\tilde{F}_0(k_x)$ are the Fourier transforms of the forces $\tilde{f}_2(x, y_1)$, $\tilde{f}_3(x, y_2)$ and $\tilde{F}_0(x - x_1)$ respectively.

Therefore,

$$\begin{aligned}&-\tilde{D}_p\left[\frac{\partial^3 \tilde{W}_{p1}(k_x, y_1)}{\partial y_1^3} - k_x^2(2-\nu)\frac{\partial \tilde{W}_{p1}(k_x, y_1)}{\partial y_1}\right]_{y_1=L_1} \\ &+\tilde{D}_p\left[\frac{\partial^3 \tilde{W}_{p2}(k_x, y_2)}{\partial y_2^3} - k_x^2(2-\nu)\frac{\partial \tilde{W}_{p2}(k_x, y_2)}{\partial y_2}\right]_{y_2=0} = \tilde{F}_0(k_x).\end{aligned} \tag{B.25}$$

$$\begin{aligned}&-\tilde{D}_p\begin{bmatrix}\tilde{B}_1\left\{\tilde{k}_{y1}^3 - k_x^2(2-\nu)\tilde{k}_{y1}\right\}e^{\tilde{k}_{y1}L_1} + \tilde{B}_2\left\{\tilde{k}_{y2}^3 - k_x^2(2-\nu)\tilde{k}_{y2}\right\}e^{\tilde{k}_{y2}L_1} \\ +\tilde{B}_3\left\{\tilde{k}_{y3}^3 - k_x^2(2-\nu)\tilde{k}_{y3}\right\}e^{\tilde{k}_{y3}L_1} + \tilde{B}_4\left\{\tilde{k}_{y4}^3 - k_x^2(2-\nu)\tilde{k}_{y4}\right\}e^{\tilde{k}_{y4}L_1}\end{bmatrix} \\ &+\tilde{D}_p\begin{bmatrix}\tilde{C}_1\left\{\tilde{k}_{y1}^3 - k_x^2(2-\nu)\tilde{k}_{y1}\right\} + \tilde{C}_2\left\{\tilde{k}_{y2}^3 - k_x^2(2-\nu)\tilde{k}_{y2}\right\} \\ +\tilde{C}_3\left\{\tilde{k}_{y3}^3 - k_x^2(2-\nu)\tilde{k}_{y3}\right\} + \tilde{C}_4\left\{\tilde{k}_{y4}^3 - k_x^2(2-\nu)\tilde{k}_{y4}\right\}\end{bmatrix} = \tilde{F}_0(k_x).\end{aligned} \tag{B.26}$$

(viii) Continuity equation for plate $p2$ and beam $b2$; equal displacement to the plate at $y_2 = L_2$ of plate $p2$

$$\tilde{W}_{p2}(k_x, y_2)\Big|_{y_2=L_2} = \tilde{W}_{b2}(k_x) \tag{B.27}$$

$$\tilde{C}_1 e^{\tilde{k}_{y1}L_2} + \tilde{C}_2 e^{\tilde{k}_{y2}L_2} + \tilde{C}_3 e^{\tilde{k}_{y3}L_2} + \tilde{C}_4 e^{\tilde{k}_{y4}L_2} - \tilde{W}_{b2}(k_x) = 0. \tag{B.28}$$

(ix) Sliding condition; beam $b2$ is assumed infinitely stiff to torsion along $y_2 = L_2$ of plate $p2$

$$\left.\frac{\partial \tilde{W}_{p2}(k_x, y_2)}{\partial y_2}\right|_{y_2=L_2} = 0 \tag{B.29}$$

$$\left.\frac{\partial \tilde{W}_{p2}(k_x, y_2)}{\partial y_2}\right|_{y_2=L_2} = \tilde{C}_1 \tilde{k}_{y1} e^{\tilde{k}_{y1}L_2} + \tilde{C}_2 \tilde{k}_{y2} e^{\tilde{k}_{y2}L_2} + \tilde{C}_3 \tilde{k}_{y3} e^{\tilde{k}_{y3}L_2} + \tilde{C}_4 \tilde{k}_{y4} e^{\tilde{k}_{y4}L_2} = 0. \tag{B.30}$$

(x) Force equilibrium condition; the force on plate $p2$ are equal and opposite to the respective force on beam $b2$

$$\tilde{D}_p \left[\frac{\partial^3 \tilde{W}_{p2}(k_x, y_2)}{\partial y_2^3} - k_x^2(2-\nu)\frac{\partial \tilde{W}_{p2}(k_x, y_2)}{\partial y_2}\right]_{y_2=L_2} = \tilde{F}_4(k_x) \tag{B.31}$$

Combining equation (B.4) and (B.31) results in

$$\tilde{D}_p \left[\frac{\partial^3 \tilde{W}_{p2}(k_x, y_2)}{\partial y_2^3} - k_x^2(2-\nu)\frac{\partial \tilde{W}_{p2}(k_x, y_2)}{\partial y_2}\right]_{y_2=L_2} = \left(\tilde{D}_b k_x^4 - m'_{b2}\omega^2\right)\tilde{W}_{b2}(k_x). \tag{B.32}$$

Therefore,

$$\begin{aligned} &\tilde{D}_p \left[\begin{array}{l} \tilde{C}_1\left\{\tilde{k}_{y1}^3 - k_x^2(2-\nu)\tilde{k}_{y1}\right\}e^{\tilde{k}_{y1}L_2} + \tilde{C}_2\left\{\tilde{k}_{y2}^3 - k_x^2(2-\nu)\tilde{k}_{y2}\right\}e^{\tilde{k}_{y2}L_2} \\ +\tilde{C}_3\left\{\tilde{k}_{y3}^3 - k_x^2(2-\nu)\tilde{k}_{y3}\right\}e^{\tilde{k}_{y3}L_2} + \tilde{C}_4\left\{\tilde{k}_{y4}^3 - k_x^2(2-\nu)\tilde{k}_{y4}\right\}e^{\tilde{k}_{y4}L_2} \end{array}\right]. \\ &-\left(\tilde{D}_b k_x^4 - m'_{b2}\omega^2\right)\tilde{W}_{b2}(k_x) = 0 \end{aligned} \tag{B.33}$$

The equations representing boundary conditions (B.11), (B.13), (B.16), (B.18), (B.20), (B.23), (B.26), (B.28), (B.30) and (B.33) can be expressed in a matrix form. For simplification, new variables α_i and β_i are introduced by

$$\begin{aligned}
\alpha_1 &= \tilde{k}_{y1}^3 - k_x^2(2-\nu)\tilde{k}_{y1}, \\
\alpha_2 &= \tilde{k}_{y2}^3 - k_x^2(2-\nu)\tilde{k}_{y2}, \\
\alpha_3 &= \tilde{k}_{y3}^3 - k_x^2(2-\nu)\tilde{k}_{y3}, \\
\alpha_4 &= \tilde{k}_{y4}^3 - k_x^2(2-\nu)\tilde{k}_{y4}.
\end{aligned} \tag{B.34}$$

$$\begin{aligned}
\beta_1 &= \tilde{k}_{y1}^2 - k_x^2\nu, \\
\beta_2 &= \tilde{k}_{y2}^2 - k_x^2\nu, \\
\beta_3 &= \tilde{k}_{y3}^2 - k_x^2\nu, \\
\beta_4 &= \tilde{k}_{y4}^2 - k_x^2\nu.
\end{aligned} \tag{B.35}$$

Then, the matrix form of the equations in the wavenumber domain is

$$\mathbf{Ku} = \mathbf{F} \tag{B.36}$$

where the dynamic stiffness matrix $\mathbf{K}$ is

$$\mathbf{K} = \begin{bmatrix}
1 & 1 & 1 & 1 & 0 & 0 & 0 & 0 & -1 & 0 \\
\tilde{k}_{y1} & \tilde{k}_{y2} & \tilde{k}_{y3} & \tilde{k}_{y4} & 0 & 0 & 0 & 0 & 0 & 0 \\
\alpha_1 & \alpha_2 & \alpha_3 & \alpha_4 & 0 & 0 & 0 & 0 & \frac{\tilde{K}_{b1}}{\tilde{D}_p} & 0 \\
e^{\tilde{k}_{y1}L_1} & e^{\tilde{k}_{y2}L_1} & e^{\tilde{k}_{y3}L_1} & e^{\tilde{k}_{y4}L_1} & -1 & -1 & -1 & -1 & 0 & 0 \\
\tilde{k}_{y1}e^{\tilde{k}_{y1}L_1} & \tilde{k}_{y2}e^{\tilde{k}_{y2}L_1} & \tilde{k}_{y3}e^{\tilde{k}_{y3}L_1} & \tilde{k}_{y4}e^{\tilde{k}_{y4}L_1} & -\tilde{k}_{y1} & -\tilde{k}_{y2} & -\tilde{k}_{y3} & -\tilde{k}_{y4} & 0 & 0 \\
\beta_1 e^{\tilde{k}_{y1}L_1} & \beta_2 e^{\tilde{k}_{y2}L_1} & \beta_3 e^{\tilde{k}_{y3}L_1} & \beta_4 e^{\tilde{k}_{y4}L_1} & -\beta_1 & -\beta_2 & -\beta_3 & -\beta_4 & 0 & 0 \\
-\alpha_1 e^{\tilde{k}_{y1}L_1} & -\alpha_2 e^{\tilde{k}_{x2}L_1} & -\alpha_3 e^{\tilde{k}_{y3}L_1} & -\alpha_4 e^{\tilde{k}_{y4}L_1} & \alpha_1 & \alpha_2 & \alpha_3 & \alpha_4 & 0 & 0 \\
0 & 0 & 0 & 0 & e^{\tilde{k}_{y1}L_2} & e^{\tilde{k}_{y2}L_2} & e^{\tilde{k}_{y3}L_2} & e^{\tilde{k}_{y4}L_2} & 0 & -1 \\
0 & 0 & 0 & 0 & \tilde{k}_{y1}e^{\tilde{k}_{y1}L_2} & \tilde{k}_{y2}e^{\tilde{k}_{y2}L_2} & \tilde{k}_{y3}e^{\tilde{k}_{y3}L_2} & \tilde{k}_{y4}e^{\tilde{k}_{y4}L_2} & 0 & 0 \\
0 & 0 & 0 & 0 & \alpha_1 e^{\tilde{k}_{y1}L_2} & \alpha_2 e^{\tilde{k}_{y2}L_2} & \alpha_3 e^{\tilde{k}_{y3}L_2} & \alpha_4 e^{\tilde{k}_{y4}L_2} & 0 & \frac{\tilde{K}_{b2}}{\tilde{D}_p}
\end{bmatrix} \tag{B.37}$$

where $\tilde{K}_{b1} = \tilde{D}_b k_x^4 - m'_{b1}\omega^2$ and $\tilde{K}_{b2} = \tilde{D}_b k_x^4 - m'_{b2}\omega^2$. Also, the displacement vector $\mathbf{u}$ in terms of the wave amplitudes in the plate and the transformed beam displacements is

$$\mathbf{u} = \left[\tilde{B}_1(k_x) \;\; \tilde{B}_2(k_x) \;\; \tilde{B}_3(k_x) \;\; \tilde{B}_4(k_x) \;\; \tilde{C}_1(k_x) \;\; \tilde{C}_2(k_x) \;\; \tilde{C}_3(k_x) \;\; \tilde{C}_4(k_x) \;\; \tilde{W}_{b1}(k_x) \;\; \tilde{W}_{b2}(k_x)\right]^T, \tag{B.38}$$

and the force vector is

$$\mathbf{F} = \begin{bmatrix} 0 & 0 & 0 & 0 & 0 & 0 & \tilde{F}_0(k_x)/\tilde{D}_p & 0 & 0 & 0 \end{bmatrix}^T. \tag{B.39}$$

Thus, if the excitation force is known, the response of the beams and the plates can be found from the solution of equation (B.36) as follows.

$$\mathbf{u} = \mathbf{K}^{-1}\mathbf{F} \tag{B.40}$$

As the response of the coupled structure consisting of infinite beams and the infinitely long finite width plate is identified, the response of a finite structure such as the structure shown in Figure 44 can be obtained based on a Fourier series expansion as explained in [2]. For example, the response of beam $b1$ is written as

$$\tilde{w}_{b1}(x) = \frac{\tilde{W}_{b1,0}}{2} + \sum_{n=1}^{\infty} \tilde{W}_{b1,n} \cos(k_{x,n}x) \tag{B.41}$$

where $k_{x,n} = n\pi/L_x$ and $\tilde{W}_{b1,n} = \tilde{W}_{b1}(k_{x,n})$ is the n^{th} component of the motion of the coupled beam $b1$, which is defined in equation (B.40).

B.2 Numerical analysis

Numerical analysis is carried out for the structure consisting of finite subsystems shown in Figure 44 where the ends of both finite beams and the corresponding two edges of the plate are assumed to be sliding. The relevant dimensions of the structure are given in Table 4.

Firstly, the transfer mobility is investigated when the external point force is applied at $x = 1.51\,\text{m}$ and $y = 0.5\,\text{m}$ on the plate and compared with that predicted using FEM. The corresponding results are shown in Figure B.2. A difference in level between them is observed near 9 Hz. This is because the corresponding FEM result is truncated due to the frequency resolution used (0.5 Hz), otherwise it can be seen that they are in good agreement.

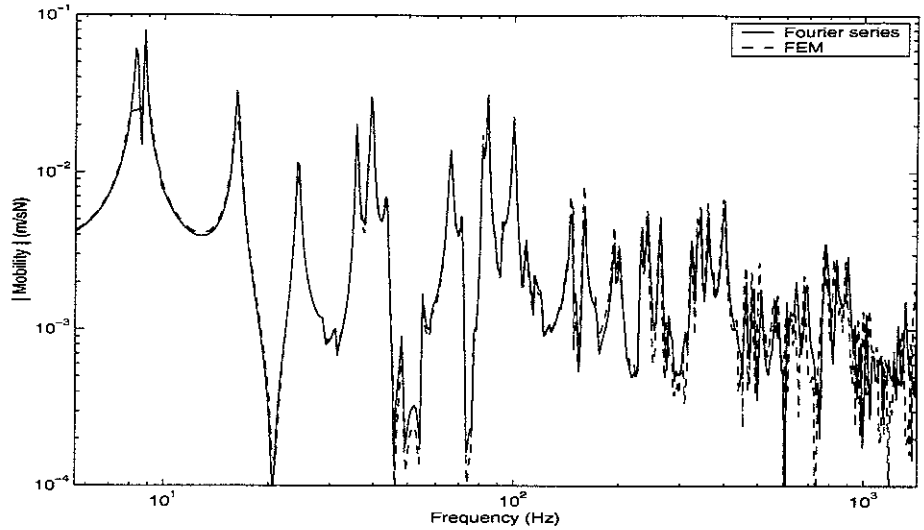

Figure B.2. Transfer mobility comparison for the plate-excited coupled structure as Figure 44 (response at $x = 0.0\,\mathrm{m}$ of beam $b1$, point force applied at $x = 1.51\,\mathrm{m}$, $y = 0.5\,\mathrm{m}$ on the plate).

In addition to the transfer mobility, the power balance relationship is also investigated. If the plate is excited, the power balance relationship for such a structure shown in Figure 44 is already presented in Figure 45 (b). The corresponding powers are shown in Figure B.3. It can be seen that the power balance between the total input power, the transferred powers and the dissipated power in the plate holds.

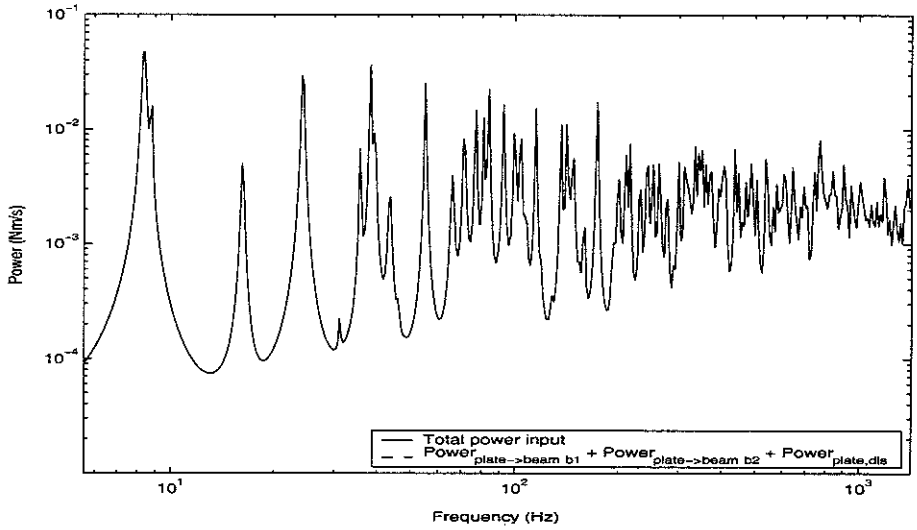

Figure B.3. Comparison of power balance for the beam-plate-beam structure as Figure 44 (point force applied at $x = 1.51\,\mathrm{m}$, $y = 0.5\,\mathrm{m}$ on the plate).